DETERMINING MECHANISMS OF SENSITIVITY AND RESISTANCE TO HSP90 INHIBITION IN NON-SMALL CELL LUNG CANCER

Thesis submitted for the degree of

Doctor of Philosophy

at the University of Leicester

by

Edward William Preston Law MBiochem (hons)

Department of Cancer Studies

University of Leicester

February 2016

Abstract

Determining mechanisms of sensitivity and resistance to HSP90 inhibition in non-small cell lung cancer – Edward Law

BACKGROUND: HSP90 is a molecular chaperone which supports the maturation of numerous client proteins, many of which are involved in oncogenic signaling pathways such as PI3K/AKT, MAPK and JAK/STAT. HSP90 is an appealing target for small molecule inhibitors due to its ability to simultaneously downregulate multiple oncogenic conduits. Results in the clinic have been mixed and biomarkers of response to HSP90 inhibitors for patient stratification remain obscure.

RESULTS: 1. EML4-ALK is a HSP90 client which degrades in response to HSP90 inhibition. Variants of EML4-ALK exist with disparate structures and stabilities. This chapter demonstrates differential stability of EML4-ALK variants and cell line sensitivity in response to HSP90 inhibition. A RT-PCR test to identify variants from FFPE tumour tissue is developed for tissues from the CHIARA trial to link variant status and response to ganetespib. **2.** Characterisation of a cell line resistant to ganetespib, and verification that high UGT1A levels prevent ganetespib from inhibiting HSP90 in a NSCLC context. **3.** Array-based analysis of genome-wide copy number alterations in the GALAXY-1 trial, which examined ganetespib plus docetaxel (G-D) in the second line setting against docetaxel alone (D), following platinum-based chemotherapy in NSCLC patients. Three CNAs were associated with sensitivity to ganetespib plus docetaxel: loss in cytoband 18q23, and gains in 11q13.3 and 16q22.3. Patients with multiple CNAs may represent a group of patients who perform badly on docetaxel but respond much better with the addition of ganetespib.

SUMMARY: Several putative biomarkers which are predictive of response to ganetespib are identified in this study. The relationship between EML4-ALK variant stability and ganetespib response may shed light on HSP90 client selection. Genome wide CNA analysis associated with randomized clinical trial survival data has identified putative biomarkers of efficacy to ganetespib plus docetaxel.

Acknowledgments

The completion of this PhD was a task like no other I have undertaken. There are many people whose contributions were invaluable to its completion and I hope to recognise them here.

Firstly, I'd like to thank David Proia, Vienna Reichart and all the staff at Synta Pharmaceuticals for providing ganetespib and collaborating with us on several projects.

I'd like to thank members of the university for their help with certain aspects of this work. Howard Pringle helped me to develop the RT-PCR methodology for detecting EML4-ALK variants from patient tissue. He was also an invaluable resource and has a magnificent mind, which he was more than happy to allow me to tap into. Don Jones and Rajinder Singh helped greatly with the design and execution of the mass spec experiments. Furthermore, I'd like to thank Don in his role as postgraduate tutor for his endless patience and pastoral support. Richard Bayliss and Mark Richards were wonderful collaborators for the EML4-ALK portion of this work and I was very grateful to be able to publish some of my research with them. Rob Hastings and Callum Rakhit have been invaluable collaborators for the CNA work.

I'd like to thank the people in the labs at CCRCB in Belfast where I began this journey for welcoming me into the scientific world. I have been lucky enough to make a lifelong friend in Ben, who has been a wonderful support throughout my time as a PhD student. Thanks go to Annabel for her ability to cheer me up and for help with some of the clinical data. I'd like to thank Ian for his help with data analysis and for regular chats. Josh and Munisha helped me so much during my time it's impossible to quantify. My sister and brother-in-law provided me with a second home at the darkest of times, and I'll be forever grateful.

Dean you have been a wonderful supervisor. Whenever I was struggling you knew exactly how to motivate me and put me back on track. Your incredible enthusiasm for science is infectious and I know you will continue to develop the vast number of ideas you have and help improve patient lives. Sara, without you there is no chance I would have finished this PhD. You have been formidable: you pushed me when I needed it, you listened to my ideas and called me on the stupid things I said and did, which helped me to develop as a scientist. You were an incredible emotional support for me throughout, even at the most awful times, and I can never thank you enough for that.

Finally, to my parents. Thank you for everything. You encouraged me to think for myself and discover the excitement that science brings. Any future success I obtain will be yours too.

Abbreviations

17-AAG	17-N-allylamino-17-demethoxygeldanamycin
17-DMAG	17-Dimethylaminoethylamino-17-demethoxygeldanamycin
18S	18S ribosomal RNA
5-FU	5-fluorouracil
A1	BCL-2-related protein A1
aCGH	Array comparative genomic hybridisation
ADME	Absorption, Distribution, Metabolism and Excretion
AHA1	Activator of HSP90 ATPase 1
AIF	Apoptosis Initiating Factor
ALK	Anaplastic Lymphoma Kinase
ALT	Alanine Aminotransferase
APAF1	Apoptotic protease activating factor 1
AST	Aspartate aminotransferase
ATP	Adenosine triphosphate
BAD	Bcl-2-associated death promoter
BAF	B-allele frequency
BAK	BCL-2 homologous antagonist/killer
BAX	BCL-2 associated X protein
BCL2	B-cell lymphoma 2
BCL-B	Bcl-2-like protein 10
BCL-W	BCL-2-like protein 2
BCL-XL	BCL-2 regulated gene, long isoform
BFB	Breakage-fusion-bridge cycles
BH	BCL-2 homology
BID	BH3 interacting-domain death agonist
BIM	BCL-2-like protein 11
BRAF	v-Raf murine sarcoma viral oncogene homolog B
CBS	Circular Binary Segmentation
CDC37	Cell division cycle 37 homolog
CDKN2A	Cyclin-dependent kinase inhibitor 2A
cfDNA	Circulating free DNA
CHIP	C-terminus of Hsp70-interacting protein
CI	Confidence Interval
c-MET	MET proto-oncogene, receptor tyrosine kinase
CNAs	Copy number alterations
CNV	Copy number variation
c-RAF/RAF-1	RAF proto-oncogene serine/threonine-protein kinase
CRC	Colorectal cancer
CSF	Cerebral-spinal fluid
CTLA-4	Cytotoxic lymphocyte antigen 4

CUL5	Cullin-RING E3 ubiquitin ligase Cullin-5
DHFR	Dihydrofolate reductase
DISC	Death-inducing signalling complex
DNA	Deoxyribonucleic acid
DRT	Direct ratio testing
ECOG	Eastern Cooperative Oncology Group
EGF	Epidermal growth factor
EGFR	Epidermal growth factor receptor
eLDH	Elevated Lactate Dehydrogenase
EML4	Echinoderm microtubule protein-like 4
EML4-ALK	Echinoderm microtubule protein-like 4-anaplastic lymphoma kinase
ENU	N-ethyl-N-nitrosourea
ER	Endoplasmic reticulum
ERBB2	Erb-B2 Receptor Tyrosine Kinase
ERK	Extracellular signal-regulated kinase
FAK	Focal adhesion kinase
FCS	Foetal calf serum
FGFR	Fibroblast growth factor receptor
FISH	Fluorescence *in situ* hybridisation
FoSTeS	Fork stalling template switching
GISTIC	Genomic identification of significant targets in cancer
GLAD	Gain and loss analysis of DNA
GRP94	Glucose-regulated protein 94
GTP	Guanosine triphosphate
GTPase	Guanosine triphosphate hydrolase
HBA	Haemoglobin A
HDAC	Histone deacetylase
HER2/neu	Receptor tyrosine kinase erbB-2
HGF	Hepatocyte growth factor
HIF-1α	Hypoxia-inducible factor-1
HPRT	Hypoxanthine-guanine phosphoribosyltransferase
HR	Hazard Ratio
HSC70	Heat shock 70 kDa protein 8
HSE	Heat shock element
HSF1	Heat shock factor 1
HSP	Heat shock protein
HSP27	Heat shock protein 27
HSP72	Heat shock 70 kDa protein 1
HSP90	Heat shock protein 90
hTERT	Telomerase reverse transcriptase
HTPG	High temperature protein G
IAP	Inhibitor of apoptosis
IL-3	Interleukin-3
IP6K2	Hexakisphosphate kinase-2

IP7	Disphosphoinositol pentakisphosphate
KDAC	Lysine deacetylase
KIF5b	Kinesin-1 heavy chain
KRAS	Kirsten rat sarcoma viral oncogene homolog
MAP	Mitogen activated protein
MAPD	Median absolute pairwise difference
MCL-1	Myeloid cell leukemia-1
MEF	Mouse embryonic fibroblasts
MEK	Mitogen-activated protein kinase kinase
MIP	Molecular Inversion Probe
MMBIR	Microhomology mediated break-induced repair
MMP2	Matrix metalloproteinase-2
MOMP	Mitochondrial outer membrane permeablisation
mTOR	Mechanistic target of rapamycin
NAHR	Non-allelic homologous recombination
NGS	Next generation sequencing
NHEJ	Non-homologous end-joining
NOXA	Phorbol-12-myristate-13-acetate-induced protein 1
NPM	Nucleophosmin
NPM-ALK	Nucleophosmin-Anaplastic Lymphoma Kinase
NQO1	NAD(P)H:quinone oxidoreductase 1
NSCLC	Non-small cell lung cancer
ORR	Overall response rate
OS	Overall survival
p53	Tumor protein p53
PBS	Phosphate-buffered saline
PCR	Polymerase chain reaction
PD	Pharmacodynamic
PFS	Progression-free survival
p-GP	P-glycoprotein
PIK3	Phosphatidylinositol-4,5-bisphosphate 3-kinase
PIK3CA	Phosphatidylinositol-4,5-bisphosphate 3-kinase, catalytic subunit alpha
PK	Pharmacokinetic
PKB/AKT	Protein kinase B
PP5	Protein phosphatase 5
PPIase	Peptidylprolyl isomerase
PTEN	Phosphatase and tensin homolog
PUMA	p53 upregulated modulator of apoptosis
qPCR	Quantitative polymerase chain reaction
ROS	Reactive oxygen species
SCLC	Small cell lung cancer
SCNA	Somatic copy number alteration
SHR	Steroid hormone receptor
SMAC	Second mitochondria-derived activator of caspases

SNP	Single nucleotide polymorphism
STAT3	Signal transducer and activator of transcription 3
STIP1	Stress-induced phosphoprotein 1
TAPE	Tandem Atypical Propeller in EMLs
TFG	TRK-fused gene
TKI	Tyrosine kinase inhibitors
TRAP1	TNF receptor-associated protein 1
TYMS/TS	Thymidylate synthase
UGT1A	Uridine-5’-diphosphate glucuronosyltransferase 1A
VEGF	Vascular endothelial growth factor
v-SRC	SRC Proto-Oncogene, Non-Receptor Tyrosine Kinase Viral Oncogene Homolog
WES	Whole exome sequencing
WGS	Whole genome sequencing

"It did not matter if this interpretation was true or false… It was a working link between imagination and reality, like love." – Ferruccio Ritossa

In memory of Nick

Contents

Table of figures

Table of tables

Chapter 1 - Introduction

1 Introduction

1.1 What is cancer?

Searching for the phrase “what is cancer” online will provide three definitions of the word. Firstly, “A disease caused by an uncontrolled division of abnormal cells in a part of the body”. Secondly, “A malignant growth or tumour resulting from an uncontrolled division of cells” and finally, “An evil or destructive practice or phenomenon that is hard to contain or eradicate”. That final description is the most striking, yet perhaps the most accurate: the disease, cancer, is synonymous with a great evil which cannot be controlled. This is the public perception of the illness, but what really is cancer?

Cancer is uncontrolled cell growth indeed, however there are multiple factors which influence this process. Hanahan and Weinberg released an updated version of the “Hallmarks of Cancer” in 2011, which demonstrates several different biological capabilities that cancers can develop, and potential strategies under development to counteract them [1]. These include sustained proliferative signalling (signals telling the cells to divide), evading growth suppressors (natural mechanisms in cells to prevent uncontrolled growth), resistance against cell death, development of cell immortality, angiogenesis (development of new blood vessels to fuel further tumour development), metastasis/invasion (migration and colonisation of cancer cells to new sites in the body), reprogramming of energy metabolism and evading immune destruction. Many of these hallmarks are able to be targeted by specific drugs, a good example being angiogenesis: a hallmark with several agents in development such as bevacizumab, a drug which targets vascular endothelial growth factor (VEGF) and prevents new blood vessel growth in tumours. However, cancers are often able to circumvent the loss of one of these key biological abilities. Still, what if it was possible to block many of these cancer hallmarks simultaneously? That has been the promise of a class of drugs known as HSP90 inhibitors for some time, however they have yet to fulfil that potential, which will be discussed later. Lung cancer in particular, where many cancer hallmarks are often present, represents a group of tumours stubbornly resistant to therapeutic progress. The question is, can our knowledge of lung cancer mutations or genetic alterations predict response to HSP90 inhibitors in this tumour subtype? The aim of

Figure 1.1-1 *The Hallmarks of cancer. Obtained from Hanahan and Weinberg, (2011)*

this thesis is to attempt to answer that question in part by looking at several contextually disparate but thematically similar projects within the non-small cell lung cancer landscape.

1.2 Lung cancer

Lung cancer is currently the second most common cancer in the UK and is responsible for around 13% of new cancer diagnoses [2]. However, it is the most common cause of cancer death: over 20% of all cancer mortalities in the UK, and the 5-year survival rate in Europe is less than 15% [2]. Risk factors for the development of lung cancer include tobacco smoke (estimated to be responsible for 80% of lung cancer deaths), radon, asbestos, air pollution and a family history of the disease. It is divided into small and non-small cell groups (SCLC and NSCLC, 15% and 85% of cases respectively).

1.3 Non-small cell lung cancer

Non-small cell lung cancer (NSCLC) is classified into the morphological subgroups squamous cell carcinoma (~ 25% of cases), adenocarcinoma (~40%) and large-cell carcinoma (~15%). 5-year survival rates remain stubbornly poor for NSCLC patients: those patients presenting with advanced metastatic cancer have a median survival of around 1 year [3]. Pathological classification alone garnered some improvement with conventional chemotherapies; for example it was found that cisplatin-pemetrexed therapy conveyed a survival advantage over cisplatin-gemcitabine in adenocarcinoma (overall survival (OS) 12.6 v 10.9 months) compared to squamous-cell carcinoma, however cisplatin-gemcitabine was more successful than cisplatin-pemetrexed in squamous cell carcinoma (overall survival 10.8 v 9.4 months) [4]. However, such gains are relatively modest, and much work has been completed on understanding the genetics which drive these tumours in order to improve clinical outcome.

1.3.1 Driver mutations and targeted therapy in NSCLC

A revolution in cancer treatment was the discovery of mutated genes which drive tumour growth, and subsequent development of specific inhibitors. The receptor tyrosine kinase, epidermal growth factor receptor (EGFR), is mutated in around 15% of

NSCLCs, and led to the development of specific tyrosine kinase inhibitors such as gefitinib [5]. In patients, activating mutations within EGFR around the ATP binding pocket were found to sensitise the tumour to gefitinib [6]. Overexpression which is found in approximately 40-60% of NSCLC was previously thought most significant, but it did not correlate with responses [7]. Phase III trials of gefitinib in patients selected for sensitising EGFR mutations significantly improved progression free survival (PFS): Mok et. al demonstrated a 9.6 month vs 6.3 month improvement of gefitinib vs standard chemotherapy (Hazard Ratio (HR) 0.48 95%, Confidence Interval (CI) 0.36–0.64) which was reversed in patients with wild type EGFR (1.6 months vs 5.5 months HR 2.85, 95% CI 2.05–3.98) and Lee et al observed similar outcomes (EGFR mut+ve PFS 8.4 months vs 6.7 months, HR 0.613, 95% CI 0.308–1.221, EGFR mut-ve PFS 2.1 months vs 6.4 months 1.517, 95% CI 0.880–2.615) [8].

Another major "oncogenic driver" in human NSCLC is Kirsten rat sarcoma viral oncogene homolog (KRAS) [9]. Found in approximately 25% of adenocarcinomas, KRAS mutations have been shown to bestow resistance to EGFR inhibitors via inactivation of the KRAS Guanosine triphosphate hydrolase (GTPase): constitutive KRAS signalling to pro-growth mitogen activated protein (MAP) kinase pathway results [10]. Over 30 years of work has gone into RAS inhibitor research, however no drug has successfully entered the clinic, leading many researchers to consider RAS proteins "undruggable". There are many reasons for this, but one is that, unlike protein kinases which generally bind ATP in the micromolar affinity range, the binding site of RAS proteins for GTP is in the picomolar affinity range, making highly specific inhibitor development problematic, and therefore there had been little success in the treatment of KRAS mutated NSCLC [11]. However, inhibition of farnesyl transferase with lonafarnib [12], which prevents farnesylation of Ras proteins and limits their ability to translocate to the plasma membrane, showed no survival advantage over standard chemotherapy, although these patients were not stratified for KRAS mutation status (overall survival 144 days vs 168 days respectively, HR 0.863, 95% CI 0.619-1.205). However, a recent phase 2 trial combining the mitogen-activated protein kinase kinase (MEK) inhibitor selumetinib with docetaxel in patients with mutated KRAS resulted in a 37% objective response rate and an overall survival of 9.4 months versus 5.2 months for docetaxel

alone [13]. However, the trade-off was a high rate of grade 3 or above adverse events and the study didn't analyse wild type KRAS patients and therefore this oncogene may not be a predictive factor. KRAS remains a stubborn patient subgroup to treatment.

Numerous other mutations and translocations have been identified and are being targeted for clinical development such as, v-Raf murine sarcoma viral oncogene homolog B (BRAF), receptor tyrosine kinase erbB-2 (HER2/neu), phosphatidylinositol-4,5-bisphosphate 3-kinase, catalytic subunit alpha (PI3KCA) and echinoderm microtubule protein-like 4-anaplastic lymphoma kinase (EML4-ALK) [14]. **Table 1.3-1** summarises current progress.

Molecular target/driver oncogene	Prevalence (%)	Approved therapies	Potential treatments in clinical trials	Potential treatments in preclinical development
Adenocarcinoma predominant				
KRAS mutations	25-30	None	Cytotoxic chemotherapy + MEK inhibitors (selumetinib, trametinib and others). PI3K inhibitors, FAK inhibitors	KRAS G12C inhibitors, KRAS inhibitors, MEK and PI3K inhibitors, JAK/TBK1/IKKε inhibitors
EGFR mutations	15-20	Gefitinib, erlotinib, icotinib, afatinib	CO1686, AZD9291, cetuximab + afatinib. HSP90 inhibitors (AUY922 etc)	Mutation-specific EGFR inhibitors
ALK rearrangements	3-7	Crizotinib, ceritinib, alectinib	PF-06463922, TSR-011, AP26113, ASP3026, X-396, Hsp90 inhibitors (AUY922 etc)	ALK inhibitors (more potent)
ROS1 rearrangements	1-3	None	Crizotinib, ceritinib, PF-06463922	ROS inhibitors, HSP90 inhibitors
HER2 mutations	1-3	None	ERBB/HER2 inhibitors (neratinib etc), mTOR/PI3K inhibitors (temsirolimus etc)	HER2 inhibitors, HSP90 inhibitors
BRAF mutations	1-3	None	Vemurafenib, dafrafenib, MEK inhibitors (selumetinib, trametinib etc), dasatinib	RAF inhibitors
RET rearrangements	1	None	Cabozantinib, vandetanib, sunitinib, ponatinib	RET inhibitors, HSP90 inhibitors
MET amplification	1	None	Crizotinib, tivantinib, onartuzumab, + other MET inhibitors	MET inhibitors
NRAS mutations	1	None	None	MEK inhibitors
PIK3CA mutations	1	None	PI3K inhibitors (buparlisib etc)	PI3K inhibitors, mTOR inhibitors
NTRK1 rearrangements	<1	None	Crizotinib	TRKA inhibitors
AKT mutations	<1	None	None	Pan-AKT inhibitors
MEK mutations	<1	None	None	MEK inhibitors
Squamous cell carcinoma predominant				
FGFR1 amplifications	20	None	FGFR inhibitors (AZD4547, JNJ-42756493, BGJ398, ponatinib etc)	FGFR inhibitors (more potent)
FGFR2/3/4 mutations and rearrangements	5-10	None	FGFR inhibitors (AZD4547, JNJ-42756493, BGJ398, ponatinib etc)	FGFR inhibitors (more potent)
PIK3CA mutations	5-10	None	PI3K inhibitors (buparlisib etc)	PI3K inhibitors, mTOR inhibitors
DDR2 mutations	3-5	None	Dasatinib	DDR2 inhibitors (more potent)

Table 1.3-1 *Driver oncogenes and inhibitors in development for adenocarcinoma and squamous cell carcinoma. Adapted from [15].*

The development of resistance to targeted agents such as tyrosine kinase inhibitors (TKI) is a common consequence of targeted therapy due to the high selective pressure on a single protein or a few proteins in the cell: either combination therapy should be considered, or mechanisms of resistance to new, target-specific therapies must be elucidated and overcome in order to maximise clinical benefit. For example, patients treated with EGFR TKIs gefitinib or erlotinib always relapse after treatment: the threonine to methionine mutation (T790M) was found to render gefitinib ineffective via steric hindrance in the catalytic site of EGFR [16]. Interestingly in H1975 cells which harbour the T790M mutation, knockdown of the pro-survival B-cell lymphoma 2 (BCL2) protein leads to increased sensitivity and apoptosis in response to gefitinib [17]. More work needs to be undertaken to fully understand the mechanism: is there a direct link to EGFR inhibition, or is it purely inhibition of the pro-survival BCL2? Dynamic assessment of BH3 proteins and other proteins involved in apoptosis may help this [18] Nevertheless, amplification of the MET tyrosine kinase in a "kinase switch" phenomenon is capable of maintaining pro-survival protein kinase B (PKB/AKT) signalling as an alternative resistance mechanism [19].

One further issue in development of targeted agents to some of these driver oncogenes is the limited availability of patients who express some of these mutations. For example, patients with NTRK rearrangements, AKT and MEK mutations account for less than 1% each of lung adenocarcinoma patients, meaning access to patient tumours for research and development, as well as initiating clinical trials, becomes problematic, especially if these patients are not routinely screened for such mutations. There may also be problems obtaining funding for research of such rare mutations.

Many of these mutated driver oncogenes are clients of the chaperone HSP90. Inhibitors of HSP90 exploit the dependence of oncogenic proteins on HSP90 for survival and maturation, and downregulation of multiple oncogenic pathways could help prevent the resistance observed to more specific inhibitors. For example, it has been demonstrated that EML4-ALK expressing H3122 cells resistant to crizotinib due to the gatekeeper mutation L1196M, remain sensitive to the HSP90 inhibitor 17-AAG and downregulate p-ALK, p-AKT and p-ERK downstream signalling pathways [20].

Development of HSP90 inhibitors has held much promise, but to date has not delivered on the theoretical potential.

1.4 The drug development process and HSP90

1.4.1 Considerations in drug development

Successful drug development requires an integrated "bench to bedside" approach from basic research to the clinic and back again. Figure 1.4-1 outlines this process [21]. Traditionally the Food and Drug Administration has required preclinical studies based on pharmacokinetic (PK) parameters known as Absorption, Distribution, Metabolism and Excretion (ADME) with emphasis on safety and toxicology. There was little emphasis on understanding the pharmacokinetic-pharmacodynamic (PK-PD) relationship at the preclinical drug development stage to understand potential drug efficacy.

The realisation that understanding the mechanism of drug action and its movement in the body may help more drugs succeed in clinical trials has led to some improvement, for example the Biopharmaceutical Classification System was developed to predict oral absorption at the *in vitro* stage and is now used by the FDA [22]. Another area in development is the ability to predict blood-brain-barrier penetration, however reliable *in vitro* models are still out of reach despite some successes [23]. Such analysis may have helped predict that some EML4-ALK positive NSCLC patients treated with crizotinib, progress due to poor CNS penetration: earlier modification of the compound may have avoided this [24].

A lack of understanding of the PK-PD relationship of novel compounds may help to explain the historical failings of HSP90 inhibitors, despite clear promise from preclinical studies.

Figure 1.4-1 *The process of drug development. Obtained from Zhang CH and Zhang P, 2013*

1.4.2 HSP90 as a target of small molecule inhibitors

One of the first HSP90 inhibitors to be investigated was the natural compound geldanamycin. This drug binds in the N-terminal ATP binding region of HSP90: the result is a disruption in HSP90 conformational cycling, prevention of the formation of an active ATPase which locks the complex in an intermediate state whereupon an E3 ubiquitin ligase such as the C-terminus of HSP70-interacting protein (CHIP) is recruited leading to client protein degradation [25, 26]. These inhibitors however failed due to poor oral bioavailability, instability and liver toxicity [27].

17-AAG (17-N-allylamino-17-demethoxygeldanamycin) was derived from geldanamycin and was the first HSP90 inhibitor to reach the clinic [28]. However, this first-in-class derivative of geldanamycin had drawbacks such as hepatoxicity, indicated by increased levels of serum transaminases: possibly due to the reactive oxygen species created by redox reactions involving geldanamycin's quinone moiety and NADPH-cytochrome P450 reductase [29-31]. Another problem of the geldanamycin derivative 17-AAG is solubility, and therefore 17-DMAG was developed, which is a more potent HSP90 inhibitor, however again was discontinued due to a poor toxicity profile [32]. This class of inhibitors have generally shown little clinical efficacy to date. New strategies should be developed, such as combination with chemotherapy or other targeted agents, or development of HSP90 inhibitors with a more favourable safety profile utilising a more thorough PK-PD analysis, plus an even higher affinity for HSP90 and produce a sustained downregulation of HSP90 clients which drive NSCLC such as EML4-ALK: downregulation of its downstream signalling pathways could yield significant advantage in ALK positive NSCLC [33, 34].

Second generation inhibitors are starting to look more thoroughly at the PK-PD relationship and many modifications over the first generation have been made to reduce toxicity and improve affinity for HSP90. For example the second generation inhibitor NVP-AUY922 is a resorcinol derivative of radicicol without a benzoquinone moiety which causes toxicity and has a very binding affinity for the HSP90 ATP-binding pocket [35]. Many have now entered clinical trials.

1.4.3 Clinical trials of HSP90 inhibitors in NSCLC

Clinical trials of HSP90 inhibitors in NSCLC have to date produced mixed results. One trial investigated the use of the second generation 17-AAG analogue IPI-504 monotherapy in EGFR wild type and EGFR mutated NSCLC patients [36]. Only a 7% overall response rate was observed in the population as a whole, however of these, EML4-ALK rearranged patients seemed to achieve the best responses (two partial responses, one stable disease) [36].

The results of NCT01031225 trialling ganetespib as monotherapy in NSCLC have recently been published [37]. This study separated 98 NSCLC patients into three genetically distinct cohorts: A, with mutant EGFR; B, with mutant KRAS or C, no EGFR/KRAS mutations. Progression free survival at 16 weeks was 13.3%, 5.9%, and 19.7% respectively. Interestingly, 4 patients achieved partial response, and retrospective analysis revealed all of these to harbour EML4-ALK translocations. This translated to a 50% partial response rate for ALK positive patients in this trial. Ganetespib appears to have significant efficacy in this subgroup of patients; however, why half of ALK positive patients did not respond to treatment is uncertain. No further trials of ganetespib monotherapy in ALK positive NSCLC patients have been conducted, however a single report of a crizotinib-resistant EML4-ALK variant 3 positive patient showed tumour shrinkage following three once-a-week doses of ganetespib at 200mg/m^2 [38]. It is likely ganetespib may need to be used in combination with other drugs to improve response rates for ALK-negative patients.

Results from the GALAXY-1 phase II trial (NCT01348126) of patients with advanced non-small cell lung adenocarcinoma randomised to docetaxel with or without ganetespib post first line chemotherapy have also been announced [39]. In a retrospective analysis, patients diagnosed with advanced disease greater than 6 months before randomization (chemosensitive patients), exhibited longer survival if treated by means of docetaxel with ganetespib than without it (N = 177): PFS (adjusted HR = 0.74, P = 0.0417); OS (adjusted HR = 0.69, P = 0.0191). Chemoresistant patients did not see such benefit, and no other patient subgroups produced any benefit including K-Ras mutation status, elevated lactate dehydrogenase (eLDH), ECOG status, smoking status or prior chemotherapy regimen [39].

Another trial looking at the HSP90 inhibitor AUY922 in combination with erlotinib in EGFR-mutated lung cancer with acquired resistance to EGFR tyrosine kinase inhibitors (NCT01259089) reported a partial response rate of only 16% and the subsequent phase II was limited due to side effects such as ocular toxicity [40]. Many of these trials have not met expected endpoints, but a better understanding of HSP90's mode of action may help to develop superior drugs.

1.4.4 HSP90 structure, function and isoforms

The heat-shock response was first discovered by Ferruccio Ritossa in 1962, when by chance, an accidental increase in temperature of an incubator led to an unusual pattern in the puffs of *Drosophila* salivary glands and rapid RNA synthesis [41-44]. Later work identified a 90kDa protein which coprecipitated with the v-src protein from the Rous Sarcoma virus, more of which coprecipitated at higher temperatures, later identified as HSP90 [45, 46]. Ritossa's inaugural work led to the discovery of multiple classes of heat shock proteins (HSPs), the nomenclature of which has recently been standardised taking into account their molecular weights: HSP100, HSP90, HSP70, HSP60, HSP40 and smaller heat shock proteins such as HSP27 [47, 48]. Heat shock proteins constitute a group of molecular chaperones that work cooperatively in a dynamic process to ensure correct folding and therefore function of cellular proteins. They play a role in intracellular protein positioning, ligand binding and phosphorylation, prevention of aggregate formation and regulates ubiquitin-mediated proteasomal degradation [49].

The ATP-ase dependent HSP90 chaperone enables the formation of meta-stable, readily activated client proteins many of which form part of proliferative signalling networks [50]. Its importance might be reflected by the fact that in normal cellular conditions HSP90 accounts for 1-2% of total protein content [49]. HSP90 consists of three conserved domains including the amino-terminal (N) domain, the middle (M) domain and the carboxy-terminal (C) domain [25]. The N domain contains an ATP binding site known as the Bergerat fold: ATP-binding delivers the resources for conformational change and protein folding [25]. The M domain harbours a charged

linker region with binding sites for ATP, HSP90 clients and co-chaperones: sansalvamide A-amide has been reported to bind to the N-middle domain, allosterically preventing binding of C-domain clients such as IP6K2 and FKBP52 [51]. The C-terminal domain contains another ATP binding site responsible for the dimerization of HSP90, which is required for the formation and function of the chaperone complex [25].

HSP90 cycles through clearly identifiable conformations freely under normal conditions, which are in dynamic equilibrium (figure 1.4-2) [52, 53]. Binding of ATP to the nucleotide binding site in the N-domain forces direction to this cycling [54]. ATP binding leads to a repositioning of amino acids in the N-domain to form a "lid" over the nucleotide binding site [55]. During this process, HSP90 is transitioned from an open "V-shaped" state to a closed conformation, when N-domains become dimerised [55]. Once in a closed conformation, the residues in the M-domain are now able to aid in forming an ATPase site, where ATP is hydrolysed releasing ADP and an inorganic phosphate, causing the HSP90 dimer to resume an open conformation [54]. However, chaperone cycling is not quite as simple as this, due to the effect of co-chaperones which can interrupt and alter the conformational cycle and help sequester specific client proteins to HSP90 [56]. In the cases of steroid hormone receptors (SHR), several distinct stages are required for correct maturation. First, sequestration to HSP90 via association with the co-chaperone HOP, which also stabilises HSP90 in the open conformation followed by the formation of an intermediate asymmetric conformation upon binding of peptidylprolyl isomerase (PPIase) [56]. Subsequent binding of ATP and p23 induce a closed conformation, and finally ATP is hydrolysed, allowing release of all co-chaperones and the mature steroid hormone receptor [56]. Structural studies, such as the crystal structure of HSP90 in complex with the co-chaperone p23 which demonstrated yeast HSP90 in a "closed" state, helped to elucidate HSP90's mechanism of action, though there is still room for refinement and a greater understanding of client recruitment and affinity [55].

The upregulation of heat-shock proteins in response to environmental stressors is known as the heat shock response. Heat shock factor 1 (HSF1), one of a number of heat shock factors, is the "master regulator" governing this response. In times of

Figure 1.4-2 *The HSP90 Chaperone cycle, obtained from Trepel et. al (2010)*

stress, monomeric HSF1 dissociates from HSP90 and HSP70, trimerises, is hyperphosphorylated and subsequently moves into the nucleus, where it binds to *cis*-acting heat shock elements (HSEs) found in or near heat shock genes to activate transcription of heat shock proteins including HSP90 [47]. The upregulation of HSP70 in response to HSP90 inhibition is likely due to loss of HSP90 sequestering HSF1, allowing it to gain transactivating ability [57, 58].

There are several members of the HSP90 family all with distinct structures and functions. Cytosolic inducible (HSP90α) and constitutively active (HSP90β) isoforms of HSP90 arose in mammals by a gene duplication event [59]. Differences in functionality are poorly understood, although it is known that the α-isoform more readily dimerises: a pre-requisite to function [49, 60]. HSP90α has been linked to invasiveness of fibrosarcoma cells via extracellular involvement with matrix metalloproteinase-2 (MMP2), and geldanamycin treatment of zebrafish embryos resulted in the loss of HSP90α-expressing muscle pioneer cells [61, 62]. Conversely, HSP90β appears to be important throughout germ cell development [63]. Hsp90α has been shown to be better at activating some Hsp90 clients, like v-Src, over Hsp90β [64]. Furthermore, PU-H71, a drug with a purine scaffold, was demonstrated to have an increased potency against Hsp90α [65]. HSP90N was previously thought to make up another cytosolic member of the HSP90 family: a 75kDa protein which replaces the N-terminal ATPase domain with a small hydrophobic sequence and binds Raf-1 with high affinity, leading to c-Ras independent MAP-kinase signalling [66]. However, Zurawska *et al.* later shed doubt on the reproducibility of the original study and suggested HSP90N was a by-product of a chromosomal translocation between chromosomes 3 and 14 [67]. HSP90 is highly conserved: for example, prokaryotic HSP90, HTPG (High Temperature Protein G), has around 40% sequence identity with the human variant, and mouse HSP90α has 99% sequence identity with human HSP90α variant 2, lacking only a single glutamic acid residue.

TNF receptor-associated protein 1 (TRAP1) is a mitochondrial-linked member of the HSP90 family of chaperones identified from a yeast two-hybrid screen [68]. TRAP1

lacks the highly charged hinge region found within the N-terminal domain of HSP90α/β isoforms and is unable to interact with HSP90 co-chaperones such as p23 or Hop: TRAP1 does however remain sensitive to inhibition with N-terminal HSP90 inhibitors such as geldanamycin [69]. TRAP1 plays an important antiapoptotic role in the mitochondria where it acts to protect against DNA damage caused by reactive oxygen species (ROS) such as hydrogen peroxide, whilst also interfering with caspase 3 [70]. It is no surprise that TRAP1 is often found overexpressed in cancers [71]. In NSCLC cell lines, loss of TRAP1 reduced mitochondrial membrane potential, ATP production and subsequent cell proliferation [72]. The same study also found high TRAP1 levels to be a prognostic factor for disease recurrence in NSCLC patients (HR: 2.554, 95% CI 1.085–6.012, p-value=0.03) [72]. Whilst this is very interesting, the drugs available for this study are not specific to TRAP1, although this could be an interesting future study.

The HSP90 homolog glucose-regulated protein 94 (GRP94) is located in the endoplasmic reticulum (ER), where it is heavily involved in protein chaperoning and maturation of clients such as MHC class II proteins, Toll-like receptors and Apo B [73]. In addition, along with other calcium sequester proteins such as calsequestrin, GRP94 has 15 calcium binding sites with low affinity for Ca^{2+} ions, allowing it to act as a calcium carrier to keep a pool of calcium ions in the sarcoplasmic reticulum [74]. It is also stated to be important for quality control of proteins to prevent misfolded and mutated proteins from maturing and it is known to bind peptides for presentation to and stimulation of T-cells [73].

1.4.5 HSP90 co-chaperones

There are multiple co-chaperones that can associate with HSP90 and which affect both the rate of HSP90 cycling and specificity of client proteins including CDC37, HOP, CNS1, p23, CPR6 and CPR7. Cell division cycle 37 homolog (CDC37) selects only protein kinase client proteins whilst stress-induced phosphoprotein 1 (STIP1) is specific for steroid hormone receptors [25]. Activator of HSP90 ATPase 1 (AHA1) is another key co-chaperone, knockdown of which has been shown to increase sensitivity to HSP90 inhibitors [75]**.** Conventionally, such co-chaperones deliver clients to HSP90 and/or alter the precise timing and conformational changes HSP90 undergoes in order to allow correct folding of specific clients**.** HSP90 client proteins interact with the M

domain of HSP90 and cochaperones transitorily as HSP90 moves between its open and closed positions [49]. In the case of protein kinase clients, HSP70 and HSP40 chaperones interact with newly translated kinases, after which both HOP and CDC37 are involved in recruiting the kinase to HSP90 and stabilising the HSP90-kinase complex [56]. Following this, AHA1 accelerates the HSP90 conformational cycle and increases HSP90 ATPase activity to allow release of a fully mature kinase proteins [56, 76]. Interestingly, proteins in the same family can have drastically different affinities with HSP90: exactly why is not clear, however a recent study suggests it is a combination of co-chaperone specificity (such as kinase recognition via the co-chaperone CDC37) and favouring interactions with thermodynamically unstable proteins [77].

Further to this, some co-chaperones are involved in HSP90's other known functions, such as the CHIP-ubiquitin ligase, which catalyses the addition of ubiquitin to client proteins in order to direct them to the proteasome for degradation and prevent further chaperone-mediated maturation [78]. Meanwhile the cochaperone protein phosphatase 5 (PP5) is able to dephosphorylate CDC37 at Ser13, preventing HSP90-CDC37 mediated maturation of protein kinase clients [79].

The HSP70 family of chaperones are comprised of several members expressed constitutively (such as HSC70) or as a response to stress (such as HSP72) [47]. They are generally involved in aiding folding of new polypeptides and in the formation of multiprotein complexes including HSP90 to deliver functional proteins [47]. The rapid induction of some HSP70 members in response to stress helps cells to cope with unfolded or mutated proteins, and this attribute is important for cancer cell survival: as a consequence, HSP70 proteins are often overexpressed in this disease state [47]. In addition, HSP70 plays a key antiapoptotic role in cancer cells via several mechanisms including: interaction with death receptors DR4 and DR5 preventing extrinsic apoptosis pathway activation [80]; binding of BAX to prevent its mitochondrial translocation and induction of mitochondrial outer membrane permeablisation (MOMP) [81] and also binding to APAF1 to prevent correct apoptosome formation thus inhibiting apoptosis [82]. It has been demonstrated that co-targeting of HSP70 family members HSC70 and HSP72 increases the efficacy of HSP90 inhibition with 17-

AAG including reduced proliferation, increased apoptosis and loss of HSP90 clients [83]. Like HSP70, HSP90 also plays a key role in cancer, and aids in cancer cells developing and maintaining many of the classic hallmarks of cancer [84].

1.4.6 The role of HSP90 in cancer

HSP90's ability to form meta-stable complexes is hijacked in the stressful, hypoxic and acidotic cancer microenvironment where expression of mutant, conformationally unstable oncogenic proteins leads to an increased requirement for active HSP90, which is generally upregulated in many cancers [49, 85-90]. The HSP90 interactome is vast (an updated list can be found at: http://www.picard.ch/downloads/HSP90interactors.pdf) and includes many protein kinases and transcription factors.

Therefore, HSP90's primary role in cancer is that it enables functionality of many pro-oncogenic clients responsible for multiple hallmarks of cancer [1, 91]. Pro-oncogenic signalling proteins such as BRAF, FAK, ERBB2, mutant cKIT, mutant EGFR and BCR-ABL allow for growth signal self-sufficiency [47, 92]. HSP90 helps to promote angiogenesis via its chaperoning of clients such as HIF-1α, STAT3 and VEGFR1/2 [93].

HSP90α, known to be secreted from cells to encourage angiogenesis, stabilises matrix-metalloproteinase-2 (MMP-2) via the HSP90 M-domain preventing MMP-2 degradation, ultimately allowing for MMP-2 to be secreted and aid in extracellular matrix breakdown and cancer cell migration [94]. HSP90 enables evasion of apoptosis by chaperoning anti-apoptotic proteins such as Bcl-2 and survivin [95, 96]. More directly, HSP90 inhibits apoptosis by forming a complex with apoptotic protease-activating factor-1 (APAF-1), preventing the formation of an active apoptosome via cytochrome c-mediated oligomerisation [97]. Furthermore, HSP90 binds to hexakisphosphate kinase-2 (IP6K2); constraining production of disphosphoinositol pentakisphosphate (IP7) and preventing apoptosis [98].

Cancer cell immortalisation is aided due to the interaction between HSP90 and the catalytic subunit of telomerase: telomerase reverse transcriptase (hTERT) [99]. HSP90

collaborates with its cochaperone p23 to stabilise the hTERT and RNA subunit (hTR) structure [100]. Additionally, in oral cancer cell models, HSP90 binds to the hTERT promoter region inducing hTERT expression, and this effect was abrogated by the addition of geldanamycin, however it remains unclear if this is important in other cancer subtypes [101]**.** Chaperoning of proteins involved in the cell cycle such as CDK4/6 and Cyclin D prevents susceptibility to anti-growth signalling [102]. Thus with a single HSP90 drug, it's possible to target multiple cancer hallmarks simulataneously.

Chromosomal instability has been shown to be induced by HSP90 inhibition-generated proteotoxic stress as a result of HSP90's role in kinetochore assembly: over longer periods of growth where HSP90 was inhibited this aneuploidy resulted in drug resistant cells with gain in chromosome 15 [103]. Genomic instability is controlled to a certain extent by HSP90 clients. Therefore there is a logical connection between the use of DNA damaging agents in combination with HSP90 inhibitors in order to increase the cancer cell sensitivity [27]. 17-AAG has been demonstrated to reduce CHK1 and CDC25A expression, inducing G2/M cell cycle arrest, and has also been shown to sensitise lung cancer cell lines to radiotherapy through the induction of degradation of CDC25C and CDC2 which causes cell cycle arrest [104-106].

Inhibition of HSP90 allows for rapid downregulation of several oncogenic pathways simultaneously. Lower HSP90 levels correlate with better overall survival in NSCLC, and so recent studies have investigated whether this molecule could be a therapeutic target [107-109]. HSP90 exists predominantly in a "superchaperone complex" in malignant cells, whereas it is mostly uncomplexed in normal cells, making tumour cells much more sensitive to HSP90 inhibition with 17-AAG: it was found that 17-AAG bound to HSP90 with 100-fold greater affinity in tumour cells than normal cells, and a similar effect was observed in normal and tumour samples from the breast and colon [90]. This selective sensitivity of tumour cells for HSP90 inhibitors is a potential strategy for targeting oncogenic drivers which utilise downstream signalling pathways comprised of HSP90 client proteins such as MEK, STAT3 and AKT: one such driver may be the fusion protein EML4-ALK. EML4-ALK has been identified as an exquisitely sensitive client of HSP90 and is effectively degraded in vitro with the HSP90 inhibitor 17-AAG and in xenografts with 17-DMAG: both geldanamycin derivatives [110].

Another HSP90 inhibitor IPI-504 emulated the result in NSCLC cell lines and xenografts and demonstrated dephosphorylation of key targets downstream of ALK: AKT, extracellular signal-regulated kinases 1/2 (ERK1/2) and signal transducer and activator of transcription 3 (STAT3) [111].

1.4.7 Echinoderm microtubule protein-like 4-anaplastic lymphoma kinase

Echinoderm microtubule protein-like 4-anaplastic lymphoma kinase (EML4-ALK) fusions have been some of the most intensely studied driver oncogenes, and are known clients of HSP90: "clients" refers to groups of substrates which interact with and utilise HSP90 in their maturation. Anaplastic lymphoma kinase (ALK) was originally identified in a truncated form; fused to the RNA-binding protein nucleophosmin (NPM) in t(2:5) rearranged anaplastic large-cell non-Hodgkins lymphoma [112]. The transforming capability of this chimeric protein was shown to be twofold. First the kinase function of the ALK portion was shown to be essential to transformation with ALK-truncated mutants and second, a full NPM region is required for NPM-ALK oligomerisation and oncogenesis [113]. This observation led to further characterisation of full length ALK: a 1620 amino acid receptor tyrosine kinase related to the insulin receptor subfamily of tyrosine kinases [114]. ALK is not normally expressed in the lung and seems to be more prominent in the brain and nervous system particularly during development [114]. Its normal function is not well understood, although it has been linked to adult neuronal tissue repair, behaviour, memory and fertility [115].

In 2007 Soda et. al. identified two variants of an oncogene formed from a fusion of the intracellular kinase domain of ALK to two differently truncated echinoderm microtubule-associated protein-like 4 (EML4) variants in non-small cell lung cancer patients [116]. Subsequent studies have identified multiple locations of the chromosome 2p inversion, leading to alternate truncations of EML4: around 11 EML4-ALK variants have now been described [116-128]. Alternative fusion partners of ALK have also been observed including KIF5b (kinesin-1 heavy chain) and TFG (TRK-fused gene) [129, 130]. In most of these variants the intracellular tyrosine kinase domain of ALK, beginning at exon 20, is conserved [128]. Two of the most common variants are variant 1 (E13;A20 – representing the exon breakpoint in EML4 that is joined to exon

20 of ALK) and variant 3a/b (E6a/b;A20); together these account for around 60% of ALK positive tumours [116, 117, 128]. EML4-ALK positive tumours as a whole now account for around 4-7% of non-squamous cases: this still accounts for approximately 40,000 EML4-ALK positive cases being diagnosed every year [131-133].

The fusion of EML4 to ALK results in the transformation of a the transmembrane ALK receptor into a stabilised cytoplasmic fusion protein, with constitutively activated mitogenic tyrosine kinase function [3]. Oligomerisation via EML4's coiled-coil domain most likely promotes stability of the oncoprotein [116] and autonomous activation of multiple pro-survival and growth pathways including the AKT, MEK/ERK and JAK/STAT pathways [111, 117, 134]. Targeting EML4-ALK directly could yield therapeutic advantages. Indeed, inhibition of EML4-ALK in addicted cell lines such as NCI-H3122 leads to increased expression of the pro-apoptotic BH3-only protein BIM and apoptosis induction [135]. In 2010 Kwak et. al demonstrated significant efficacy of the ALK inhibitor crizotinib in ALK-positive patients: an overall response rate of 55% was achieved, which is a great improvement compared with an average response rate of 10% with standard second line chemotherapy [136, 137]. A phase I study demonstrated a 60·8% objective response rate (95% CI 52·3-68·9), including three complete responses and 84 partial responses in ALK-positive patients [19]. However, most tumours treated with crizotinib will select for resistance over time and patients relapse within 12 months [20].

Multiple resistance mechanisms have been reported against the tyrosine kinase inhibitor crizotinib. The first study published in 2010 demonstrated two mutations in the ALK kinase domain within cells isolated from a relapsed patient treated with crizotinib: C1156Y and L1196M "gatekeeper mutations" which flank both sides of the ATP binding site [138]. These mutations were shown to induce increased resistance to crizotinib and an inability of the drug to dephosphorylate ALK [138]. This is similar to other gatekeeper mutations such as the canonical T790M mutation of EGFR resistance mutation in response to EGFR inhibition. Further suggested resistance mechanisms include: multiple gatekeeper mutations in ALK, microenvironment-secreted ligands such as epidermal growth factor (EGF) or hepatocyte growth factor (HGF) enabling bypass of ALK signalling, ALK copy number gain and coactivation of other oncogenic

drivers such as EGFR or KRAS [20, 139-141]. This indicates alternative populations within the EML4-ALK patient background which will require new treatment strategies. These resistance mechanisms ultimately increase pro-survival signalling pathways and prevent initiation of cell death mechanisms such as apoptosis. An additional complication has been identified in that crizotinib has low penetration into the cerebral-spinal fluid (CSF), which negatively affects the drug's performance in brain-metastasised adenocarcinoma [142, 143]. Next generation ALK inhibitors such as ceritinib and alectinib are in development in order to circumvent some of these issues, due to their higher affinity for EML4-ALK and better CNS penetration [3]. The ASCEND-1 trial (NCT01283516) of ceritinib in EML4-ALK positive patients reported a median overall response rate (ORR) of 58% [144]. The phase I/II AF-001JP trial of alectinib in crizotinib-resistant patients reported over a 90% response rate in a phase I study, and much higher CNS penetration [145, 146]. Response to ALK inhibitors is not always simple or predictable: one recent study revealed that a crizotinib-resistant patient became resensitised to crizotinib after treatment with the third generation ALK inhibitor lorlatinib due to the development of the lorlatinib-resistant mutation L1198F which surprisingly augments crizotinib binding [147]. Targeting gene-level driver mutations like EML4-ALK with HSP90 inhibitors is another promising strategy for treatment of NSCLC patients, as it could circumvent common resistance mechanisms to ALK inhibitor therapy such as gatekeeper mutations and upregulation of bypass pathways such as EGFR, due to its pleiotropic mode of action and downregulation of pro-survival, pro-proliferative signalling pathways after inhibition of HSP90.

1.4.7.1 Ganetespib

Ganetespib (also known as STA-9090, fig.4) is a small, triazolone-containing inhibitor of HSP90's N-domain ATP binding region [31]. X-ray crystallography data of ganetespib bound to this region, with the HSP90 N-terminal region in a closed conformation, revealed a more tightly bound interaction due to increased hydrogen bonding than earlier HSP90 inhibitors [31] In contrast to 17-Dimethylaminoethylamino-17-demethoxygeldanamycin (17-DMAG), treatment of rats with high doses of ganetespib does not raise serum levels of the transaminases aspartate aminotransferase (AST) and alanine aminotransferase (ALT), suggesting reduced hepatoxicity of this drug. The

same study demonstrated improved potency and tumour penetration of ganetespib against geldanamycin derivatives [31]. As a result, ganetespib has entered several clinical trials for lung cancers (table 1.4-1),

Study	Drug	Phase	Status
NCT01348126	Ganetespib/docetaxel	II/III	Terminated
NCT01031225	Ganetespib	II	Completed
NCT01562015	Ganetespib	II	Completed
NCT01798485	Ganetespib/docetaxel	III	Terminated
NCT02192541	Ganetespib/Ziv-Aflibercept	I	Recruiting
NCT01579994	Ganetespib/crizotinib	I	Active, not recruiting

Table 1.4-1 *Table of clinical trials involving ganetespib in NSCLC*

Ganetespib, like other HSP90 inhibitors, has been shown to enable degradation of EML4-ALK and depletes cells of multiple oncogenic signalling proteins including EGFR, MET, AKT in addition to dephosphorylation of both STAT3 and ERK [38]. This makes it a promising strategy; allowing simultaneous downregulation of multiple prosurvival pathways and activation of cell death mechanisms. Little work has been conducted on looking at surrogate PD markers such as looking at HSP90 client targets such as CDK4 throughout tumour biopsies pre and post drug. However, the limited PK-PD work performed on early HSP90 inhibitors like 17-AAG did not help it to remain in the clinic: a more comprehensive approach is needed [148]. Angiogenesis is another key hallmark of cancer, and colorectal cancer (CRC) models treated with ganetespib demonstrated decreased angiogenic activity related to a reduction in hypoxia-inducible factor-1 alpha (HIF-1α) and STAT3 expression levels [149]. The same group found that ganetespib represses epithelial to mesenchymal transition, motility and invasive behaviour [150].

Ganetespib has demonstrated synergy with several other targeted agents and chemotherapies. The MET-kinase inhibitor crizotinib is redundant in MET-kinase domain mutated cells, however mutated MET remains dependent on HSP90 for proper functionality, and *in vitro* experiments combining crizotinib and ganetespib in MET-driven models have demonstrated significant synergy and dephosphorylation of key downstream effectors AKT and ERK1/2 [151]. Focal adhesion kinase (FAK) mediates cell adhesion and polarity but it also is involved in cell survival via downstream signalling to the prosurvival AKT pathway. Combination of ganetespib with the FAK inhibitor PF-573228 resulted in reduced IC50 values, loss of AKT-pathway activity and induction of caspase-3 cleavage [152]. Ganetespib has been shown to sensitise cells to 5FU and doxorubicin chemotherapies and interestingly, in lung adenocarcinoma cell lines and xenografts, was able to induce radiosensitisation [150, 153, 154]. Importantly, ganetespib exhibited significant synergism with docetaxel in non-small cell lung cancer cell lines and reduced tumour volume with concurrent higher apoptosis in xenografts: this data helped to initialise clinical trials for non-small cell lung cancer patients [155].

1.4.8 Mechanisms determining response to HSP90 inhibitors

HSP90 inhibitors are not effective in every patient and multiple molecular mechanisms leading to increased resistance or sensitivity have been proposed to explain this.

Mutations in human or yeast HSP90 have been reported to enhance or inhibit HSP90 ATPase activity, depending on how they affect ATP-lid closure and HSP90 dimerisation [156]. However, to date no activating mutations have been reported to induce resistance to HSP90 inhibitors in humans, likely because mutations that affect inhibitor-binding would also prevent ATP-binding [156]. Nevertheless, *Humicola fuscoatra,* a fungus which produces the HSP90 inhibitor radicicol, possesses the amino acid isoleucine at position 33, where a leucine residue normally resides; this results in a slight increase in the size of the hydrophobic pocket, causing an increased hydration state of radicicol [157]. Consequently, *H. fuscoatra* benefits from a reduced affinity for radicicol at the ATP-binding site of HSP90 and is resistant to the inhibitor's effects [157]. A similar outcome has been observed for geldanamycin in *Streptomyces hygroscopicus* [158]. Thus, the prospect of a mutation in mammalian HSP90 which confers resistance to N-terminal inhibitors cannot be ruled out.

HSP90 undergoes several post-translational modifications which alter its function and binding of clients such as phosphorylation, S-nitrosylation and acetylation [25]. In the yeast *Saccharomyces cerevisiae,* mutations in key lysine deacetylases (KDACs) Hda1 and Rpd3 confer increased sensitivity to HSP90 inhibition with geldanamycin [159]. Furthermore, inhibition of the histone deacetylase HDAC6 in human leukemic cell line models has been shown to cause hyperacetylation of HSP90 with a higher affinity for 17-AAG: greater degradation of HSP90 clients and reduced clonogenic survival results from this combination approach [160].

It is unknown if HSP90 amplification itself translates into resistance to HSP90 inhibition. The Broad Institute screen of "Copy Number Alterations Across Multiple Cancer Types" suggests amplification of HSP90AB1, which codes for the HSP90β isoform, is observed across all cancer types, although significant recurrence is seen only in lung, hepatocellular and ovarian cancers [161]. Further, in a study of 481 breast

cancer samples, HSP90AA1 and HSP90AB1 amplifications were markers of poor prognosis in HER2 negative breast cancer [162].

The drug efflux pump P-glycoprotein (P-gp) has been linked to resistance to 17-AAG, and 17-DMAG [163-165]. However, one study suggested silencing of HSP27 or HSP70, both upregulated in response to HSP90 inhibition, completely abolished the effect of overexpressed P-gp, and therefore its role in resistance is downgraded [165]. HSP90 had previously been linked to P-gp when it was demonstrated that HSP90beta stabilises P-gp, and knockdown of HSP90beta and p-gp synergistically increases doxorubicin sensitivity in resistant cells [166].

The quinone-metabolising enzyme NAD(P)H:quinone oxidoreductase 1 (NQO1) metabolises the ansamycin family of HSP90 inhibitors including geldanamycin, 17-AAG and 17-DMAG into more potent hydroquinone forms [167, 168]. Reduced NQO1 results in decreased sensitivity to this class of inhibitors [163, 168]**.** Another metabolic mechanism of resistance involves the uridine-5'-diphosphate glucuronosyltransferase 1A (UGT1A) family. These are normally expressed in the liver from a complex locus where they catalyse the addition of UDP-glucuronic acid to small molecules which increases their solubility and aids excretion [169]. Higher expression levels of UGT1A were associated with increased resistance to ganetespib in a panel of colorectal cancer cells, and RNAi or propofol-mediated inhibition of UGT1A activity demonstrated increased sensitivity to ganetespib in intrinsically resistant colorectal and bladder cancer cells respectively [170, 171].

An upshot of HSP90 inhibition is degradation of client proteins via ubiquitination and proteasomal degradation [172]. Cullin-RING E3 ubiquitin ligase Cullin-5 (CUL5) is responsible for ubiquitination of some HSP90 clients such as ERBB2 and HIF-1α, and reduction in CUL5 causes delays in detectable loss of client activity and client degradation: the corollary is a reduction in sensitivity of cells to HSP90 inhibitors [173, 174]. Interestingly, combination of HSP90 inhibitors with a proteasome inhibitor may prove synergistic: simulataneous client inhibition and toxic build up of misfolded proteins, as in the case of PU-H71 in combination with bortezomib in Ewing's sarcoma models [175]. Further, combination of 17-AAG with bortezomib in a stage 1 trial in

multiple myeloma resulted in a 27% response rate made up of 2 complete and 8 partial responses [176].

It is thought that tumours may become resistant through de novo and/or acquired resistance mechanisms. Intratumour heterogeneity is a major factor – over 60% of somatic mutations found within renal carcinomas have been shown to be undetectable across the whole tumour mass and, furthermore, there is evidence of convergent evolution for loss of tumour suppressors such as PTEN (Phosphatase and tensin homolog) via multiple inactivating mutations [177]. Therefore, targeted therapeutic agents will tend to select for resistant subpopulations within the tumour mass, eventually rendering that drug ineffective as the resistant subpopulation becomes dominant. Whilst "drug holidays" may help to reduce the development of resistance such as has been demonstrated for crizotinib, patient tumour sequencing in combination with better drugs with high specificity and low toxicity will allow the development of novel combinatorial strategies so that resistance can be overcome [178]. However, elucidating resistance mechanisms will allow the development of new therapeutics which overcome the tumour's resistance to other targeted agents, leading to the transformation of cancer into a long-term but manageable disease.

Efforts have been made to predict resistance mechanisms to some targeted agents. For example, a study in 2011 utilised a rapid N-ethyl-N-nitrosourea (ENU) screen of Ba/F3 cells containing EML4-ALK variant 1 to identify point mutations in the ALK kinase domain under crizotinib selection pressure [139]. The authors successfully reproduced mutations that had been previously identified in patients [138]. A similar technique using NPM-ALK identified multiple point mutations in the ALK region which conferred resistance to crizotinib, however were still sensitive to HSP90 inhibition [38]. This strategy could be equally useful in predicting mutations in the ATP binding region of HSP90 which confer resistance.

Resistance can also be generated using an insertional mutagenesis approach. Gene-trap mutagenesis involves the stable insertion of a promoterless viral vector ROSAFARY into cells which randomly mutates genes [179]. Applying drug selection pressure would select for cells in the population where the mutation has occurred in a

gene important for resistance to that drug. These clones can then be screened by sequencing or microarray analysis. A similar retrotransposon "Slingshot" is able to look at the role of both gain and loss of function mutations in drug resistance [180].

Furthermore, the Sanger "Genomics of Drug Sensitivity" project has screened many drugs across thousands of cell lines, and then looked for common genetic changes that confer sensitivity or resistance to a particular drug. The geldanamycin derivative HSP90 inhibitor 17-AAG is featured in this screen (Fig 3.). Mutations in the tumour suppressor PTEN and the cyclin-dependent kinase inhibitor 2A (CDKN2A) confer sensitivity whilst ALK mutations confer resistance to 17-AAG 17-N-allylamino-17-demethoxygeldanamycin) [181]. These data may be useful for understanding genetic alterations affecting sensitivity and resistance to the next generation HSP90 inhibitor ganetespib.

1.5 Copy number variation

Gene-level mutations have been shown to drive many cases of NSCLC, however there remains a large proportion of patients where the driving factors are unknown. Somatic copy number alterations (CNAs) as putative drivers or biomarkers in lung cancer remain poorly understood in general and no data is available in relation to HSP90 inhibitors.

Copy number variation (CNV) is part of a group of genomic structural changes including rearrangements, indels, translocations and inversions [182]. A CNV is defined as a DNA segment of 1kb or greater which has increased (insertion/duplication/gain) or decreased (loss/deletion) copies compared to a reference genome [182]. Around 0.8% of the human genome differs in terms of copy number between any two people in normal conditions [183, 184]. Copy number variation does correlate with gene expression levels in several studies, although it is far from a complete correlation, with one study finding CNVs responsible for only 17.7% of gene expression variation [185] . Other work has suggested copy number change for around 5% of genes is correlated with changes in gene expression via a

dosage effect (more/less copies) [182]. Individuals with trisomy 21 display phenotypes associated with Down syndrome, however 56% of genes on chromosome 21 show no increase in expression levels from receipt of an extra chromosomal copy [186, 187].

1.5.1 Mechanisms of copy number change

CNVs can be generated via mechanisms such as non-allelic homologous recombination (NAHR) or non-homologous end-joining (NHEJ) [188]. Additionally, DNA replication-based mechanisms have been noted to be responsible for genomic structural variation. These include processes such as fork stalling template switching (FoSTeS), microhomology mediated break-induced repair (MMBIR) and breakage-fusion-bridge (BFB) cycles [188]. Furthermore, catastrophic large-scale genomic rearrangements have been identified in disease genomes via a mechanism dubbed chromothripsis, allowing for multiple potentially pathogenic rearrangements to occur at once [189]. This process has recently been shown to produce an EML4-ALK fusion (normally formed via inversion) in a NSCLC patient-derived cell line [190].

CNVs can lead to complex phenotypes rather than just a simple gene-dosage effect, where gene copy number is proportional to expression and protein level. In fact, for a small percentage of genes, a significant negative correlation between copy number and gene expression has been suggested [183]. Copy number gains may occur where the breakage point falls within part of a gene, causing disruption and leading to a reduced expression level of the relevant protein: this can lead to a haploinsufficiency where not enough protein is produced to maintain normal functionality [191]. In patients with spastic paraplegia type 2, a duplication event downstream of the PLP1 gene was postulated to negatively regulate the expression of PLP1, phenocopying a direct PLP1 mutation [192].

Conversely, loss in a region containing transcriptional repressor elements could lead to increased gene expression [191]. Unexpected phenotypic effects can also be produced by compound heterozygosity (where recessive alleles are revealed) [182]. Further still, gene-dosage compensatory mechanisms have been described, such as the Xist transcript, which overlays one of the X-chromosomes in female mammals, rendering it inactive [186].

An early example of copy number alteration described in humans was an additional copy of the haemoglobin A (HBA) gene, which appears to have no phenotypic effect, whereas a loss causes α-thalassemia due to reduced haemoglobin levels [186]. Many developmental diseases have now been associated with copy number changes such as Prader-Willi syndrome, Gorlin-Goltz syndrome (PTCH1 deletion leading to basal cell carcinoma) and famously deletion in RB1 which gives rise to retinoblastoma. However recently there has been more interest in the role genomic instability, and copy number change in particular, plays in cancer [191, 193].

1.5.2 Somatic copy number alteration in cancer

Enhanced genomic instability through mechanisms such as reactive oxygen species (ROS)-induced DNA damage, acidosis-generated chromosomal breaks, telomere damage and centrosome amplification leads to an increase in somatic copy number alteration (SCNA) within cancer cells [194, 195]. In 2010 Beroukhim and colleagues published copy number data from over 3000 cancer samples spanning 26 histologies and found 158 focal SCNAs (<1 chromosomal arm) to be significantly altered [196]. This study found that any one tumour sample compared to a normal sample on average had more genomic amplifications (17% vs 0.35%) and deletions (16% vs 0.1%), with NSCLC tumours exhibiting around 50 SCNAs on average [196]. Members of the BCL2 family of anti-apoptotic proteins were particularly enriched across multiple cancer types: MCL-1 was amplified in 83% of lung cancer specimens, when inclusive of high and low-level amplification and 1q polysomy [196]. Specific knowledge such as this regarding copy number alteration in cancer allows for development of therapeutic strategies.

Patients with amplification of HER2 in breast cancer can be targeted with the monoclonal antibody Herceptin (Trastuzumab), which blockades the HER2 receptor, induces a cytotoxic immune response, reduces HER2 shedding and prevents downstream MAPK and PI3K pathway signalling [197]. Response rates upwards of 50% were reported when combined with taxanes [198]. EGFR is amplified in approximately 9% of advanced NSCLC cases: along with an increase in phosphorylated, activated EGFR, amplification could represent a “bypass” mechanism of resistance to crizotinib in EML4-ALK positive patients, and may be targetable [199, 200]. Combining targeted

therapies to overcome such a bypass mechanism may be a successful strategy, however there are several unknown variables to be investigated such as possible increased toxicity, or a complex and unexpected drug interaction across complex signalling pathway networks [201]. Focal amplification of FGFR1 in around 20% of squamous cell carcinomas of the lung may be a marker of poor prognosis, however specific inhibitors are in development for this marker [202]. MET amplification has been observed as a mechanism of resistance MET antibody and may additionally aid resistance to EGFR inhibitors [203, 204].

SCNAs can be prognostic: MYCN amplification in neuroblastoma is a classic example of a gene amplification event bestowing a poor prognosis [205]. Homozygous deletion of the tumour suppressor CDKN2A is a very common event in NSCLC (around 50%) and mesothelioma (75%), which leads to unchecked CDK4 activity, phosphorylation of pRb and cell cycle progression: CDKN2A is a marker of a more aggressive phenotype and represents a poor prognosis for mesothelioma patients definitively, and possibly NSCLC patients too [206, 207].

Furthermore, in a meta-analysis of 9 studies of NSCLC patient cohorts, an increase in MET copy number was a predictor for worse outcome, although this effect was only significant when studies were grouped which featured mainly adenocarcinoma patients [208]. PTEN loss and PIK3CA gain have also been cited as markers of poor outcome for NSCLC patients treated with gefitinib [209]. Clearly, copy number status has a key and unexplored role to play in understanding therapeutic response.

1.3.1.1 SCNAs and resistance to therapeutics

It is well documented that patients with amplifications in DHFR, thymidylate synthase (TYMS) and BCR-ABL exhibit resistance to methotrexate, 5-fluorouracil (5-FU) and Imatinib respectively [210-213]. In NSCLC, copy number change is associated with resistance to different drugs for several genes such as ALK, EGFR, MET and VEGFR2. It is now possible to understand distinct regional copy number changes over time, and significant intratumour heterogeneity has been demonstrated for renal carcinoma [177]. Similarly, NSCLC tumours display temporal and spatial heterogeneity in terms of copy number changes [214]**.** In a study of 7 NSCLC patients, 4 had whole genome

doublings, and some displayed intratumoral heterogeneity for recurrent copy number changes such as PTEN and CDKN2A loss [214]. Further still, intratumoral heterogeneity for known driver mutations was observed [214]. Combined with the fact that somatic copy number alterations can affect multiple genes at once, often in complex ways, there is need for a drug strategy which affects multiple pro-oncogenic signalling pathways simultaneously. This is where a "network drug", such as HSP90 inhibitors, which negatively regulate many pro-oncogenic signalling pathways simultaneously, could prove useful. However, the most powerful clinical trials recently in NSCLC have all been focused on immunotherapy approaches.

1.6 Immunotherapy and NSCLC

Immunotherapy refers to a wide range of therapeutics with the intention of activating or reactivating the immune response in order to destroy cancer cells. One type of immunotherapy is antitumour vaccines, which uses immunogenic tumour-related antigens with an adjuvant to activate the normal immune response. In a phase III trial (known as START) of the vaccine tecetomide (which contains exposed mucin1 core expressed by over 80% of lung adenocarcinomas), in the second line setting, patients who previously received sequential chemoradiosensitivity achieved an improved median overall survival (30.8 vs. 20.6 months, P=0.012) [215]. However, probably the biggest success story of immunotherapy in NSCLC so far has been with checkpoint inhibitors.

Ipilimumab, an anti-cytotoxic lymphocyte antigen 4 (CTLA-4) antibody utilises the idea that tumour cell death releases antigens which can be taken advantage of to boost the immune response to tumour cells. A randomised phase II study of ipilimumab in conjuction with standard chemotherapy produced a marked overall response rate for patients treated with ipilimumab and chemotherapy against chemotherapy alone (32% vs 18%) [216]. Phase III trials are under way.

The anti-PD-1 inhibitor nivolumab was assessed in a phase III trial (Checkmate 017) of patients with squamous histologies in the second line setting versus standard docetaxel alone [217]. Median overall survival significantly increased by 3.2 months (9.2 vs. 6.0 months, P<0.001), leading to rapid approval of this drug by the FDA in

squamous NSCLC in the second line setting. Work is also ongoing on PD-L1 antibodies such as atezolizumab which may boast a more positive toxicity profile due to blockade of PD-1/PDL-2 interaction. This drug in a phase one (POPLAR) trial achieved a 100% ORR in PD-L1 positive patients. In a phase III trial,in the second and third line setting, overall survival was greater for the atezolizumab arm (11.5 vs. 9.5 months, HR=0.77, P=0.11) however this did not reach significance [218].

Chapter 2 – Materials and Methods

2 Materials and Methods

2.1 Safety

A class II microbiological safety cabinet was used for all cell culture operations. Solid waste was disinfected with 1000ppm Presept® (Thermo Fisher Scientific, Waltham, MA, USA) then autoclaved at 132°C for 15 minutes before incineration. Liquid waste was treated with 1000ppm Presept® overnight. No glassware was used in cell culture experiments. Spillages were cleared up with paper towels or a spill kit and disinfected with Presept® before disposal. Surfaces were additionally wiped down with 70% industrial methylated spirit. A COSHH risk assessment was carried out for each procedure, considering the risks of every substance used and manual handling procedures. Genetically modified application forms were completed to assess risk of using specified microorganisms and the intended genetic modifications and were approved by the MRC Toxicology Unit Biological Safety Committee.

2.2 Cell culture

2.3 Materials

Tissue culture flasks (T25, T75, T175), serological pipettes (1, 5, 10, 25mL), 2mL cryotubes and multi-well plates (6, 12, 24, 96 well) were purchased from Greiner Bio One Ltd (Stonehouse, UK). Falcon tubes (15 and 50mL), pipette tips (10, 20, 200, 1000 µl) and 1.5mL Eppendorf tubes were supplied by Starlab (UK) Ltd (Milton Keynes, UK). P60 and P90 plates were obtained from Thermo Fisher Scientific (Waltham, MA USA).

2.3.1 Cell lines

Wild type mouse embryonic fibroblasts (MEF) cells were a kind gift from Dr Scott Oakes (UCSF, San Francisco, CA, USA). NCI-H2228 cells were provided by Dr Stephen Gray (Institute of Molecular Medicine, St James's Hospital, Dublin, Ireland) at passage 27; Interleukin-3 (IL-3) dependent Ba/F3 cells were provided by Professor Martin Dyer (MRC Toxicology Unit, Leicester, UK) at passage 12. NCI-H3122 cells were obtained from the NCI Tumor Repository (Frederick, MD, USA). Non-small cell lung cancer cell line NCI-H460 was a kind gift from the Drug Resistance Group (CCRCB, Queen's

University Belfast, UK). NSCLC cell line Calu-3 was a kind gift from Dr Gavin Morris (University of Nottingham, Nottingham, UK) passage 30. Mesothelioma cell lines MSTO and NCI-H28 were purchased from ATCC (Middlesex, UK). Cell line authentication is currently underway in the lab for all cell lines, but it is important to note MEF, H460, H28 and MSTO cell lines may be at high passage, and ideally should be compared against newer, low passage cell lines.

2.3.2 Mycoplasma testing

Cells were tested every 1-2 months for the presence of mycoplasma by polymerase chain reaction (PCR). Cells in exponential growth phase were cultured for 48-72 hours and 1mL media was subsequently extracted, boiled at 100^{o}C for 10 minutes and 2µl used in a PCR reaction with primers (Sigma-Aldrich, Gillingham, Dorset, UK) Myco-FW (5'-ACTCCTACGGGAGGCAGCAGTA-3') and Myco-RV (5'-TGCACCATCTGTCACTCTGTTAACCTC-3') and the following conditions: 95^{o}C for 2 minutes, followed by 35 cycles of 95^{o}C 30s, 56^{o}C 30s, 72^{o}C 45s, plus an extra 10 minutes at 72^{o}C. Samples were held at 4^{o}C before running on a 2% agarose gel with 1kb ladder (Invitrogen, Thermo Fisher Scientific). The presence of a band around 800bp constituted a positive result. Cells found to be positive were either disposed of or treated with Plasmocure^{TM} (InvivoGen, San Diego, CA, USA) and retested regularly.

2.3.3 Growth media

All cells were cultured in Roswell Park Memorial Institute (RPMI) medium 1640, 2mM Glutamax and 10% Foetal Calf Serum (FCS) (Gibco, Thermo Fisher Scientific). Ba/F3 cells were additionally supplemented with 10% WEHI-3b conditioned media as a source of IL-3 until after electroporation (WEHI-3b cells obtained from Cell Lines Service, Eppelheim, Germany). 250ug/mL Hygromycin B (Invitrogen, Thermo Fisher Scientific) was added to Ba/F3 –EML4-ALK transfected cells.

2.3.4 Cell line maintenance

Cell lines were kept in exponential growth phase in T25, T75 or T175 flasks at 37^{o}C/5% CO_2 in humidified incubators (Thermo Fisher Scientific). Suspension cell lines (Ba/F3) were inspected daily and prevented from reaching confluence by 1:10 – 1:100 dilutions with appropriate media. Adhesive cell lines were allowed to grow to

approximately 80% confluence and subsequently passaged: media was removed, cells were washed with 1x phosphate buffered saline (PBS) and cells were incubated at 37^{o}C with 1x trypsin/EDTA (Gibco, Thermo Fisher Scientific) for up to 15 minutes until cellular detachment. Trypsin was inactivated with fresh media containing FCS and sub-cultured at a cell line appropriate ratio.

2.3.5 Freezing cell lines

Cells were allowed to reach 80% confluency in T175 flasks before media was removed, cells washed with 1x PBS and trypsinised (if appropriate) with 1x trypsin/EDTA. 10mL fresh medium was added and cells were pelleted by spinning down for 5 minutes at 200x*g*. Cells were then resuspended in 10-15mL freezing medium containing 70% RPMI, 20% FCS, and 10% DMSO (Sigma-Aldrich). 1mL aliquots were transferred to cryotubes and placed into a Cryo 1^{o}C Freezing Container, "Mr Frosty" (Nalgene, Rochester, NY, USA) and stored overnight at -80^{o}C. Frozen aliquots were then transferred to liquid nitrogen (BOC Ltd., Surrey, UK) for long term storage.

2.3.6 Thawing of frozen cell lines

Frozen cells in cryotubes were removed from liquid nitrogen and quickly thawed in a water bath at 37^{o}C. Thawed cells were transferred to 10mL pre-warmed appropriate media, and spun at 200x*g* for 3 minutes. Media was removed and pelleted cells were gently resuspended in RPMI with 20% FCS, 2mM Glutamax, transferred to a T25 flask and left in an incubator overnight. The following day, cells were washed with 1x PBS and fresh media added with standard 10% FCS to remove any remaining traces of DMSO. Upon 80% confluence cells were transferred to a T75 flask.

2.3.7 Cell counts

100µl of resuspended cells were added to 10mL isoton (Beckman Coulter, Buckinghamshire, UK) in duplicate, mixed by inversion and cell numbers counted with a CASY Model TT Cell Counter and Analyser (Innovatis, Roche, West Sussex, UK).

2.4 Small-molecule inhibitors

Ganetespib (STA-9090) was a kind gift from Synta Pharmaceuticals (Lexington, MA, USA). Bortezomib (Velcade®) was from Millennium Pharmaceuticals (Cambridge MA,

USA). Crizotinib (Xalkori®) was a kind gift from Dr Sandra Van Schaeybroeck (CCRCB, Queen's University Belfast, UK). PU-H71 and Radicicol were purchased from R & D Systems Europe Ltd (Bio-Techne, Abingdon, UK). 17-N-allylamino-17-demethoxygeldanamycin (17-AAG/Tanespimycin) was purchased from Stratech Scientific Ltd (Suffolk, UK). ABT-737 was provided by Abbot (Abbot Park, IL, USA). Curcumin was a kind gift from Professor Karen Brown (University of Leicester, Leicester, UK). All powders were dissolved in DMSO to stock concentrations of 5 or 10mM, aliquoted and stored at -20^{o}C or -80^{o}C according to manufacturer recommendations. Stock concentrations were diluted to working concentrations with appropriate media before use. Aliquots did not go through more than 5 freeze-thaw cycles. Light sensitive drugs including Bortezomib, PU-H71, 17-AAG and ABT-737 were kept in the dark.

2.5 Selection of ganetespib-resistant Ba/F3-EML4-ALK variant 1 cells with ENU-mutagenesis

2x10^{6} Ba/F3 cells stably transfected with YFP-tagged EML4-ALK variant 1 were seeded in a T25 flask with complete media containing 100µg/ml ENU (Sigma-Aldrich) for 24 hours. Cells were subsequently washed 3 times with media and once with 1x PBS and allowed to settle for 24 hours. Cells were then exposed to a high dose of ganetespib for 24 hours: 200, 500 or 1000nM. Remaining cells were then washed with RPMI and replated in 96-well plates. Any proliferating colonies were grown up to sufficient numbers and then drugged again in the above fashion. Potentially resistant clones were brought up and tested by viability assay, caspase assay and western blot against an isogenic parental control.

2.6 Preparation of plasmid DNA for transfection

2.6.1 Transformation of E.coli with plasmid DNA

One vial of One Shot® TOP10 chemically competent *E.coli* cells per plasmid were thawed on ice. 1-5µl of DNA (around 50ng) was added to each vial, mixed gently and left on ice for 30 minutes. The cells were then heat-shocked for 30 seconds at 42^{o}C and placed on ice for 2 minutes. 250µl of pre-warmed S.O.C medium was added to

each vial which was then shaken horizontally at 225rpm for 1 hour at 37°C. 50-100µl of transformed mixture was aseptically spread on a pre-warmed LB agar plate containing 50µg/mL ampicillin, allowed to dry and then inverted and incubated for 16 hours overnight at 37°C. The following day, one colony per plasmid was picked and placed in 200mL LB Broth with ampicillin (100µg/mL) and shaken at 225 rpm horizontally overnight at 37°C.

2.6.2 Purification and extraction of plasmid DNA

Plasmid DNA was extracted and purified using the Qiagen Plasmid Maxi Kit (Qiagen, Limburg, Netherlands) according to manufacturer's instructions and quantified on a Nanodrop 2000 (Thermo Fisher Scientific).

2.7 Transfections

2.7.1 Transient overexpression of plasmid DNA

MEF or NCI-H3122 cells were transiently transfected with YFP-empty vector, YFP-cytoplasmic ALK or YFP-Fused EML4-ALK variants as indicated by using the X-tremeGENE HP DNA transfection reagent (Roche) according to manufacturer's instructions. Briefly, cells were seeded in 6-well plates at 150-300,000 cells/well and allowed to adhere overnight. The following day 1µg of DNA was added to 100µl OPTIMEM media (Gibco) and mixed gently. 3µl of X-tremeGENE HP DNA transfection reagent was added directly to the diluted DNA, mixed gently, and incubated for 15 minutes at room temperature. Media was replaced on adherent cells before adding the transfection mixture dropwise and gently swirling the plates. Cells were incubated for 24 hours before checking for YFP expression on a fluorescent microscope: Axiovert 135 (Zeiss, Cambridgeshire, UK) with X-cite 120 excitation lamp (Excelitas Technologies, Waltham, MA, USA).

2.7.2 Generation of stable Ba/F3-EML4-ALK cell lines

Ba/F3 cells were electroporated with the Amaxa® Cell Line Nucleofector® Kit V (Lonza, Verviers, Belgium) with the Nucleofector™ II Device (Lonza) according to manufacturer's instructions. Briefly, 12 well plates were prepared with 1mL media containing WEHI-3b conditioned media as a source of IL-3 and equilibrated to 37°C.

Cells were counted and $2x10^6$ cells per sample were spun down at 90x*g* for 10 minutes at room temperature. Each cell pellet was resuspended in 100µl Nucleofector® solution and combined with 2µg of DNA for EML4-ALK variants 1, 2, 3a or 5a. The mixture was then transferred to a certified cuvette ensuring no air bubbles and cells were electroporated in the Nucleofector™ II device with program X-001. 500µl of pre-equilibrated media was immediately added to each cuvette and gently transferred to one well of the 12-well plate. YFP-expression was checked after 24 hours by fluorescence. After a further 24 hours cells were resuspended in IL-3-free media with hygromycin B at 250µg/mL and diluted to single cell density in 96-well plates to select for stably-transfected cells. When colonies were of sufficient size they were transferred to 6-well plates and a sample was taken to screen for the presence of the EML4-ALK variant by SDS-page and immunoblotting. Clones with the highest expression levels were taken forward for analysis.

2.7.3 siRNA knockdown

10µM or 20µM stock siRNA was diluted in OPTIMEM in a tube, so that it would produce a final concentration in the plate as indicated (20-100nM) and mixed gently. 5µl of Lipofectamine™ RNAiMAX was added and incubated for 10-20 minutes at room temperature. This was transferred to a 6-well plate and pre-trypsinised cells in complete media added on top of the siRNA/RNAiMAX mixture so that they would be 50% confluent 24 hours later, which is the minimum amount of time cells were allowed to proliferate before further operations were conducted.

2.8 Cell viability and apoptosis assays

2.8.1 3-(4,5-dimethylthiazol-2-yl)-2,5-diphenyltetrazolium bromide (MTT) assay

Viability was measured by colorimetric assay utilising NAD(P)H-dependent reduction of 3-(4,5-dimethylthiazol-2-yl)-2,5-diphenyltetrazolium bromide (MTT) (Sigma-Aldrich) to formazan as a reflection of viable cell number. 3000-5000 cells per well were seeded in transparent 96-well plates and allowed to adhere overnight. Cells were then drugged as indicated for the specified time after which 10µl of 5mg/mL MTT was added to each well and incubated at 37°C/5% CO_2 for 2-3 hours. Media was then aspirated and insoluble formazan dye was dissolved with 50µl dimethyl sulfoxide (DMSO) (Sigma-

Aldrich) and gently rocked for 15 minutes. Absorbance measurements at 595nm for 0.1s per well were read on a Victor X4™ 2030 Multilabel Plate Reader (PerkinElmer Inc., Waltham, MA, USA).

2.8.2 CellTiter-Glo® Luminescent Cell Viability assay

Cell viability was additionally measured by quantification of ATP levels by conjugation to a luciferase reaction with the CellTiter-Glo® Luminescent Cell Viability assay (Promega, Southampton, UK). Suspension cells were plated at 5000-10000 cells per well in opaque 96-well plates and incubated with drug concentrations as indicated for the specified time. 50µl of CellTiter-Glo® solution was added directly to each well and the plate was incubated on a rocker in the dark for 10 minutes. Luminescence was measured on a on a Victor X4™ 2030 Multilabel Plate Reader with 0.1s readings.

2.8.3 Caspase-Glo® 3/7 Assay

Caspase 3/7 activity was measured using the Caspase-Glo® 3/7 assay (Promega). Cells were seeded at 3000-10000 cells per well and allowed to adhere overnight and treated the following day or treated with indicated drug immediately if suspension cells for the indicated concentrations and time. Caspase 3/7 activity was assayed according to manufacturer's instructions. The luminescent signal was read on a Victor X4™ 2030 Multilabel Plate Reader with 0.1s readings.

2.9 Clonogenic assays

Measurement of clonogenic potential of cells post treatment was assessed with crystal-violet based clonogenic methodology. Cells were seeded at 500 or 1000 cells in 24 or 12 well plates respectively and allowed to adhere overnight. The following day cells were treated with the indicated concentrations of drug for 24 hours after which cells were washed with 1x PBS and complete growth medium added. Cells were observed for up to two weeks, replenishing medium every 3 days until control wells had formed sufficient colonies. Cells were then washed with 1x PBS and fixed in ice cold methanol for 15 minutes. Cells were then stained with crystal violet (Sigma-Aldrich) for 10 minutes and washed thoroughly with running ddH_2O to remove any excess. Plates were left to dry at room temperature. Colonies containing at least 50 cells were then counted manually with a light microscope (Axiovert 135).

2.10 Protein Extraction, SDS-PAGE and Immunoblotting

2.10.1 Protein extraction from whole cell lysate

Cells were scraped into a 15ml falcon tube on ice and spun down at 2000rpm for 5 minutes at 4^{o}C. Supernatant was aspirated and the cell pellet was resuspended with 50-200µl RIPA buffer [50mM Tris pH7.4, 150mM NaCl, 5mM EDTA, 1% Triton X-100, 0.1% SDS] containing protease inhibitors (1 complete mini protease inhibitor tablet/10mL RIPA, Roche, Burgess Hill, UK) and phosphatase inhibitors (50mM NaF, 2mM Na_3VO_4). Cells were allowed to lyse on ice for 20 minutes. Insoluble cellular debris was removed (clarified) by centrifugation for 15 minutes at 13200 rpm at 4^{o}C. The supernatants were transferred to new 1.5mL tubes and samples were stored at -80^{o}C or taken forward for immediate analysis.

2.10.2 Protein quantification

Proteins were quantified using the standard BCA assay (Thermo Fisher Scientific) according to manufacturer's instructions. Briefly, a standard curve was generated using known quantities of bovine serum albumin (BSA). 5µl of each protein sample to be tested was then added to prepared BCA mix in a multiwall format and absorbance measured at 595nm on a Victor X4™ 2030 Multilabel Plate Reader with 0.1s readings. The protein levels in each sample could then be determined from the standard curve.

2.10.3 Protein sample preparation and Sodium Dodecyl Sulfate-Polyacrylamide Gel Electrophoresis (SDS-PAGE)

Lysates were thawed on ice if required and 0.25 volumes of 5x laemmli protein loading buffer was added to each sample. Proteins were subsequently denatured for 10 minutes at 95^{o}C. Resolving gels were prepared (8%, 10% or 12% acrylamide,), covered with methanol to prevent bubbles and allowed to polymerise at room temperature. Once polymerised, methanol was removed and the top of the gel was rinsed and dried before stacking gel was prepared and poured over the top. 1.5mm combs were inserted to create wells and the stacking gel was allowed to polymerise. Two gels each were then inserted into a mini-PROTEAN 3 electrophoresis apparatus (Bio-Rad, Hercules, CA, USA) and 1x running buffer added. A molecular weight protein ladder was first loaded (Fermentas, Thermo Fisher Scientific) followed by the protein samples

in the desired order in the wells. Electrophoresis was run at 80-100V until proteins were properly stacked and had entered the resolving gel, after which gels were run at 120-140V until the blue dye marking the front of the samples reached the end of the gel.

2.10.4 Protein transfer

Once proteins were separated they were transferred to 0.2µm nitrocellulose membrane (Amersham Protran, Thermo Fisher Scientific). One membrane and two pieces of Whatman® filter paper (Thermo Fisher Scientific) per gel were immersed in 1x transfer buffer and assembled in a transfer cassette so that the membrane was between the gel and the positively charged anode: this ensures the current moves the samples into the membrane. Transfer was then run in a Mini Trans-Blot Electrophoretic Transfer Cell (Bio-Rad) at 240mA for 90 minutes.

2.10.5 Immunoblotting

Membranes were immersed in 10% Ponceau/ddH_2O (Sigma-Aldrich) to ensure correct loading, run and transfer of samples and to ensure no bubbles are present. Membranes were then washed several times with 1x Tris-buffered saline/0.1% Tween-20 buffer (TBST) to remove the Ponceau stain. The membrane was subsequently blocked in 5% milk/TBST for one hour at room temperature with gentle rocking. Next, membranes were incubated with a suitable antibody over night at 4^{o}C. After this step, membranes were washed 3 separate times for 5 minutes with TBST and incubated for 1 hour at room temperature with the relevant horseradish peroxidase (HRP)-conjugated secondary antibody. Membranes were washed an additional 3 times for 5 minutes each in TBST. Antibodies used are listed in the Appendix.

2.10.6 Detection and autoradiography

Secondary antibodies which had bound to the primary antibody under investigation were detected by applying a 1:1 solution of Western Lightning Plus-ECL chemiluminescent reagent (PerkinElmer) for 5 minutes, removing excess reagent, placing the membrane between two sheets of acetate and overlaying a piece of double sided X-ray film (SLS, Hessle, UK). This film was developed and fixed with a SRX-101A medical film processor (Konica Minolta, Amsterdam, The Netherlands).

2.11 Cell cycle analysis

Media was removed from cells and transferred to a falcon tube on ice. Cells were washed with 1x PBS, trypsinised with 1x trypsin/EDTA and transferred to the appropriate tube. Cells were next spun down at 2000rpm for 5 minutes at 4^{o}C. Media was aspirated and pelleted cells were washed with 1mL ice cold 1% FCS/PBS. Cells were again spun down at 2000rpm for 5 minutes at 4^{o}C, supernatant removed, and fixed by adding 1mL ice cold ethanol (Thermo Fisher Scientific) dropwise whilst vortexing. Cells were placed at -20^{o}C overnight to ensure proper fixation. The following day, fixed cells were spun down at 2000rpm for 5 minutes at 4^{o}C and all ethanol removed. The pelleted cells were subsequently resuspended in 1% FCS/PBS and the spin down procedure repeated. After removal of supernatant, cells were resuspended in a solution of 1% FCS/PBS with 100µg/mL RNase A and 10µg/ml propidium iodide (Sigma-Aldrich) as the fluorescent intercalating agent. Resuspended cells were then transferred to 5mL BD FACS tubes (SLS) and incubated at 37^{o}C for 30 minutes to remove contaminating RNA. These were then run through the BD FACSCanto™ II (BD, Oxford, UK) with gating of the forward vs side scatter channels to remove debris, and the blue laser adjusted to the R-Phycoerythrin (PE, excitation max 496 nm/emission max 578nm) setting for the FL-2 channel to detect intercalated propidium iodide and remove doublets. 10,000 events were collected for each sample and data was analysed with BD FACSDiva 8.0 software to determine the proportion of cells in each phase of the cell cycle by DNA content.

2.12 Development of a real-time PCR-RQ approach for EML4-ALK variant phenotyping

2.12.1 Human tissue consent and storage

The CHIARA trial was performed according to the Declaration of Helsinki framework and was approved by the ethics committee at each participating institution. All patients from the CHIARA trial provided fully informed, written consent before enrolment. Samples were stored temporarily in the UK in accordance with the Human Tissue Act, with Dr Howard Pringle as named recipient with responsibility for the

tissues. At the end of the study, all samples were disposed of according to local standard operating procedures.

2.12.2 Preparation of cytoblocks

Cytoblocks were prepared of NCI-H460 as a negative control and NCI-H3122 and NCI-H2228 as positive controls for EML4-ALK variants 1 and 3 respectively. 3 x 80% confluent T175 flasks for each cell line were trypsinised, resuspended in complete media and spun down at 800rpm for 5 minutes at room temperature. All but approximately 0.5mL of supernatant was aspirated, which was used to resuspend the cell pellet. 10% formal saline (Formalin, Sigma-Aldrich) was added to a total volume of 15mL. Cells were gently but thoroughly mixed by inversion and left to fix for 3 hours. Fixed cells were centrifuged at 800rpm for 5 minutes and all formalin was removed. Approximately 1mL of cytoblock reagent 2 (Life Sciences International/Shandon Scientific Ltd, Cheshire, UK) was used to resuspend the cell pellet. Cytoblock cassettes (Life Sciences International) were prepared by applying 3 drops of cytoblock reagent 1 (Life Sciences International/Shandon Scientific Ltd) to each well and subsequently assembling the cassettes and cytofunnels (Life Sciences International) into the cytospin centrifuge clips (Shandon Scientific Ltd). 100µl of resuspended cell pellet was added to each cytofunnel and spun for 5 minutes at 1500rpm at room temperature on "Lo" acceleration. One drop of reagent 1 was added to each well and cassettes were immersed in 70% industrial methylated spirit (IMS, Thermo Fisher Scientific) prior to processing on a Leica ASP3000 overnight. Processed samples were embedded in paraffin wax and 5µm sections cut for further analysis. Sample processing, embedding, sectioning and hematoxylin and eosin (H&E) stains were performed as a service by the University of Leicester Core Biotechnology Services.

2.12.3 RNA extraction from formalin-fixed, paraffin embedded cytoblock or tissue sections

5µm sections of formalin-fixed, paraffin embedded cytoblock or patient tissue sections were dewaxed in xylene (Thermo Fisher Scientific) for 2 x 3 minutes and subject to rehydration steps: 99% IMS for 2 x 1 minute and 95% IMS for 1 x 1 minute. Sections were cleaned with running tap water for 1 minute. Once air dried, sections were scraped into 0.05M Tris pH 8/0.1% SDS buffer (Thermo Fisher Scientific), with

100ug/mL Proteinase K (Sigma-Aldrich) to enable protein digestion for 2 hours at 37°C. Samples were vortexed and cooled on ice. 1 volume of QIAzol lysis reagent (Qiagen) was added and samples were vortexed and left to stand for 5 minutes at room temperature. 0.1 volumes of chloroform (Thermo Fisher Scientific) was added, samples were vortexed and incubated for 3 minutes at room temperature before centrifugation at 13200rpm for 15 minutes at 4°C. The clean aqueous phase was transferred to a sterile tube, after which 1.25x volumes of absolute ethanol (Thermo Fisher Scientific) was added and the samples were vortexed. The remaining steps were performed with an RNeasy kit (Qiagen). Samples were applied to an RNeasy column and microfuged at 13200rpm for 15 seconds. Flow through was discarded and the column was washed with 700µl buffer RW1 and the microfugation repeated. Columns were then washed with 500µl buffer RPE and microfuged for 1x 15s and again for 1x 2 minutes. Columns were spun dry for 1 minute at 13200 rpm. Dry columns were transferred to clean eppendorfs and 30-100µl of RNase-free water added. A final spin at 13200 rpm was conducted to elute the RNA which was stored for short periods at -20°C.

2.12.4 Reverse transcription of cytoblock or FFPE tissue-extracted RNA

Given the likely low-quality RNA retrieved from FFPE samples, reverse transcription (RT) of RNA to cDNA was conducted using specific reverse transcription primers. RT primers were designed for HPRT1 and 18S endogenous control primers, as well as an RT primer in exon 20 near the breakpoint where ALK is fused to EML4. Each reaction consisted of: an RT-primer master mix containing all 3 RT primers described above to a final concentration of 1.3µM (Sigma-Aldrich); 2.6µM dNTPs (Sigma-Aldrich), 150 units Multiscribe RT enzyme (Thermo Fisher Scientific), 1x RT buffer (Thermo Fisher Scientific), 3mM MgCl2 (Thermo Fisher Scientific), 0.01 volumes RNase OUT (Thermo Fisher Scientific), 1µl nuclease free water and 6µl RNA. Next, the reverse transcription reaction was run on a GeneAmp® PCR System 9700 (Applied Biosystems, Thermo Fisher Scientific) as follows: 30 minutes at 16°C, 30 minutes at 42°C, 5 minutes at 85°C and then held at 4°C. Reactions included no RT-enzyme and no template controls.

2.12.5 Real-time polymerase chain reaction-relative quantification

In order to develop a variant specific assay from poor quality RNA, primers were designed across each EML4-ALK variant breakpoint which would produce a small amplicon of around 100-200bp. Additionally, custom Taqman® minor groove binder probes with a 6-carboxyfluorescein dye (MGB/6-FAM probes, Thermo Fisher Scientific) were designed, which take advantage of the 5' exonuclease activity of Taqman polymerase to separate the fluorochrome from the 3' quencher, allowing for fluorescence detection and production of a ΔRn value. Each reaction contained: 0.5 volumes 2 x Taqman FAST master mix (Thermo Fisher Scientific), 10pmols/µl of forward and reverse primers, 0.02 volumes 2µM MGB 6-FAM probe and 3.6µl of cDNA template diluted 1:5 to 1:10. The reaction was multiplexed to include HPRT1, 18S and two EML4-ALK variants in a 96-well plate (Applied Biosystems): this included positive and negative control cell lines during method development and, later, patient samples. A master mix without cDNA was added to each well of the plate, followed by 3.6µl diluted cDNA. MicroAmp™ Optical Adhesive Film (Applied Biosystems) was applied firmly and the plates were centrifuged at 2.5rpm for 30s, before running on the StepOne™ Plus Real-Time PCR system (Applied Biosystems) with the following parameters: 95^{o}C for 20 seconds, followed by 45 cycles of: 95^{o}C 1 second, 60^{o}C 20 seconds. A ΔRn threshold of 0.01 appeared to be sufficient to avoid noise and was used to derive cycle threshold (C_t) values for each sample.

2.13 Liquid chromatography-electrospray ionisation- tandem mass spectrometry (LC-ESI-MS/MS) for detection of ganetespib metabolites

2.13.1 Preparation of samples by acetonitrile precipitation

Cells and media were harvested and spun down for 5 minutes at 2000rpm at 4^{o}C. 500µl was removed for analysis of extracellular drug or metabolite levels. Remaining media was aspirated and the cell pellet was washed with 2mL 1x PBS. Cells were again spun down for 5 minutes at 2000rpm and 4^{o}C. PBS was removed and pelleted cells were resuspended in 100µl fresh PBS. 2 volumes of acetonitrile (Sigma-Aldrich) were

added to each sample for the pellet (200ul) and the media (1mL) on ice. Samples were vortexed for 1 minute, spun down for 15 minutes at 13200rpm and 4^{o}C. Supernatant was removed and samples were air dried and stored at -80^{o}C until needed.

2.13.2 LC-ESI-MS/MS

LC-ESI-MS/MS of ganetespib treated samples was kindly performed by Dr. Rajinder Singh (University of Leicester). The LC-ESI-MS/MS consisted of a Waters Alliance 2695 separations module with a 100 µL injection loop connected to a Micromass Quattro Ultima (Waters Ltd., Manchester, UK) tandem quadrupole mass spectrometer with an electrospray interface. The temperature of the electrospray source was maintained at 120ºC and the desolvation temperature at 350ºC. Nitrogen gas was used as the desolvation gas (700 L/h) and the cone gas was set to 25 L/h. The capillary voltage was set at 3.05 kV. The cone and hexapole ion tunnel voltages were 45 V and 0.0 V (Hex1), 1.0 V (Aperture) plus 1.0 V (Hex2), respectively. The mass spectrometer was tuned by using a ganetespib (20 pmol/µL) standard solution dissolved in 0.1% formic acid/acetonitrile (0.1% formic acid) (80:20 v/v) introduced by continuous infusion at a flow rate of 10 µL/min with a Harvard model 22 syringe pump (Havard Apparatus Ltd., Edenbridge, UK). Supernatants from pelleted cell samples were evaporated to dryness and re-dissolved in 30 µL of ultrapure water/methanol (80:20 v/v). Following centrifugation at 14,000 rpm for 10 min the supernatants were transferred to HPLC vials. A 10 µL aliquot of the sample was injected onto a HyPurity C18 (2.1 × 150 mm, 3 µm) column connected to a HyPurity C18 (2.1 × 10 mm, 3 µm) guard cartridge (Thermo Electron Corporation, Runcorn, UK) attached to KrudKatcher (5 µm) disposable pre-column filter. The column was eluted using a gradient with solvent A, 0.1% formic acid and solvent B, acetonitrile (0.1% formic acid) at a flow rate of 200 µL/min with a run time of 30 min. The following gradient was used: 0min-10%B, 2min-10%B, 14min-90%B, 17min-90%B, 17.1min 10%B, 25min-10%B and 30min-10%B. The column oven temperature was maintained at 30 ºC. The samples were analysed in positive electrospray ionization (ESI) mode with selected reaction monitoring (SRM) for the [M+H]+ ion transitions of ganetespib 365.1 to 323.0 m/z and 365.1 to 131.0 m/z, ganetespib glucuronides 541.1 to 365.1 m/z and ganetespib sulphates 445.1 to 365.1 m/z. The collision gas was argon (indicated cell pressure 2.5 × 10-3 mbar) and the

collision energy set at 30 eV. The dwell time was set to 200 ms and the resolution was 1.5 m/z units at peak base. The data was acquired using MassLynx software (Version 4.0).

2.14 Detection of recurrent somatic copy number alterations which significantly affect survival from the GALAXY-1 clinical trial

2.14.1 DNA isolation and CNA analysis

Genomic DNA was extracted from FFPE tumour samples of 212 patients and 40 samples from normal tissue. DNA (preferably over 80ng) was mixed with the molecular inversion probe (MIP) panel, aliquoted into two reactions per sample to be queried by A+T and G+C dNTP mixes. These mixes were subsequently hybridised to an Affymetrix GeneChip®, washed and scanned to generate CEL files of copy number data. Samples were genotyped, normalised by quantile normalisation and copy number values for all samples and markers generated using the algorithm described in: "Optimal genotype determination in highly multiplexed SNP data", European Journal of Human Genetics (2006) 14, 207–215. Samples were loaded into Nexus to perform initial segmentation and adjustment for GC content. All of the above was performed as a service by Affymetrix. All samples were then manually curated in Nexus to ensure no additional normalisation was required.

2.14.2 Sample filtering, quality control and data extraction

Partially processed samples were removed from the dataset. Where multiple samples existed for a patient, samples with the lowest median absolute pairwise difference (MAPD) score were retained. If they shared identical MAPD values, the sample with the greatest DNA quality was included. This "non-stringent" dataset (n=212) was further reduced by filtering out samples with a MAPD value of >0.6. MAPD is a gauge of the average difference in log2 ratio of pairwise probes for all probes across the genome and so is a measure of the noisiness of the data. This stringent dataset (n=165) was taken forward for analysis. The overall failure rate was approximately 22%. Copy number data was loaded into Nexus Express for Oncoscan and the ".ivg to .txt" function used to extract log2 ratio data compatible with the circular binary

segmentation (CBS) algorithm. Segmentation and recurrence detection strategy was decided by both myself and Dr Rob Hastings: most segmentation and recurrence detection was run either together or by Dr Hastings.

2.14.3 CNA Segmentation

The circular binary segmentation algorithm (CBS) was employed to identify regions of copy number aberration from log2 ratio data [219, 220]. Custom Perl and R scripts were generated to automate the process using the open source R package "DNAcopy" (Bioconductor, Fred Hutchinson Cancer Research Center, Seattle, WA, USA). In brief, copy number alteration (CNA) values were used to create an object which was mapped to the reference genome. The data was then smoothed (with the smooth command in DNAcopy) using default parameters to remove single-point outliers before segmentation. Smoothed data is then segmented into regions estimated to be equal in copy number using CBS with the default values as stated: alpha=0.01, nperm=10000, p.method="hybrid", "perm", min.width=2, kmax=25, nmin=200, eta=0.05, sbdry=NULL, trim=0.025, undo.splits=c("none", "prune", "sdundo"), undo.prune=0.05, undo.SD=3, verbose=1). A custom perl script was coded, available on request, to run CBS on multiple files and concatenate the output into one file suitable for running through GISTIC2 for recurrence detection.

2.14.4 Detection of recurrent CNAs

The GISTIC2 algorithm was used to detect genomic regions which are subject to significant levels of gain or loss across a group of samples [221]. Regions which had a copy number of 0.1 or more were labelled as gains, whilst large gains were determined to have a copy number greater than 0.9. Losses were called if copy number fell below -0.1, and large losses determined as less than -1.3. GISTIC2 utilised the frequency of the aberration across the population and greater weight was given to aberrations with higher amplitudes. A false discovery rate score ("q-value") was assigned; a threshold of 0.5 was used to determine significant recurrent CNAs initially, and this list was later manually curated (see Survival Analysis). Additional parameters used for the GISTIC2 algorithm are as follows: refgene=hg19 (reference genome), genegistic=1, smallmem=1, broad=1, brlen=0.5 conf=0.1, armpeel=1, savegene=1, gcm=extreme, qvt=0.5.

2.14.5 Survival analysis

Each recurrent CNA identified was used to select patients to construct sequential Kaplan-Meier curves and conduct log-rank survival analysis, with the aim to optimise curve separation. Overall survival in days was used as the survival metric. Hazard ratios produced were ranked by minimising p-value. Analysis was initially conducted with R and perl scripts with the CRAN package "survival" and the Bioconductor package "survcomp". Full scripts available on request. The results of this process were refined with Graphpad Prism 6.0 (GraphPad Software, Inc, La Jolla, CA, USA) and Microsoft Excel (Microsoft UK, Reading, UK). A cut-off of $p<=0.01$ for log-rank survival outputs and $q<=0.01$ for GISTIC q-values was used to minimise the risk of finding groups of patients which randomly separate the survival curves.

2.14.6 Random sampling and analysis of false discovery rate

Random sampling of the patient dataset to produce 10,000 survival curves was performed in R using library packages "survival" and "survMisc" using customised R code. False discovery rate analysis was conducted with FDRslim methodology.

2.14.7 Interrogation of COSMIC, CCLE and ganetespib cell line data

IC50 data for lung cancer cell lines for the HSP90 inhibitors 17-AAG, AUY922, and docetaxel, was downloaded from the Wellcome Trust Sanger Institute "Catalogue of Somatic Mutations in Cancer" (COSMIC) website. Ganetespib IC50 data on a panel of lung cancer cell lines was provided by Synta Pharmaceuticals. Affymetrix SNP 6.0 copy number data was obtained from the Broad Institute Cancer Cell Line Encyclopedia (CCLE) dataset. Regions of interest were searched for using the Integrated Genomic Viewer (Broad) and exported as a tab-delimited gene matrix file. Log2 ratios above 0.2 were considered a gain; above 1.0 a high gain; ratios below -0.2 were considered a loss; below -1.0 a high loss. Cell line IC50 data was then grouped by presence or absence of gains or losses. Those cell lines with CNAs at 18q23, 16q22.3 and 11q13.3 identified from the GALAXY-1 dataset were pitted against cell lines which had 0, 1, 2 or 3 of these and IC50 values were compared with boxplots.

2.14.8 Statistical analysis

Error bars indicate ± standard deviation (SD) or ± standard error (SE) as indicated. Statistical tests used are indicated in figure legends. Asterisks on graphs designate the level of significance: * p-value <0.05, ** p-value <0.01, ***p-value <0.001.

Chapter 3 – Determining the effect of EML4-ALK variant status on sensitivity to HSP90 inhibition

3 Determining the effect of EML4-ALK variant status on sensitivity to HSP90 inhibition

3.1 Introduction

The EML4-ALK fusion is present in approximately 5% of non-small cell lung adenocarcinomas, and is readily targetable by agents such as crizotinib and alectinib. Echinoderm microtubule-associated protein (EMAP)–like (EML) proteins normally aid the construction of the mitotic spindle and have been demonstrated to interact with microtubules; EML4 is key to microtubule formation [222]. Wild type length anaplastic lymphoma kinase meanwhile (ALK) crosses the cytoplasmic membrane and tends to be expressed in the brain where it plays an important role in development [223]. Normal ALK requires external ligand binding to its external receptor and internal dimerisation to activate downstream signalling pathways [223]. By contrast, ALK fusion proteins such as EML4-ALK are located within the cell exclusively and become autophosphorylated, leading to constitutive activation of downstream signalling pathways involved in cancer development such as JAK/STAT and PI3K/AKT (Figure 3.1-1) [128]. As a consequence, these cancer cells become addicted to the oncogenic signalling of EML4-ALK. ALK inhibitors like crizotinib can exploit this addiction and directly target the cytoplasmic domain of ALK in order to inhibit these downstream signalling pathways, however various resistance mechanisms develop over time: secondary gatekeeper mutations in the cytoplasmic region of ALK have been shown to render ALK inhibitors ineffective [20, 200]. Alternative therapeutic options are therefore required.

EML4-ALK has been demonstrated to be a client of the chaperone HSP90, and inhibition of HSP90 has been shown to cause rapid proteasomal degradation of the fusion protein [111]. However, multiple variants of EML4-ALK exist where the EML4 region is truncated at different breakpoints within the gene (Figure 3.1-2) [128]. It is not known what effect this has on stability of the protein and sensitivity to HSP90 inhibition. Recent X-ray crystallography work revealed the structure of a key globular domain of the related EML protein, EML1; revealed to

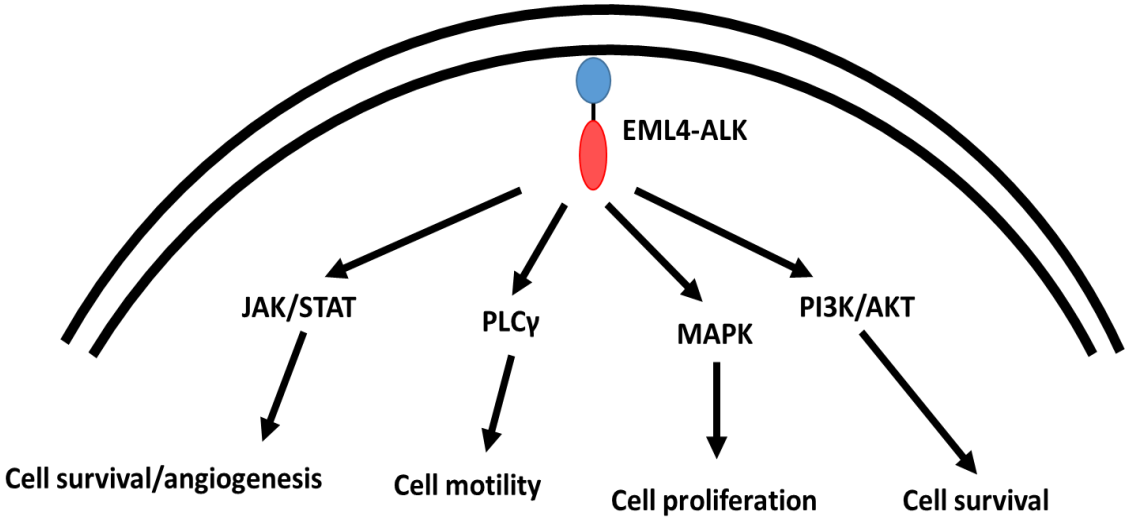

Figure 3.1-1 *EML4-ALK downstream signalling pathways*

Figure 3.1-2 *EML4-ALK variants. Obtained from Sasaki et. Al (2010)*

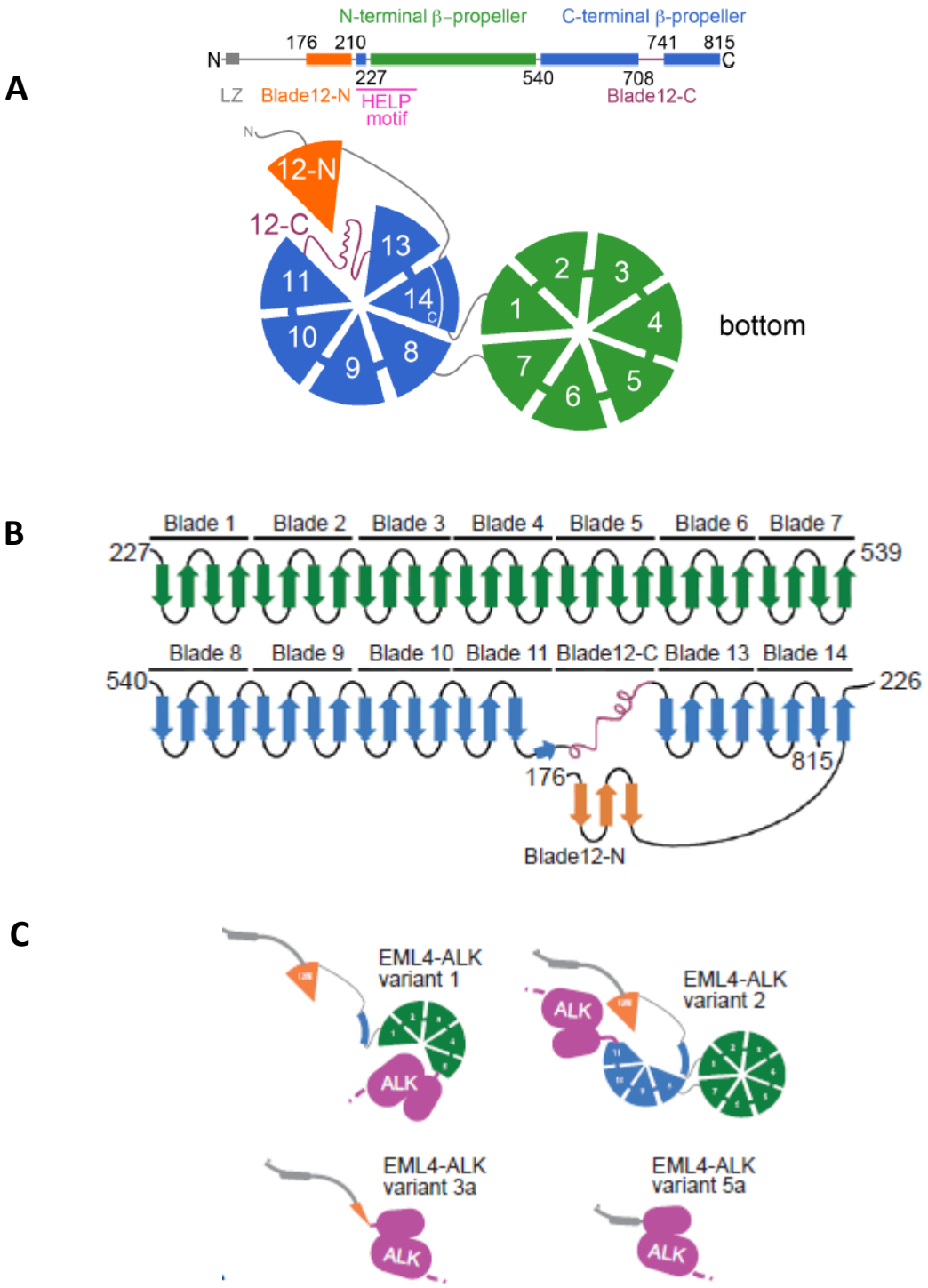

Figure 3.1-3 *The TAPE domain (A) Representation of the TAPE domain of EML1. Green blades form the N-terminal propeller, blue blades form the C-terminal region. The atypical blade 12 is made up of 3 beta sheets from the N-terminal portion of the sequence (12N, orange) and the remaining looped structure is from the C-terminal sequence (B) Secondary structure cartoon displaying that each blade is comprised of 4 beta sheets arranged in the classical propeller formation. The atypical 12th blade is clearly represented (C) Models of the EML4-ALK variants 1, 2, 3a and 5a based on knowledge of EML1 TAPE domain structure. Variants 1 and 2 contain disrupted TAPE regions, whereas 3a and 5a have little to none of this region left. Taken from Richards et al. (2014)*

be comprised of two atypical beta-propellers (N- and C-terminal propellers) oriented at a 50^{o} angle to one another [224]. This region was designated the TAPE domain (Tandem Atypical Propeller in EMLs) (figure 3.1-3)(A). Each propeller has seven "blades", encompassing 4 beta sheets, arranged in a circular fashion around a tapered channel. Uniquely blade 12 in the C-terminal propeller is comprised of two subdomains from distinct regions of the primary sequence: 12N is arranged as a three stranded beta-sheet, 12C has a fairly loosely formed looped structure. The crystal structure of EML1 provided a basis to model the likely structure of EML4-ALK fusion proteins. Variant 1 was predicted to be disrupted within the N-terminal propeller whilst variant 2 was found to be disrupted in the C-terminal region. Meanwhile variant 3 has very little of the tape domain present, with only a small part of the 12N blade remaining and variant 5, with the breakpoint at exon 2 of EML4, is predicted to have none of the TAPE domain at all (figure 3.1-3) (**C**). In addition, variant 3 was shown exclusively of all variants tested to co-localise with microtubules, further complicating the molecular dynamics at work.

The largely exposed hydrophobic core of the TAPE domain in variants 1 and 2 would render the proteins relatively unstable and therefore gives rise to the hypothesis that EML4-ALK variants may differ in their dependency on HSP90 for their continued stability in the cancer cell. Variants 3a and 5a, without such a large hydrophobic region exposed, may not be as dependent on HSP90 for stability and so HSP90 inhibition may not be as effective for these variants. However, whether this is the case remains unknown and therefore the differential stability and sensitivity of EML4-ALK variants to HSP90 inhibition will be assessed in this chapter. The potential increased stability of EML4-ALK and independence from Hsp90 may increase resistance to HSP90 inhibitor-induced cell death. Ganetespib inhibits multiple oncogenic axes simultaneously (PI3K/Akt, Ras/Raf/MEK/ERK, JAK/STAT) and has been shown to induce apoptosis in EML4-ALK expressing cell lines, however differences in apoptotic induction dependent on EML4-ALK variant remain unclear [38].

It has been recently published that specific EML4-ALK translocations may be detected from lung adenocarcinoma patient specimens by using a multiplex reverse transcription-PCR method [124]. This is of great importance because it may allow

further stratification of EML4-ALK positive patients into groups expressing specific EML4-ALK variants. Consequently, treatment of these patients can utilise a more selective strategy that is expected to be the most successful for the specific fusion variant. A recent phase I trial of the HSP90 inhibitor ganetespib in EML4-ALK positive NSCLC patients (CHIARA; NCT01562015) has provided tissues to examine if the EML4-ALK variant present is linked to survival outcome. Therefore, another aim of this chapter is to develop a RT-PCR method to detect EML4-ALK variants and apply it to patient samples from the CHIARA trial to achieve this goal.

Aims and rationale

- Determine whether EML4-ALK variants exhibit differing stabilities upon HSP90 inhibition, and whether this translates into an effect on cell viability and apoptosis The crystal structure analysis of EML1 implies the specific EML4 domains present in EML4-ALK variants exhibit different dependencies on Hsp90 for stability in the cell. Particularly, EML4-ALK variant 3, which colocalises with microtubules, may depend less on Hsp90 chaperone activity for its stability
- Using ENU-mutagenesis and sequential high doses of ganetespib, develop a cell line with acquired resistance to ganetespib: this has not been done before and would be interesting to see what mechanisms cells could use to adapt to HSP90 inhibition in patients
- Develop a RT-PCR methodology to determine EML4-ALK variants in FFPE tissue and apply to samples from the CHIARA trial of ganetespib monotherapy in NSCLC patients and look for correlation of variant with response, in order to determine if *in vitro* observations hold true in clinical samples

3.2 Results

3.2.1 EML4-ALK variants exhibit different stabilities in response to Hsp90 inhibition

In a preliminary experiment to examine differential stability of EML4-ALK variants *in vitro,* constructs containing EML4-ALK variants 1,2,3a and 5a fused to YFP, plus YFP and cytoplasmic ALK-YFP controls were transfected into wild type mouse embryonic fibroblast cells (MEF). These were then subject to 100nM of ganetespib (MEF 72h IC_{50} value) for 0, 1, 3 and 6 hours and EML4-ALK expression level monitored by western blot (figure 3.2-1).

EML4-ALK variants 1 and 2, which have large regions of exposed hydrophobic core and thus expected to depend on Hsp90 for stability, appear to start degrading after 3h treatment and cannot be detected after 6h as seen in figure 3.2-1. Conversely, variants 3a and 5a which have lost most of their N-terminal EML4 transcript and thus do not have a large hydrophobic region exposed can still be detected after 6h treatment with ganetespib. Densitometry analysis of the three biological repeats supports this view: variant 1 decreases to approximately 30% at 3 hours, and less than 3% of control by 6 hours. Variant 2 follows a similar pattern: 15% at 3 hours and 2% of control at 6 hours' exposure to ganetespib. Meanwhile variant 3 remains around 95% by the 6-hour time point, whilst variant 5 decreases to only around 60% of control by 6 hours.

To investigate this effect more thoroughly Ba/F3 cells stably expressing the EML4-ALK variants were generated. These cells become IL3-independent and EML4-ALK-dependent once the construct is stably established in the cells. Multiple clones were developed for each variant, and two clones per variant with the highest expression were selected for continued study. EML4-ALK dependence was demonstrated by treatment with the ALK-specific kinase inhibitor crizotinib in cells expressing variants 1 or 3a: treatment over 12 hours results in a dose-dependent dephosphorylation of EML4-ALK at the tyrosine 1604 phosphorylation site and simultaneous increase in PARP cleavage for both cell lines (figure 3.2-2). Low level PARP cleavage was observed without crizotinib exposure which may be due to the presence of hygromycin.

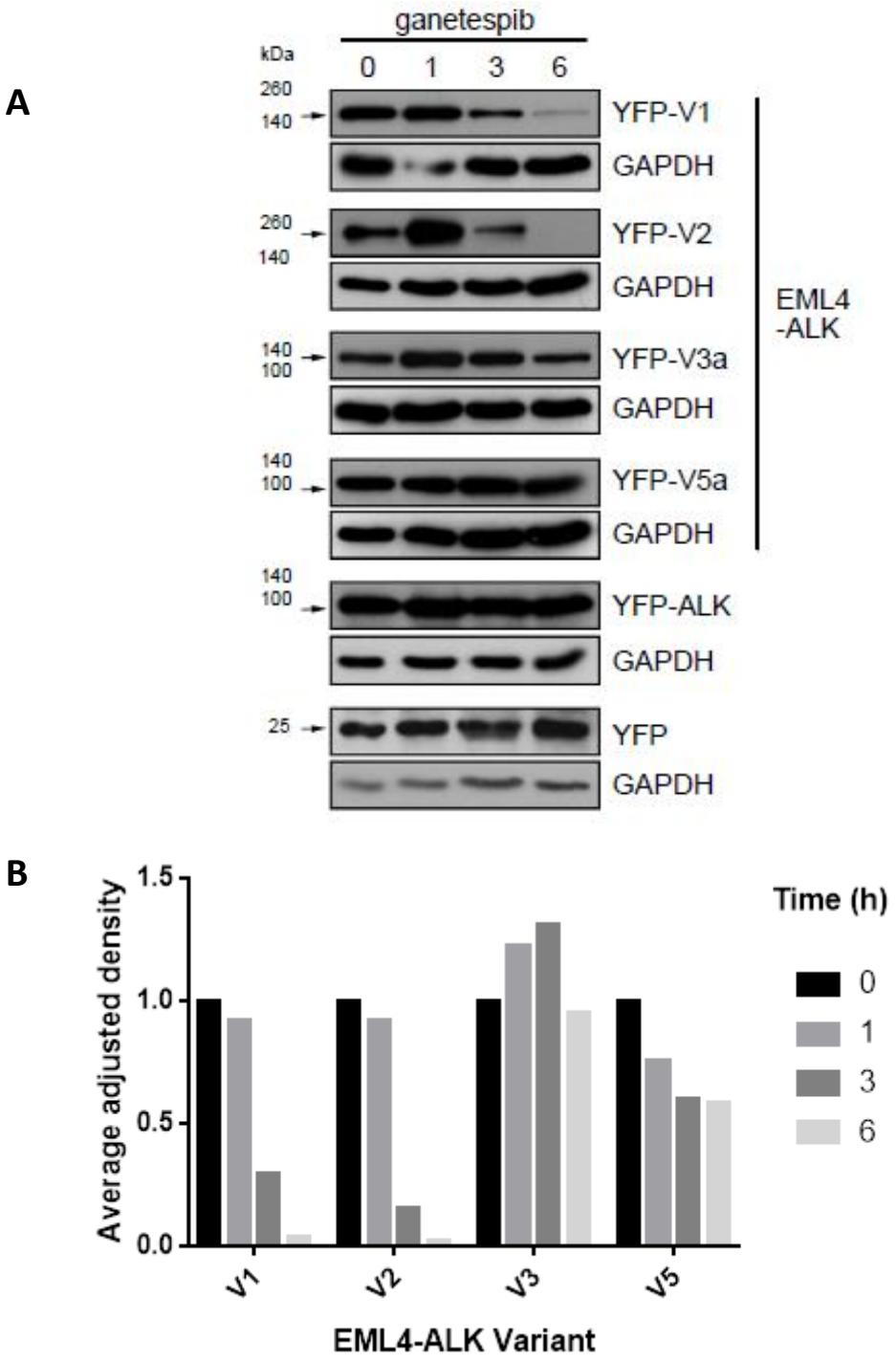

Figure 3.2-1 *Differential stability of transfected EML4-ALK variants in response to ganetespib. (A) Western blot of MEF cells transfected with empty vector (EV) cytoplasmic ALK or EML4-ALK variants 1, 2, 3a and 5a and treated with 100nM ganetespib for 0, 1 ,3 or 6h. n=3 repeats (B) Densitometry analysis of three biological replicates of YFP band intensity normalised to GAPDH control*

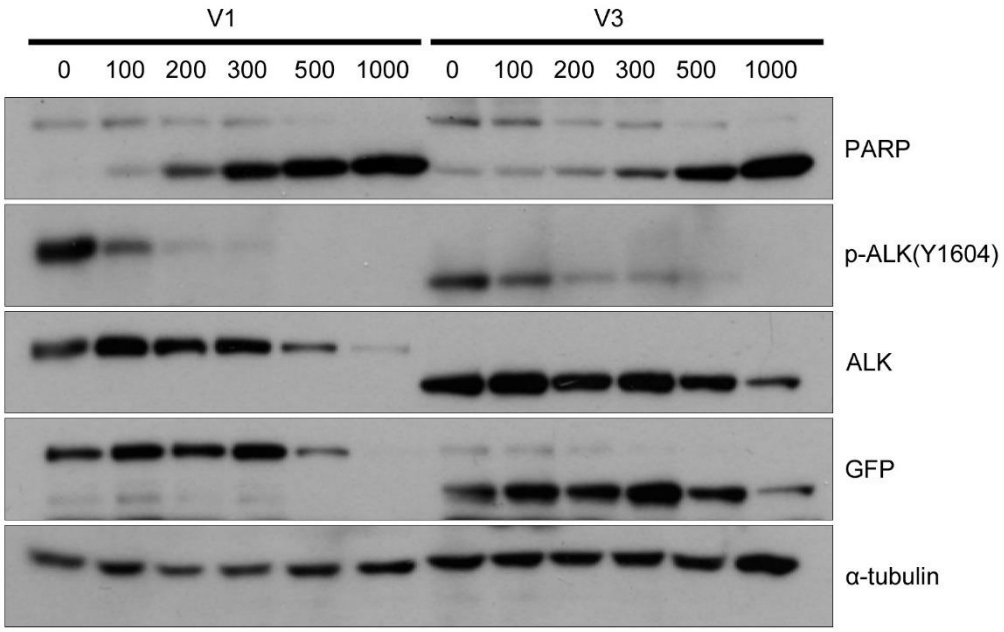

Figure 3.2-2 *Stably-transfected Ba/F3 cells are sensitive to the ALK inhibitor crizotinib. Western blot of dose-response to 12 hours of crizotinib treatment of EML4-ALK dependent Ba/F3 cells expressing variants 1 or 3a treated. n=3 biological replicates*

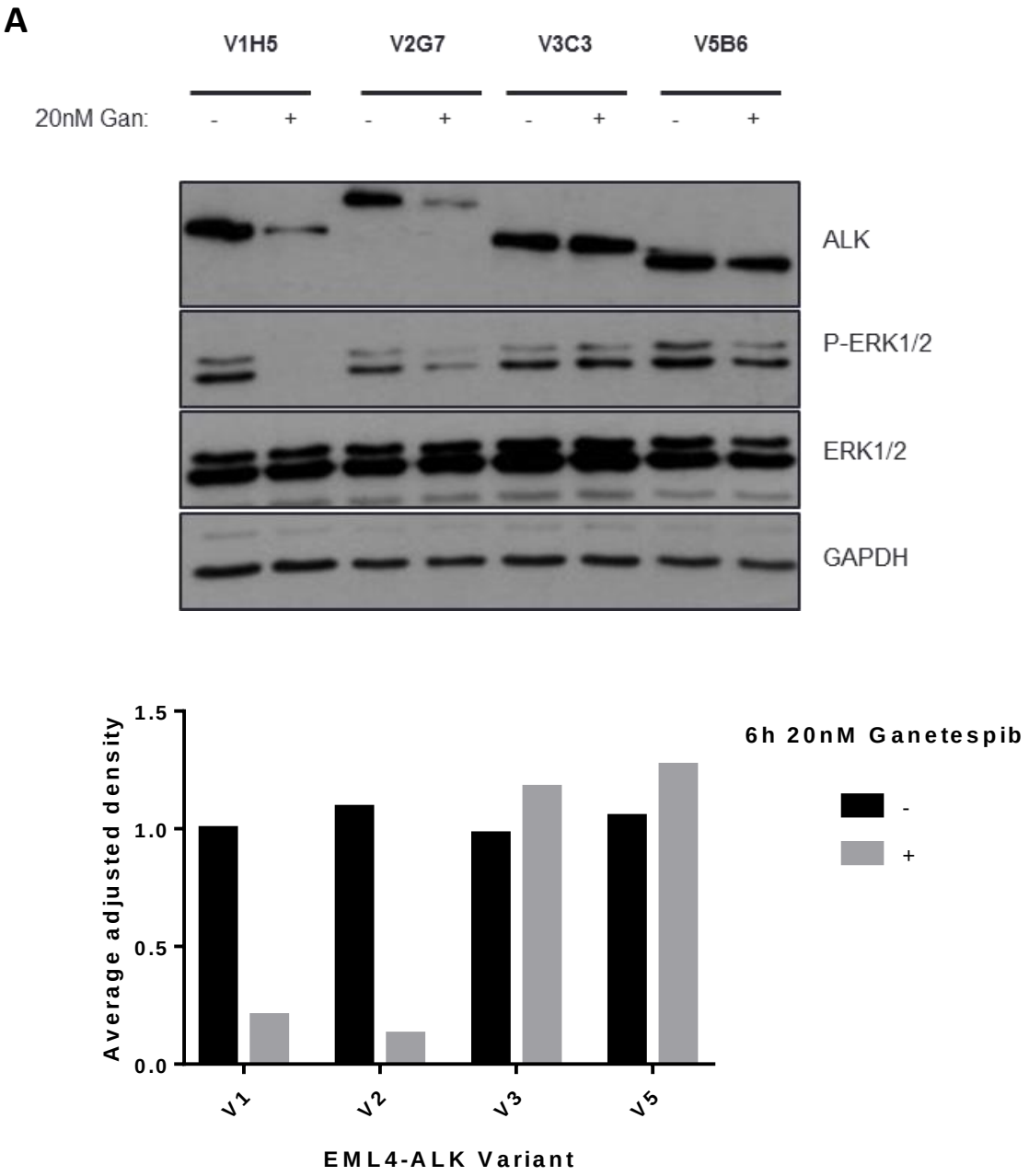

Figure 3.2-3 *Differential stability of EML4-ALK variants in stable cell lines in response to Ganetespib.* ***(A)*** *Western blot of Ba/F3 cells stably expressing EML4-ALK constructs 1, 2, 3a and 5a subjected to 20nM Ganetespib for 6h Variant designated by "Vx" followed by clone number. Representative of one of two clone sets tested. n=3* ***(B)*** *Densitometry analysis of 3 repeats of western. Bars represent average density of ALK band adjusted for GAPDH loading control*

Multiple clones were generated for variants 1, 2, 3a and 5a and two per EML4-ALK variant were selected for analysis. Cells were subjected to 20nM ganetespib for 6h based on pilot dose response data (not shown) and analysed by western blot (figure 3.2-3). Ganetespib treatment in these cells mimicked what was seen in the transient experiments: degradation of EML4-ALK variants 1 and 2 but not 3a or 5a after 6h exposure. Densitometry analysis of three biological replicates confirms this interpretation, and ALK expression was altered for each of the variants approximately as follows in response to ganetespib in comparison to the control: V1 – 21%, V2 – 13%, V3 – 118% and V5 – 127%. Given these cells are dependent on ALK for survival, downstream ALK signalling was also seen to be affected by ganetespib for variants 1 and 2 but not 3a and 5a as shown by the presence of phosphorylated-ERK, though this may also be due to the fact MEK is a known client of HSP90 and will be affected by its inhibition.

To confirm these in vitro data further, two human non-small cell cancer cell lines which express EML4-ALK variant 1 (NCI-H3122) or variant 3b (NCI-H2228) were subjected to a dose response to ganetespib for 6 hours (figure 3.2-4). These doses represent much lower concentrations than the C_{max} of 5000ng/mL observed in patients when dosed with 200mg/m^2, and the 6 hour time point selected based on an approximation to the ganetespib half-life observed in clinical studies, and because EML4-ALK degradation has been previously observed in response to IPI-504 at this time point [111, 225]. Once again whilst degradation of EML4-ALK variant 1 was seen at 20nM in H3122 cells with concurrent loss of p-ERK signalling, no observable degradation of EML4-ALK variant 3b was observed in H2228 cells, even with doses up to 500nM. Densitometry analysis suggests variant 1 expression decreased to around 40% in H3122 at 20nM, then remained around 10-20% at higher doses for this time point. Meanwhile, variant 3 in H2228 does not appear to be affected markedly by ganetespib, even at 500nM where protein levels appear around 91% of control.

Inhibition of the Hsp90 chaperone complex results in ubiquitylation and targeting of client proteins to the proteasome for degradation. To ensure ganetespib-induced degradation of EML4-ALK is proceeding via the proteasome, EML4-ALK variant 1 transfected cells were subject to 6h ganetespib at 100nM (MEF IC_{50} value 72h) alone

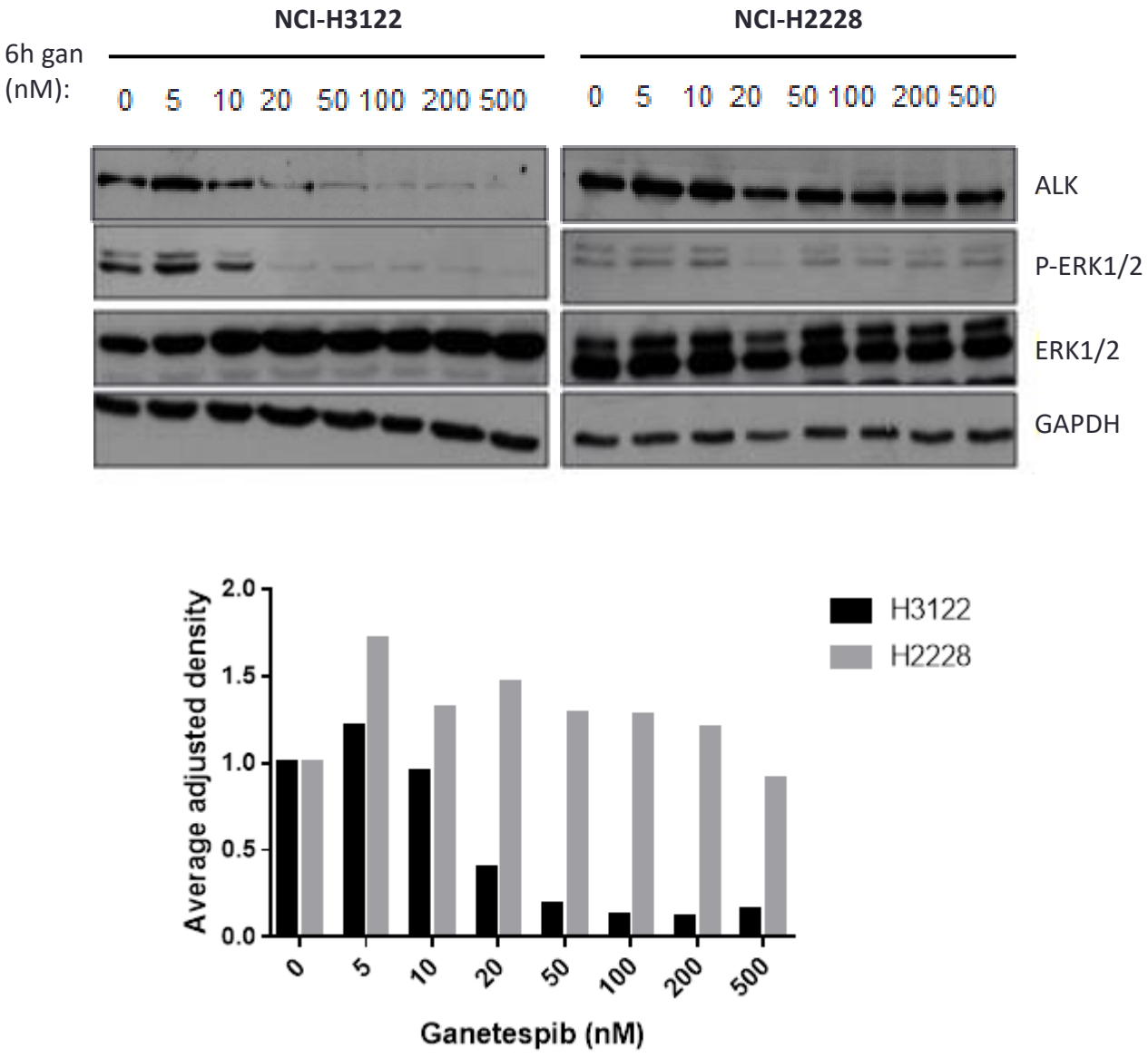

Figure 3.2-4 *Differential stability of endogenously expressed EML4-ALK variants 1 and 3b in H3122 and H2228 cells respectively. Western blot of H3122 or H2228 cells treated for 6h with increasing doses from 5 to 500nM*

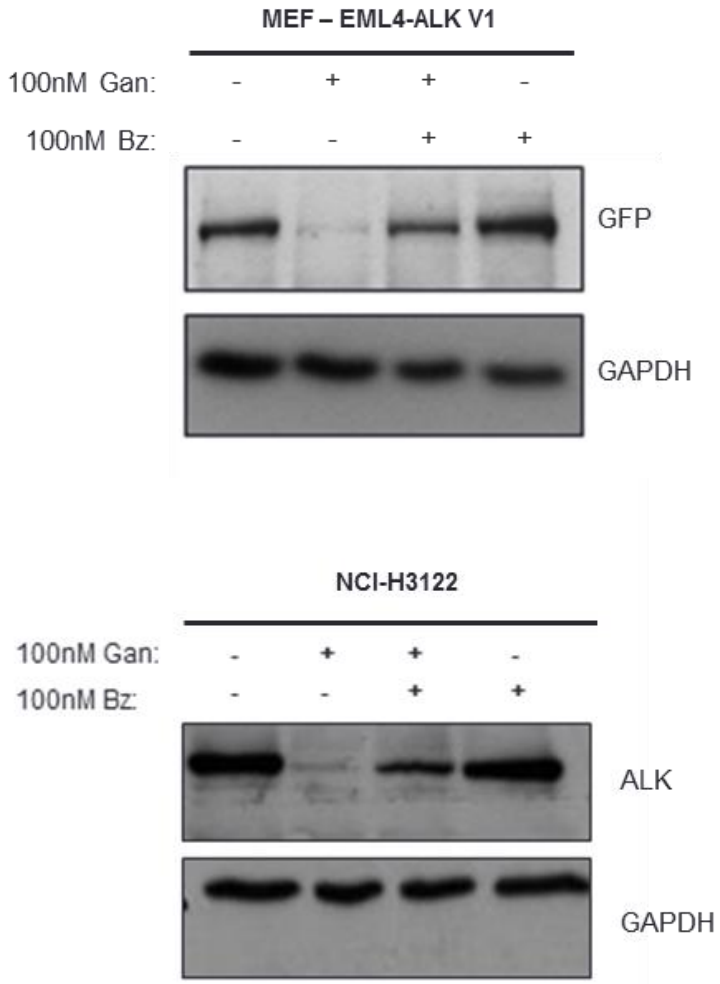

Figure 3.2-5 *Rescue of EML4-ALK variant 1 from ganetespib induced proteasomal degradation. Western blot of EML4-ALK variant 1 transfected MEF cells or H3122 cells with endogenous variant 1 treated for 6h with ganetespib and bortezomib alone or in combination. n=3 biological replicates*

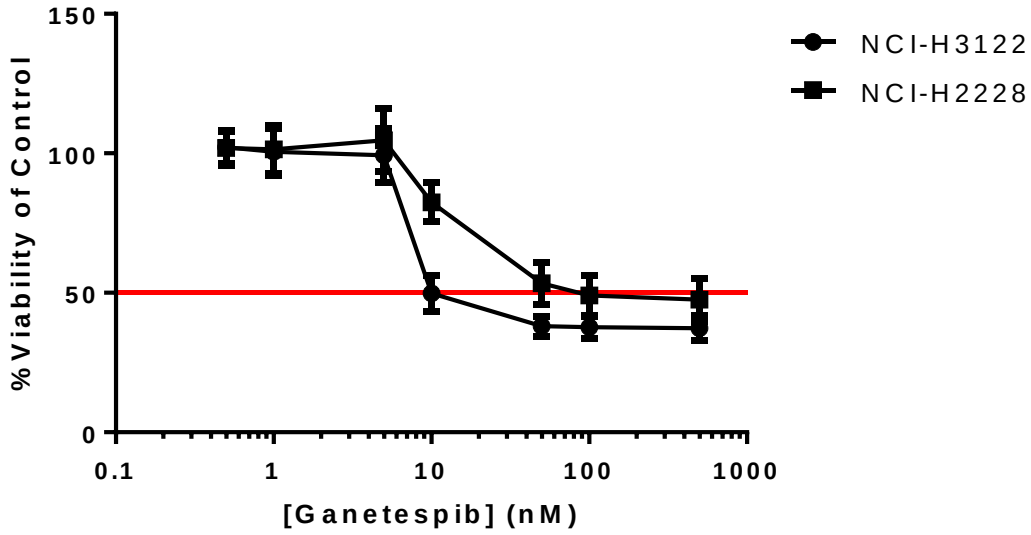

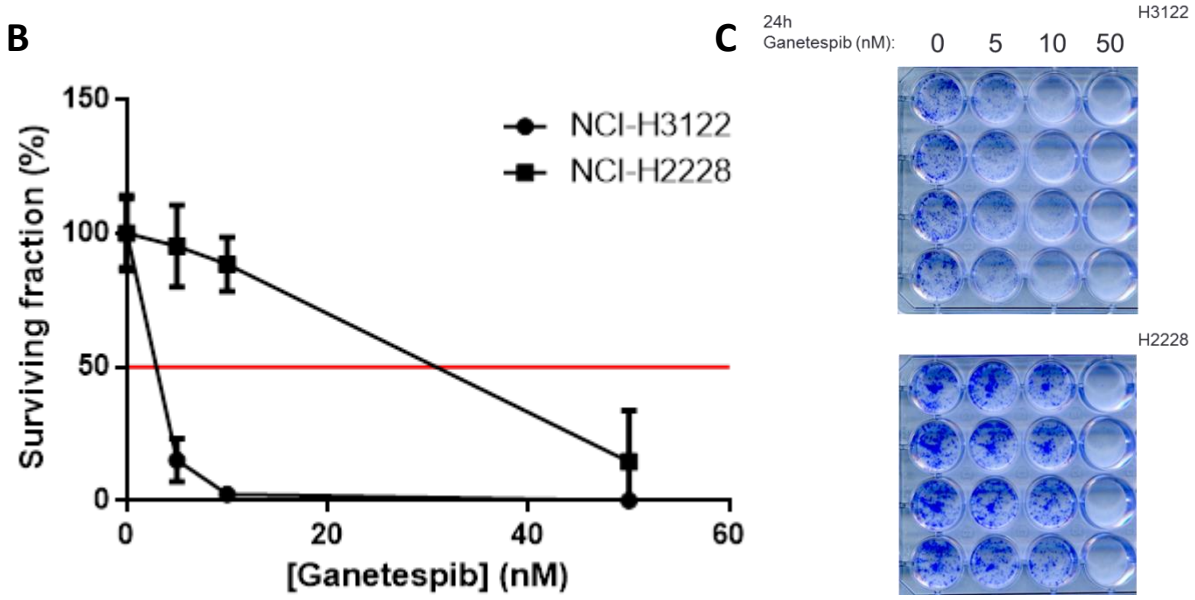

Figure 3.2-6 (A) *Short term viability of H3122 and H2228 after 72h treatment with ganetespib. IC50 values IC50 H3122 – 7.45nM (95%CI 5.13nM-10.83nM); H2228 – 17.70nM (95%CI 12.25nM-25.59nM). Represents n=3 experiments* ***(B)*** *Clonogenic assay of H3122 or H2228 cells treated with ganetespib. Graph represents the average no of colonies compared to the control. 1 colony = at least 50 cells.. Error bars represent standard deviation. n=3 experiments* ***(C)*** *Representative scans of plates used for clonogenic experiments. Error bars represent standard deviation.*

or in combination with the 26S proteasome inhibitor bortezomib (figure 3.2-5). When exposed to both drugs for 6 hours, partial rescue of the EML4-ALK fusion protein can be seen. A similar result was obtained in H3122 cells which harbour endogenous EML4-ALK variant 1.

3.2.2 EML4-ALK variants and sensitivity to Hsp90 inhibition

Given these data suggesting EML4-ALK variants 1 and 2 are much less stable than 3a and 5a in response to ganetespib in the short term, it was investigated whether this translated into a difference in cell survival over a longer period. Firstly, H3122 (V1) and H2228 (V3b) cells were subjected to a range of doses of ganetespib for 72h and tested for viability (figure 3.2-6)(A). The IC_{50} values for H3122 and H2228 were 7.45nM and 17.7nM respectively. Interestingly cells did not die completely in either cell line: cells viability reduced to around 40% even at the highest concentration of ganetespib. To assess if a difference could be observed over a longer time course a clonogenic assay was carried out. H3122 and H2228 cells were plated at 1000 cells/well of 24WP and subsequently drugged with 0,5,10 and 50nM ganetespib for 24h. The drug was then washed out and cells allowed to grow until confluency in the control well. Cells were then fixed, stained with crystal violet and colonies of over 50 cells counted in each well (figure 3.2-6**(B)**). This assay reveals that H3122 cells, which express EML4-ALK variant 1, were much more susceptible to ganetespib treatment with less than 20% colony formation at 5nM. Conversely H2228 cells, which express variant 3b, did not display much difference in colony formation until drugged with 50nM ganetespib, where the amount of colonies formed was less than 20% of the control.

There appears to be some difference in sensitivity of these cells to ganetespib, therefore the mechanism of this difference was probed further by looking at the induction of apoptosis. Cells were treated for 48h with ganetespib and then analysed for induction of apoptosis by PARP or caspase 9 cleavage, Sub-G1 and caspase 3/7 activity figure 3.2-7. Evidence of PARP and caspase 9 cleavage is seen in H3122 and H2228 cell lines at 20nM ganetespib at 48h. Whilst EML4-ALK variant 1 is degraded completely in H3122 cells by 20nM, the same is not true in H2228 cells. Significant cell

death and apoptosis was indicated for both cell lines at 10nM for both H3122 and H2228 as revealed by Sub-G1 and caspase-3/7 assay respectively (*** $p<0.001$, ** $p<0.01$).

To assess the role of the intrinsic apoptosis pathway in ALK-dependent cells after Hsp90 inhibition, BAX and BAK was silenced in H3122 cells which were subsequently treated with 20nM ganetespib for 48 hours (figure 3.2-8). BAX and BAK levels were greatly reduced in cells transfected with RNAi. A subtle induction of PARP cleavage was observed in ganetespib-treated cells subjected to negative control siRNA, which may translate into a small reduction in PARP cleavage in ganetespib-treated cells however this is unclear. There was however a significant reduction in the proportion of $subG_1$ cells after ganetespib treatment in the BAX/BAK silenced group (mean =12.5%) compared to the negative control group (mean =20.6%) ($p<0.01$), suggesting that BAX and BAK are indeed involved in cell death in this context.

H3122 and H2228 cells are not an isogenic model and have different genetic backgrounds. Therefore, there could be many other factors determining sensitivity to Hsp90 inhibition in these cell lines. Consequently, sensitivity to ganetespib was assessed in an isogenic context. First, H3122 cells were transfected with empty vector or EML4-ALK variant 3 and then plated at low density for a clonogenic assay. Cells were drugged for 24h then monitored over 1-2 weeks until colonies formed at which point colonies were counted (figure 3.2-9). No significant difference was observed in colonies formed in V3 transfected cells against empty vector transfected H3122 cells subjected to ganetespib. The transfection efficiency for variant 3 appears to be much less than that of the empty vector construct. To assess if variant 3 could rescue from ganetespib induced apoptosis, H3122 cells were transfected with YFP, EML4-ALK variant 1 or 3a and subjected to 48h 20nM ganetespib (figure 2.3-10). There appears to be no reduction in PARP or caspase-9 cleavage in V3 transfected cells suggesting no rescue from apoptosis.

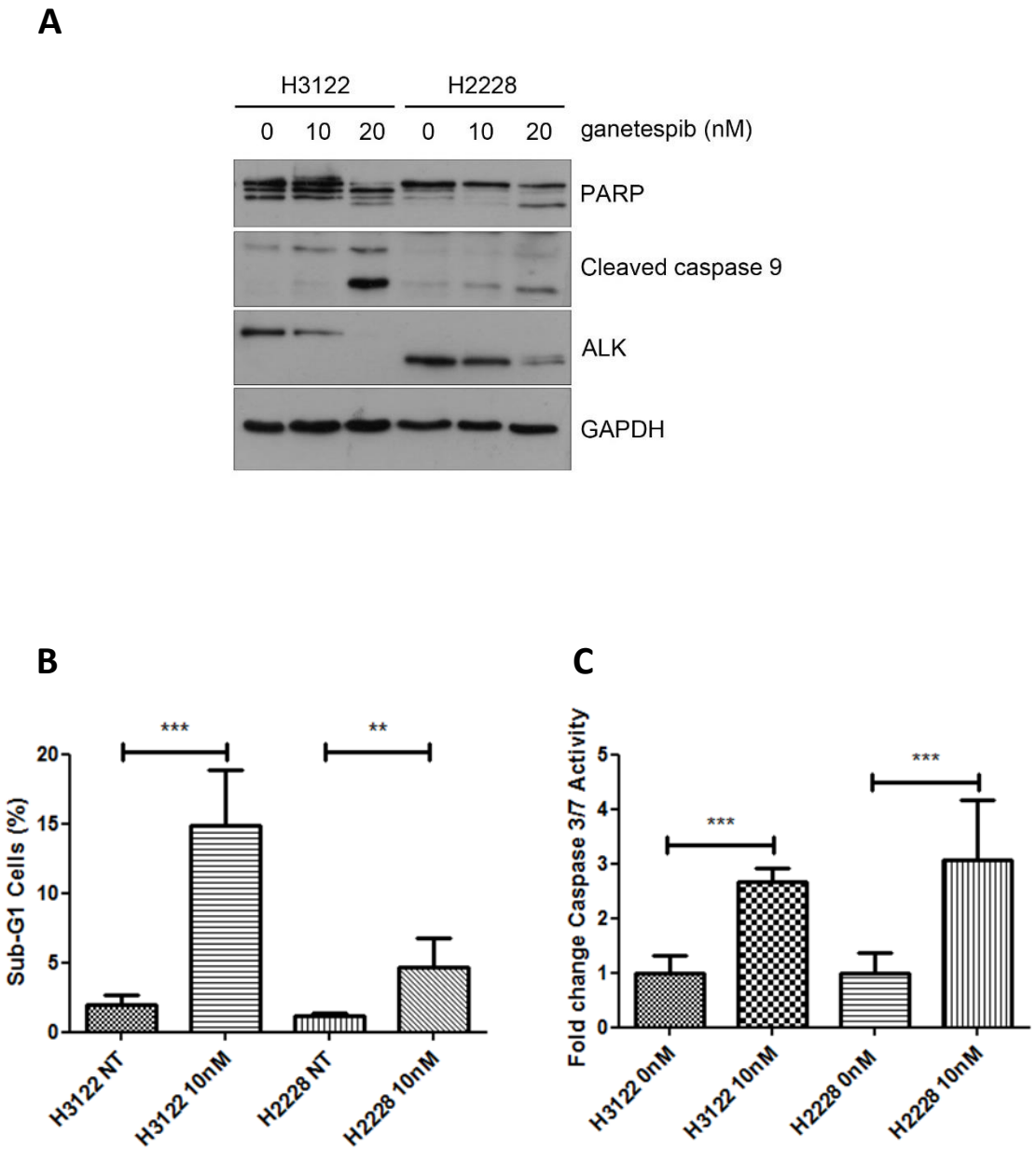

Figure 3.2-7 *Apoptosis induction in H3122 and H2228 cells in response to ganestespib. Cells were treated with ganetespib for 48h and assessed for apoptosis by* ***(A)*** *Western blot by PARP and caspase 9 cleavage,* ***(B)*** *Sub-G1 analysis and* ***(C)*** *Caspase 3/7 assay. Error bars indicate standard deviation. ** p<0.01, ***<0.001. n=3 for all experiments*

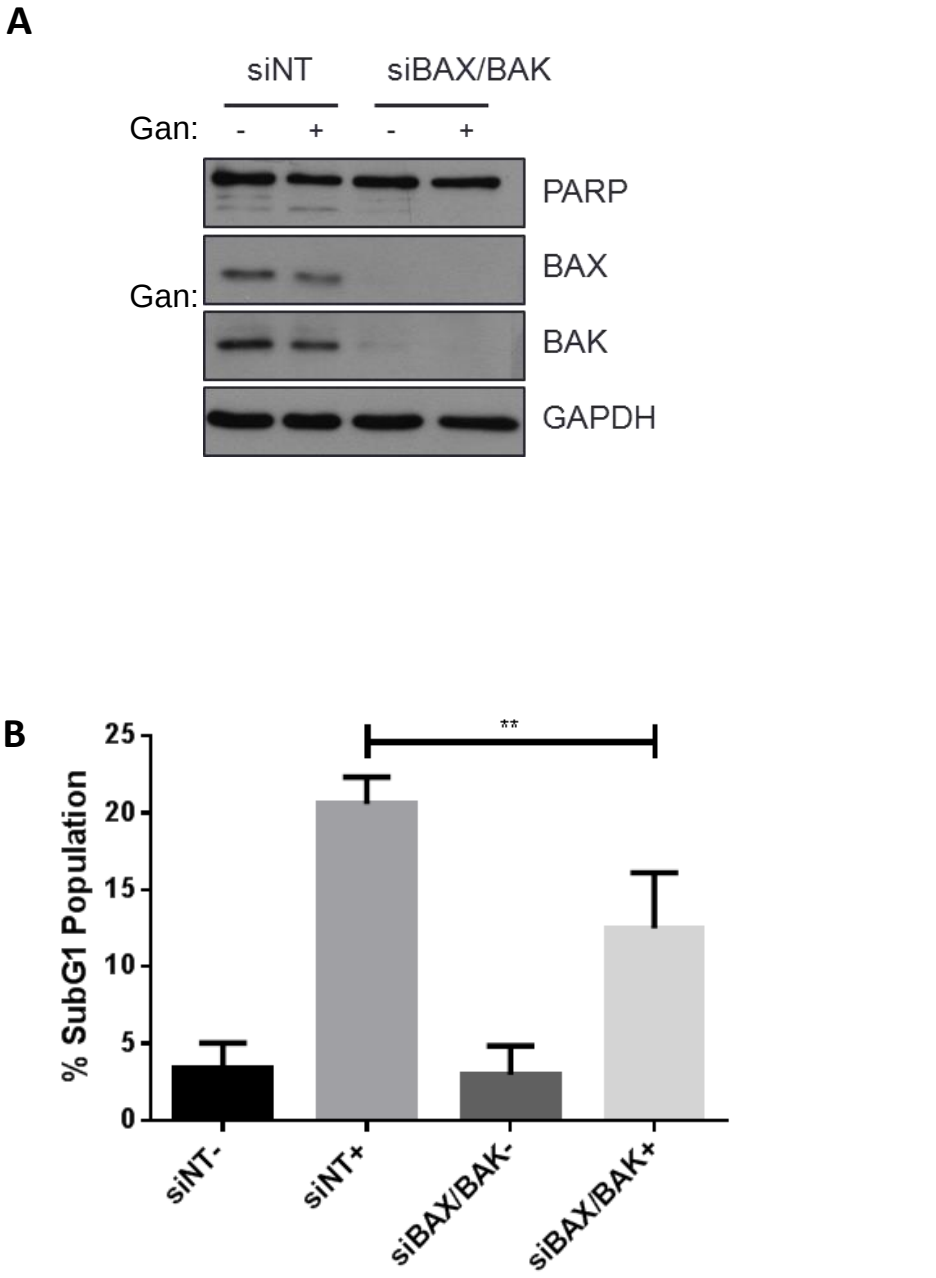

Figure 3.2-8 *Cell death in ALK-dependent H3122 cells is reduced by BAX and BAK knockdown Cells were subjected to 20nM of RNAi against BAX and BAK for 48h then treated with 20nM ganetespib for a further 48h and assessed for cell death by* ***(A)*** *Western blot by PARP cleavage and* ***(B)*** *Sub-G1 analysis. Error bars indicate standard deviation. ** p<0.01, n=3 for all experiments*

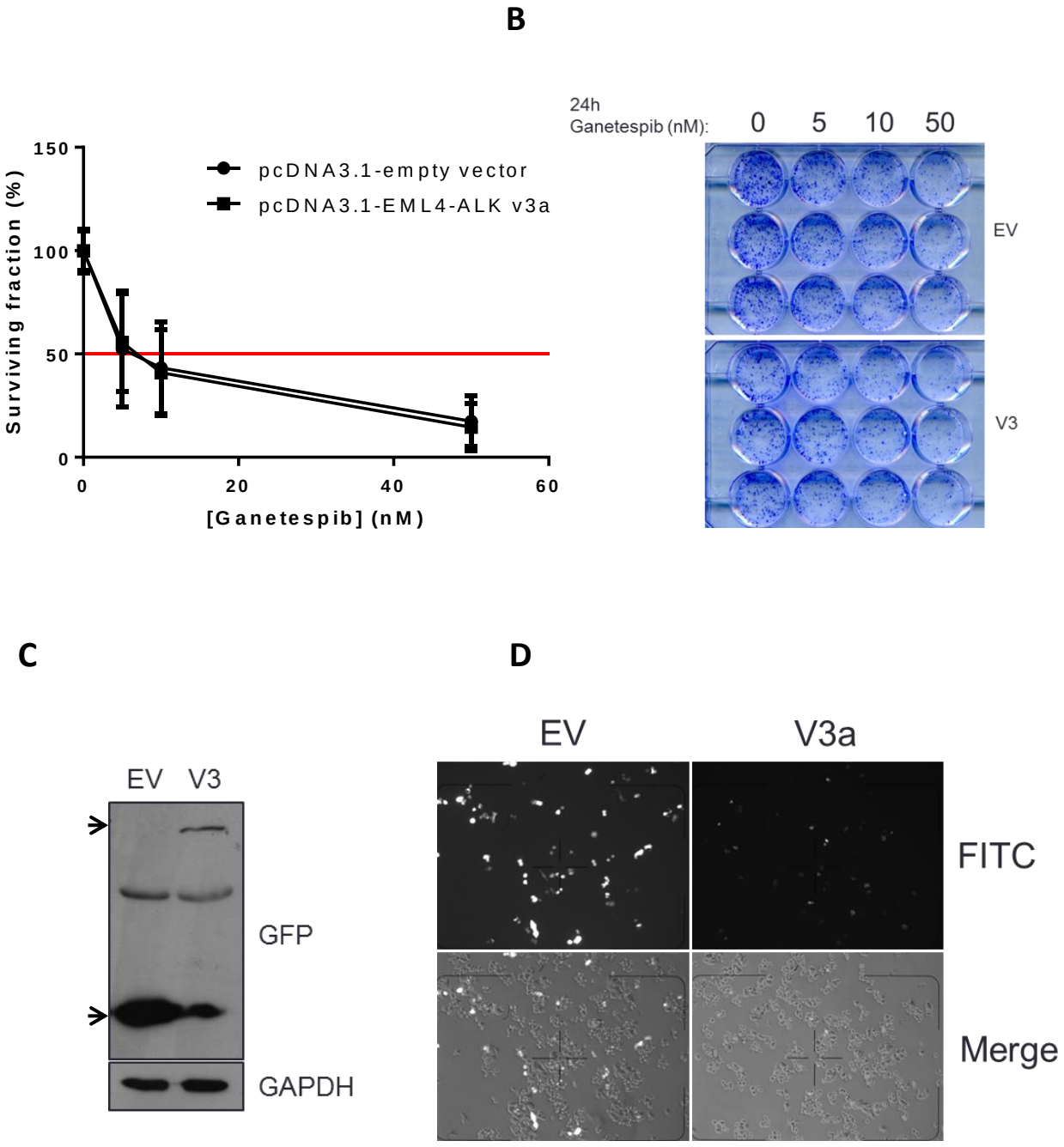

Figure 3.2-9 *Transfection of EML4-ALK variant 3 has no effect on clonogenic survival after treatment with ganetespib. Clonogenic analysis of H3122 cells transiently transfected with empty vector or EML4-ALK variant 3a and treated with ganetespib.* ***(A)*** *Average number of colonies as a percentage of control wells. 1 colony = 50 or more cells. n=3. Error bars represent standard deviation* ***(B)*** *Scanned clonogenic plates representative of 3 experiments.* ***(C)*** *Western blot of GFP expressed on day of drug addition* ***(D)*** *Phase contrast and FITC images of transfected cells on day of drugging. n=3 repeats*

Sensitivity to Hsp90 inhibition was further investigated in EML4-ALK-expressing Ba/F3 cells that were previously established. Ba/F3 cells stably overexpressing EML4-ALK variants 1 or 3a were subjected to a range of doses of ganetespib for 72h and viability assessed (figure 3.2-11)**(A)**). The IC_{50} values were determined for V1 (10.64nM, 95% CI 8.219nM to 13.79nM) and V3 (35.84nM, 95%CI 27.43nM-46.83nM). This represents a threefold increase of IC_{50} in cells expressing variant 3a compared to variant 1.

To understand if this difference in viability was linked to differential apoptotic sensitivity, Ba/F3 cells were drugged with ganetespib for 12 hours and assessed for apoptotic activity by western blot and caspase 3/7 assay (figure 3.2-11)**(B/C)**). Ba/F3 cells expressing EML4-ALK V1 displayed PARP cleavage at 20nM ganetespib, indicating apoptosis, whilst PARP remained uncleaved in V3-expressing cells at this concentration. ALK degradation was again seen in V1 cells at 20nM as well as loss of phosphorylated ERK, which was not seen in V3 cells. In addition, V1 expressing cells displayed a significant threefold increase in caspase 3/7 activity after treatment with 20nM ganetespib for 12 hours (p<0.0001), which was not observed in V3 cells.

In the cancer cell resistance to therapeutics can be intrinsic or can become acquired over time. In order to simulate acquired resistance to ganetespib in the EML4-ALK dependent context, Ba/F3 cells expressing EML4-ALK variant 1 were expressed to high doses of ganetespib several times and less sensitive clones were allowed to grow back. To assess these cells sensitivity to ganetespib, the less sensitive clone and parent cells were subjected to doses of ganetespib for 24h and assessed for viability (figure 3.2-12)(A). Parental cells expressing EML4-ALK variant 1 displayed a viability similar to when tested previously (IC_{50} 8.657nM, 95% CI 6.725-11.15nM), however cells exposed multiple times to high doses of ganetespib doubled their IC_{50} value (IC_{50} 16.45nM, 95%CI 13.68-19.77nM). To assess the difference in apoptotic sensitivity, cell lines were subjected to ganetespib for 12h and assessed by western blot and caspase 3/7 assay (figure 3.2-12)(B/C). High levels of cleaved PARP were observed in parental cells beginning at 20nM, whereas a much reduced cleavage is observed in V1GD8 cells, beginning at 50nM. ERK is dephosphorylated clearly at 50nM in both lines, suggesting ganetespib is still targeting MEK effectively in the V1GD8 line, however there does appear to be a persistence in EML4-ALK variant 1 at higher EML4-ALK levels in this line

not observed in parental cells. In addition, parental cells showed a 6-fold increase in caspase 3/7 activation in response to 20nM ganetespib, however the increase in caspase-3/7 activity observed in the less sensitive V1GD8 cell line, whilst significant, was less than 1.5 fold, suggesting a reduction in apoptotic activity.

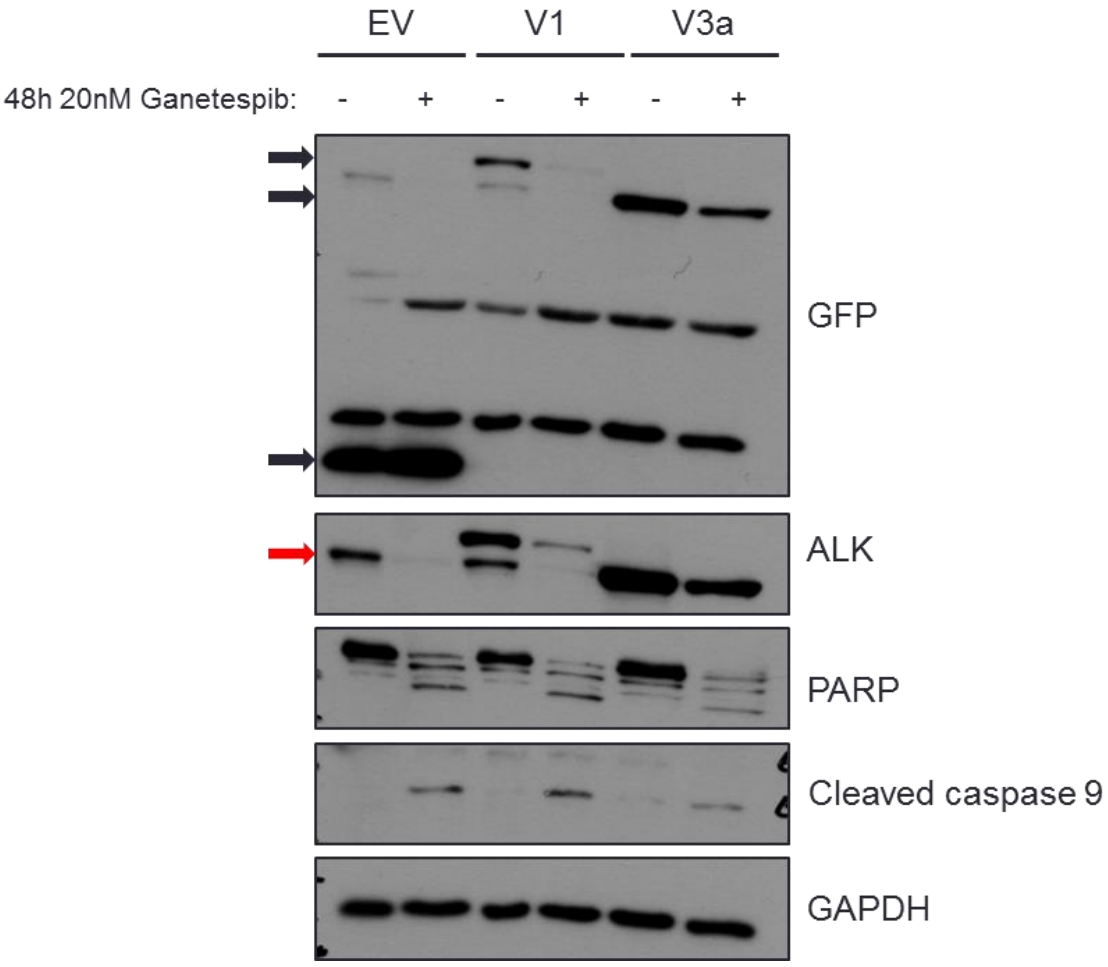

Figure 3.2-10 *Transfection of variant 3 into H3122 cells does not rescue from ganetespib-induced apoptosis Western blot of H3122 cells transfected with YFP, EML4-ALK variant 1 or 3a. Black arrows indicate YFP, V1 and V3a expression. Red arrow indicates endogenous ALK expression. Representative of n=3 experiments*

A

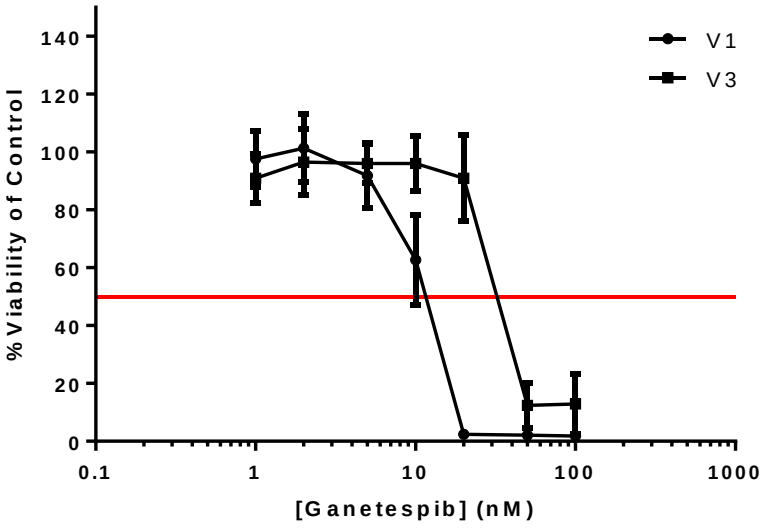

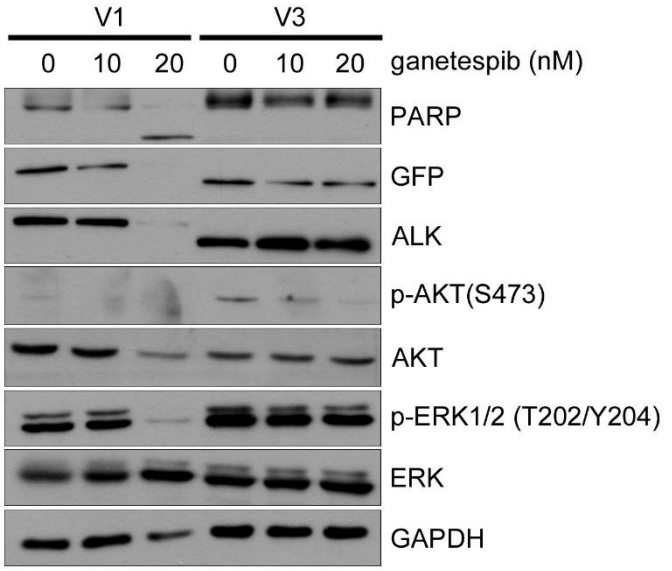

C

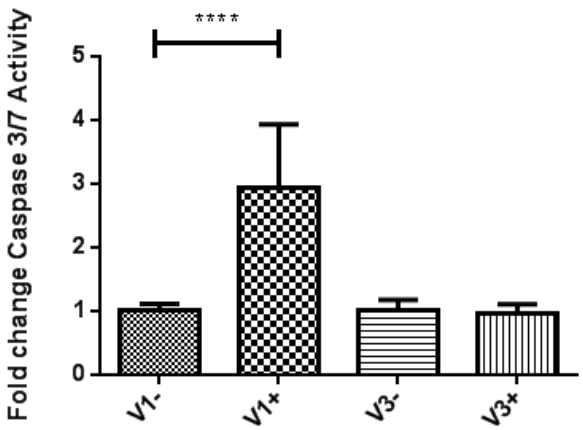

Figure 3.2-11 Differential sensitivity of Ba/F3 cells expressing EML4-ALK variant 1 or 3a (A) Cell titer glo assay of viability after 24h treatment with ganetespib 0 -100nM. - IC50 values: V1 10.64nM (95% CI 8.219nM to 13.79nM); V3 35.84nM (95%CI 27.43nM-46.83nM (B) Ba/F3 expressing EML4-ALK V1 or V3a treated with 0, 10 or 20nM ganetespib for 12 hours and assessed by western blot. (C) Ba/F3 cells treated for 12 hours -/+ 20nM ganetespib were assayed for caspase 3/7 activity (* denotes p<0.0001). Error bars represent standard deviation. n=3 biological replicates***

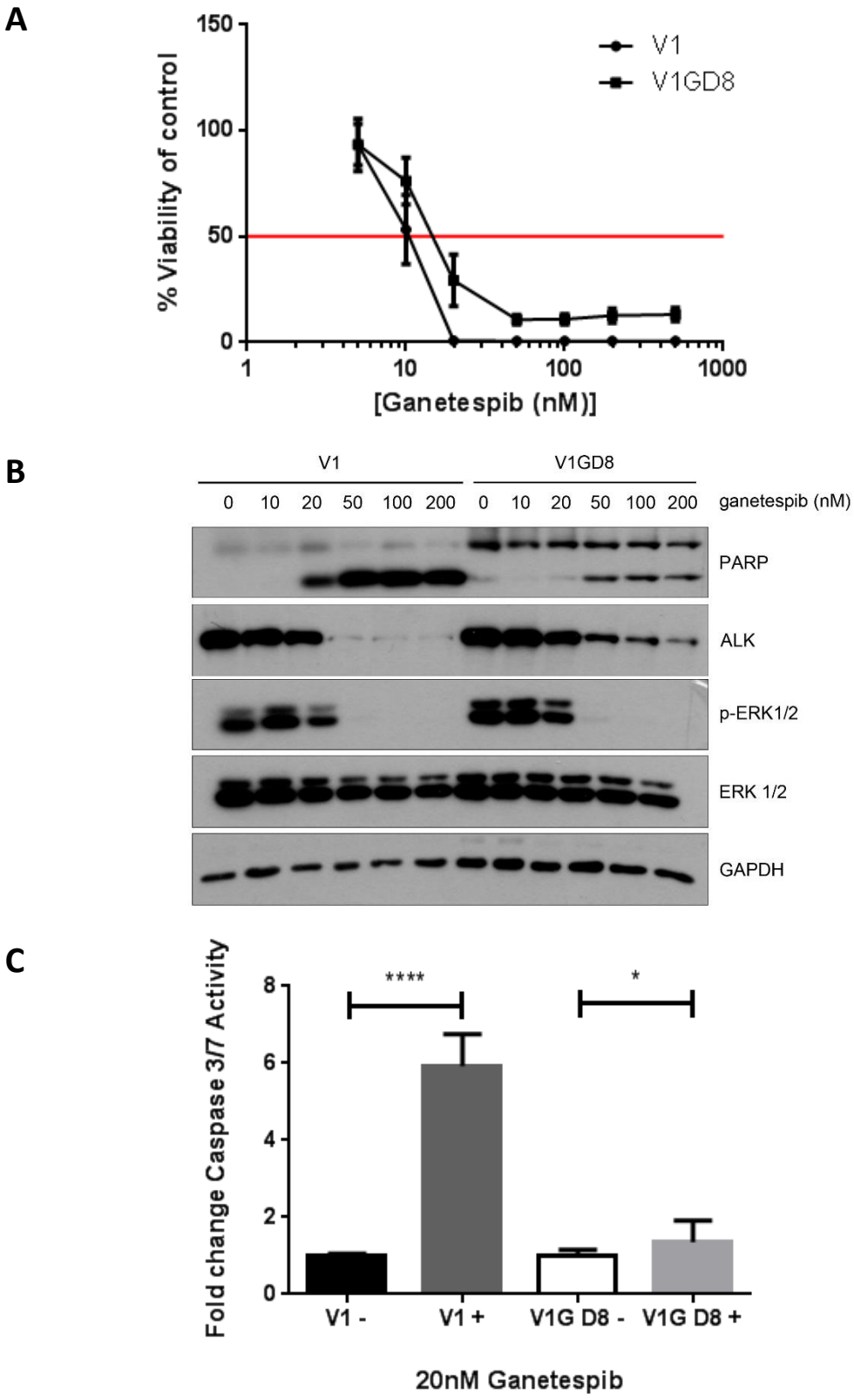

Figure 3.2-12 Development of less-sensitive Ba/F3 cells expressing EML4-ALK variant 1 by repeated drug exposure (A) Cell titer glo assay of viability after 24h treatment with ganetespib 0 -100nM. - IC50 values: V1 8.657nM (95% CI 6.725-11.15nM); V1GD8 16.45nM (95%CI 13.68-19.77nM) (B) Ba/F3 expressing EML4-ALK V1 and less sensitive V1GD8 treated with 0-200nM ganetespib for 12 hours and assessed by western blot. (C) Ba/F3 cells treated for 12 hours -/+ 20nM ganetespib were assayed for caspase 3/7 activity (* =p<0.05, ****= p<0.0001). Error bars represent standard deviation. n=3 biological replicates

3.2.3 Development of a real-time PCR method to detect EML4-ALK variants from formalin-fixed patient tissue

The results obtained *in vitro* suggests a possibility that ALK-positive NSCLC patients treated with Hsp90 inhibitors may differ in their survival outcome dependent on the EML4-ALK variant present. To test this hypothesis, a real-time PCR method was developed to detect specific variants from formalin fixed tissue FFPE from a clinical trial (FFPE). Patient tissue was limited, so the method was first tested on formalin-fixed cytoblocks of ALK- positive H3122 and H2228 cell lines with H460 as a negative control. Initially, six 5mm^2 10µm sections per cytoblock were processed by real-time PCR with primers designed to amplify small (~100-200bp) sections across the breakpoint of variants 1 and 3. Utilising a change in normalised reporter value (ΔR_n) of 0.05, the cycle threshold (C_T) values were determined for EML4-ALK variants 1, 2, 3a/b and 5a as a way of determining the presence or absence of a specific mRNA variant from these cell lines. Hypoxanthing-guanine phosphoribosyltransferase 1 (HPRT1) and the 18S ribosomal subunit were used as markers of RNA quality and efficiency of the PCR reaction.

The amplification plots and mean C_T values for each gene from six cytoblock sections each for H460, H3122 and H2228 are shown in (figure 3.2-13). HPRT1 consistently has a mean C_T value between 29.290 and 30.061 cycles for all cell lines. 18S is amplified at an early stage for all cell lines (between 10.810 and 13.054 cycles). EML4-ALK variant 1 is detected only in the H3122 cell line at 28.671 cycles, whilst variant 3a/b is only detected in H2228 slightly later at 30.992 cycles. To determine if the assay was sensitive to small amounts of tissue, the experiment was repeated with only one 10µm section per cell line (figure 3.2-14). The HPRT1 signal was detected later than previously; between 30.229 and 32.420 cycles. A similar effect was observed for 18S where the mean C_T score shifted to between 11.644 and 14.609 cycles. EML4-ALK variants 1 and 3a/b were again only detected in their reported cell lines and were detected at slightly more cycles (29.282 and 32.466 respectively).

The assay was then utilised on ALK-positive patient tissue from the CHIARA trial, including primers targeting variants 2 and 5a and using H3122 and H2228 cytoblocks as positive controls for the reaction (figure 3.2-15). Patients 1-3 amplified HPRT1 at

mean C_T values of between 29.544 and 30.680 and 18S values between 9.261 and 14.319. However, no EML4-ALK variant was detected in any of these patients. Patients 4, 5, 6 and 9 amplified HPRT1 and 18S within the expected ranged and EML4-ALK variants were detected for each of these between 24.981 and 28.916 cycles. Patients 7, 8 and 10 had high mean C_T values for 18S and no EML4-ALK variant was detected.

To assess the effect of EML4-ALK variant on clinical response, patients with positive results for EML4-ALK were combined with response evaluation criteria (stable disease, progression, partial response, complete response) (**Table 3.2-1**). Sample 6 was positive for variant 1 and this patient's best response was assessed as having stable disease after ganetespib treatment. Two patients were positive for variant 2: one was assessed as having stable disease (sample 5) and one with progressive disease (sample 9). Finally, one patient was positive for EML4-ALK variant 3 and assessed as having progressive disease (sample 4).

A

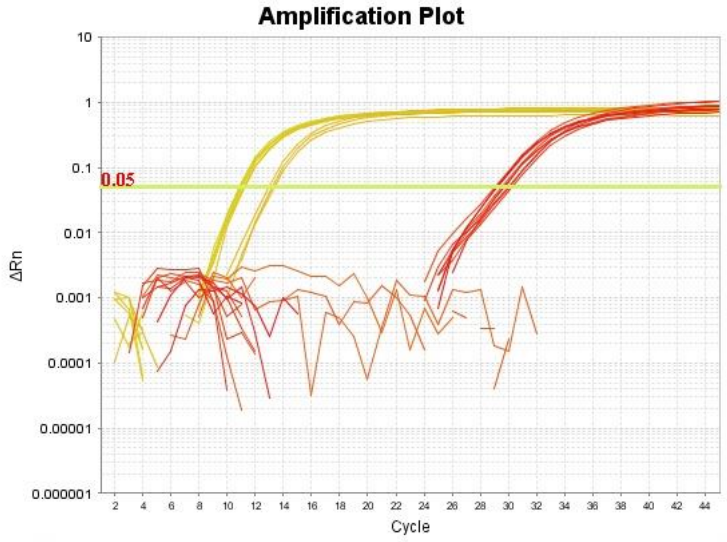

B

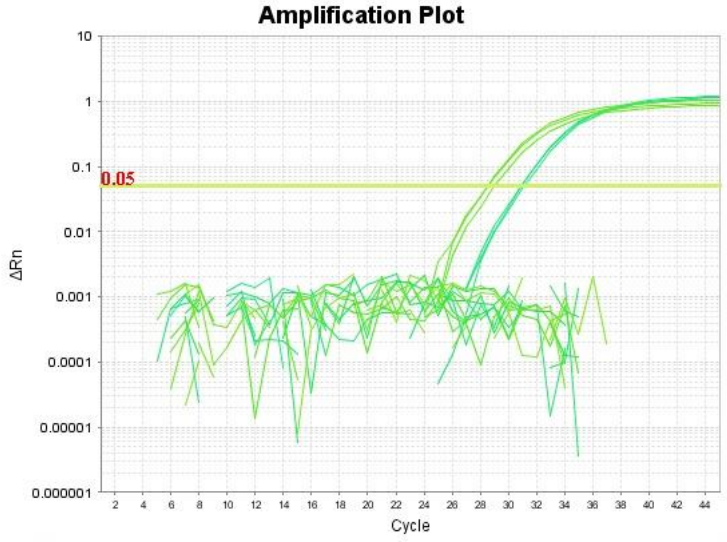

C

	Mean C_T Value			
Cell line	HPRT1	18S	EML4-ALK V1	EML4-ALK V3
H460	29.29	13.05	Undetermined	Undetermined
H3122	30.06	11.02	28.67	Undetermined
H2228	29.40	10.81	Undetermined	30.99

Figure 3.2-13 *RT-PCR analysis of HPRT1, 18S, EML4-ALK v1 and v3 using six 10µm sections from cytoblocks of H460, H3122 and H2228 cells.* ***(A)*** *Amplification plot for housekeeping genes HPRT1 (red) and 18S (orange)* ***(B)*** *Amplification plot for EML4-ALK variants 1 (green) and 3 (blue) using customised primers ΔRn set at 0.05.* ***(C)*** *Summary table of mean C_T (cycle threshold) values*

A

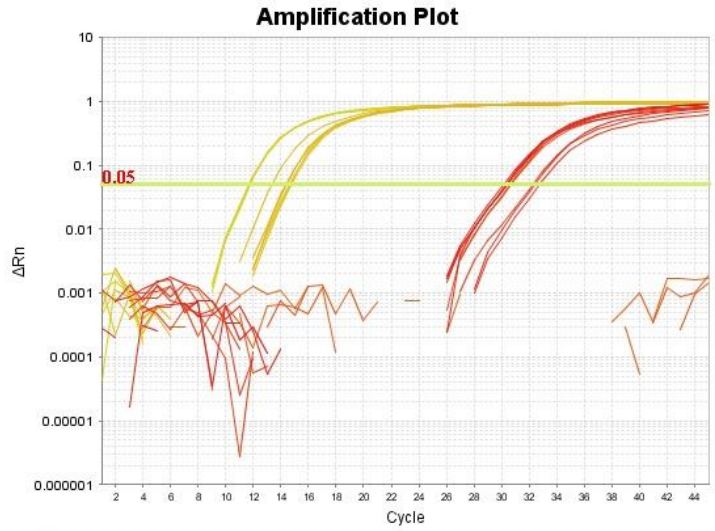

B

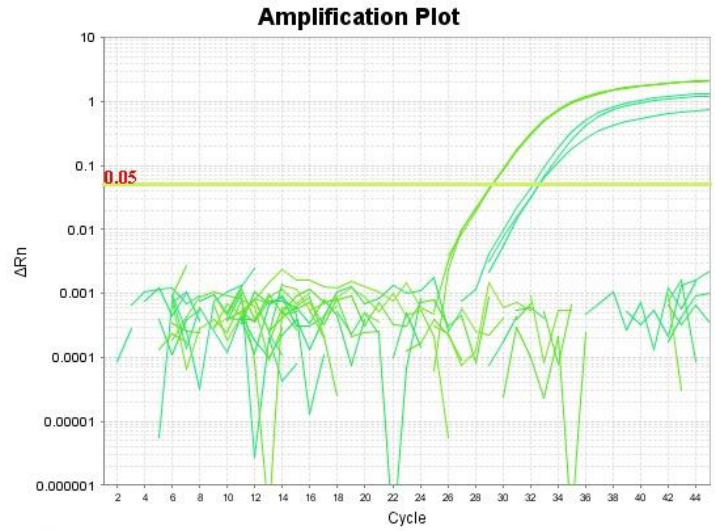

C

	Mean C_T Value			
Cell line	HPRT1	18S	EML4-ALK V1	EML4-ALK V3
H460	30.22	13.95	Undetermined	Undetermined
H3122	32.42	14.61	29.28	Undetermined
H2228	30.58	11.64	Undetermined	32.47

Figure 3.2-143.2-18 RT-PCR analysis of HPRT1, 18S, EML4-ALK v1 and v3 using one 10µm section per cytoblock of H460, H3122 and H2228 cells. (A) Amplification plot for housekeeping genes HPRT1 (red) and 18S (orange) (B) Amplification plot for EML4-ALK variants 1 (green) and 3 (blue) using customised primers. ΔRn set at 0.05. (C) Summary table of mean C_T (cycle threshold) values

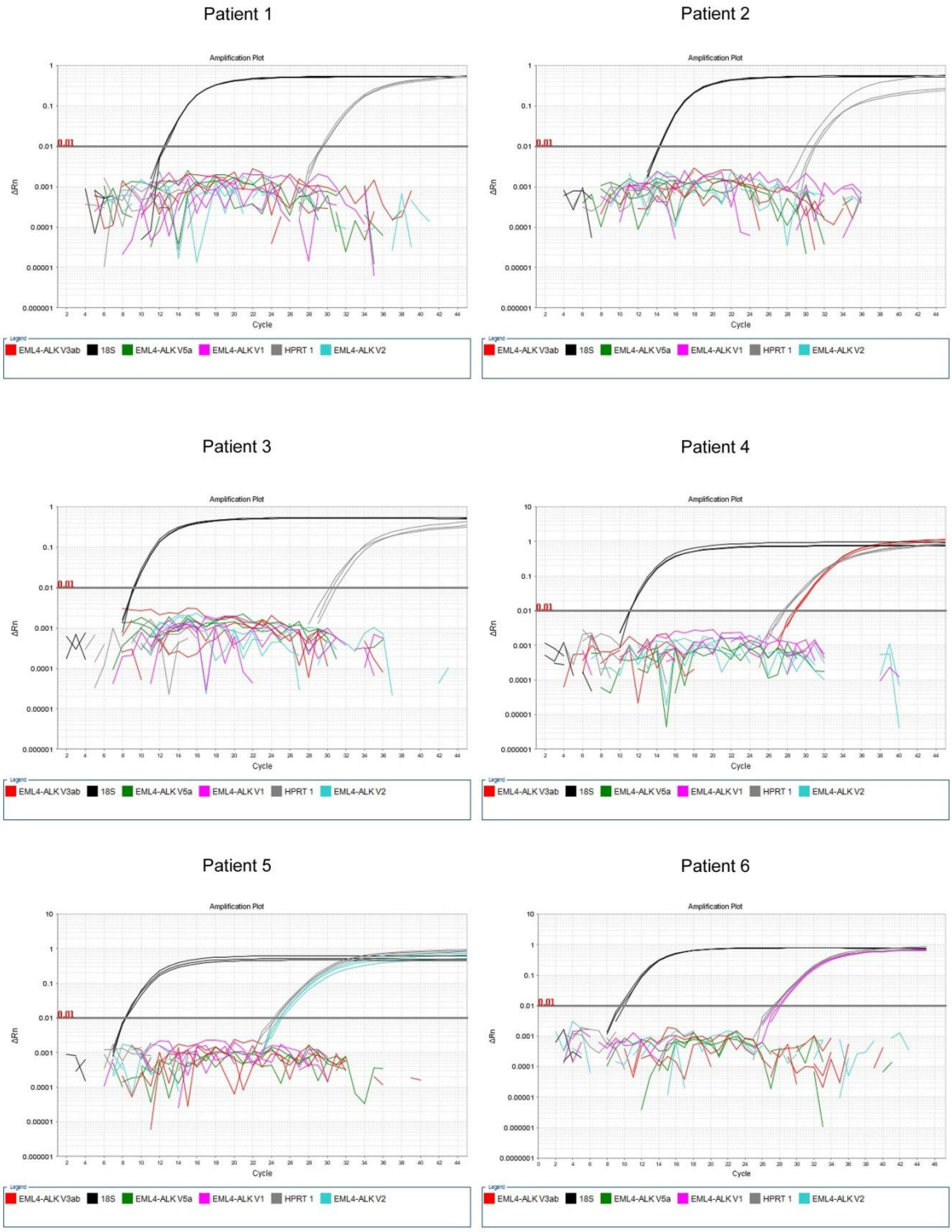

Figure 3.2-153.2-20 *Multiplexed RT-PCR analysis of HPRT1, 18S, EML4-ALK v1, v2, v3 and v5a on patient samples from the CHIARA clinical trial of ganetespib monotherapy in NSCLC. Amplification plots indicated the presence of HPRT1 (grey) and 18S (black) housekeeping genes and one of EML4-ALK variants 1 (pink), 2 (blue), 3 (red) or 5a (green). Summary table indicates mean cycle threshold values. UD=undetermined. ΔRn set at 0.01*

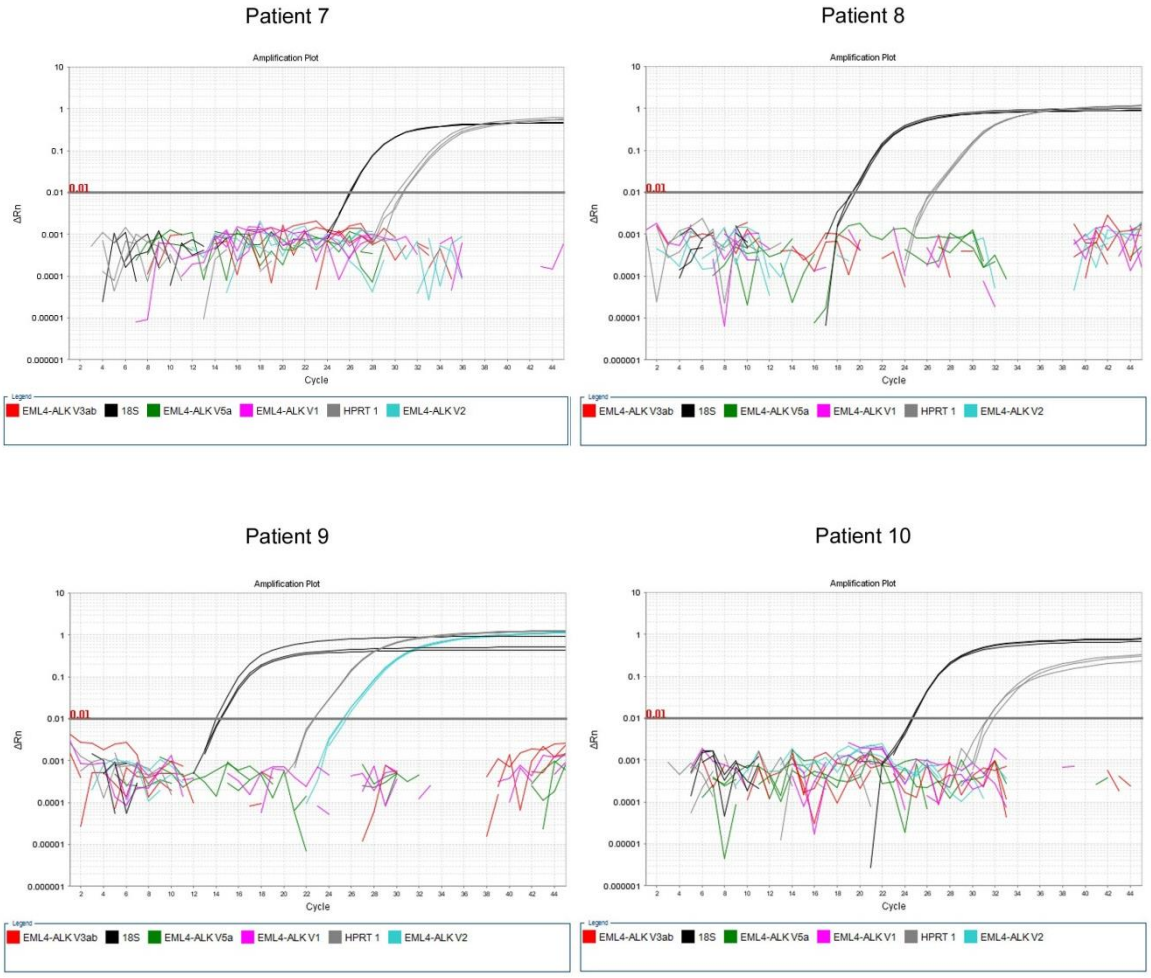

	Mean CT Value					
Patient	**HPRT1**	**18S**	**EML4-ALK V1**	**EML4-ALK V2**	**EML4-ALK V3ab**	**EML4-ALK V5a**
1	29.54	12.63	UD	UD	UD	UD
2	30.68	14.32	UD	UD	UD	UD
3	30.61	9.26	UD	UD	UD	UD
4	27.72	11.18	UD	UD	28.92	UD
5	24.44	8.39	UD	24.98	UD	UD
6	27.45	9.85	27.95	UD	UD	UD
7	30.66	26.01	UD	UD	UD	UD
8	26.61	19.65	UD	UD	UD	UD
9	22.799	14.307	UD	25.481	UD	UD
10	31.526	24.757	UD	UD	UD	UD

Figure 3.2-15 continued

Sample Number	Patient ID	Block ID	EML4-ALK variant	Breakpoint exons	Best response
1	0864-9B90	10-40178-D13	UD	UD	SD
2	0155-9A35	PVS11-17258-1A	UD	UD	SD
3	0667-9A25	4557/12	UD	UD	SD
4	0865-9A65	PS11-14030-A1	V3 (a/b)	E6:A20	PD
5	0864-9C57	CD12-9940	V2	E20:A20	SD
6	0864-9C25	H12-8081-A1	V1	E13:A20	SD
7	0864-9B04	LS12-8352-A1	UD	UD	PR
8	0718-9A02	CJ12-1807	UD	UD	SD
9	0718-9A11	12SJ-2086	V2	E20:A20	PD
10	0721-9B34	19597/09	UD	UD	SD

Table 3.2-1 *Summary table of patients achieving a positive result from EML4-ALK phenotyping and associated clinical response. PD = progressive disease, SD = stable disease, PR = partial response. UD = undetermined*

3.3 Discussion

The effective treatment of EML4-ALK fusion positive lung tumours was hailed as a key moment for personalisation of cancer therapy, as it took only 3 years from discovery by Soda *et al.* in 2007 to the first phase I clinical trial of the ALK-targeted therapy crizotinib in NSCLC patients in 2010 by Kwak *et al.* [116, 136]. However as previously discussed, several resistance mechanisms have been found to crizotinib and alternative therapeutic options have been sought, one of which is HSP90 inhibitors.

Early data, now published, suggested that the structure of the EML4 portion of the fusion protein, the TAPE domain, is important to its stability [224]. Longer EML4-ALK variants such as variants 1 and 2 have disrupted beta propellers (within the TAPE domain) revealing a large amount of hydrophobic core residues, suggesting increased instability [224]. It has been suggested that the inherent stability of proteins is a key factor in how much the HSP90 chaperone machinery is involved in propagating their development and survival in the cancer cell [77]. It was thus hypothesised that variants of EML4-ALK which are more unstable, are more dependent on HSP90 for stability and thus more sensitive to HSP90 inhibitors. Using transient EML4-ALK overexpression, stable exogenous expression and endogenous-expressing cell lines this work has clearly demonstrated *in vitro* downregulation of more unstable variants 1 and 2 which have a large region of exposed hydrophobic core, whereas variants without this exposed region like 3 and 5 are more resistant to degradation with HSP90 inhibitors. Furthermore, this difference in stability appears to translate into a small difference in cell viability, with variant 3-expressing H2228 cells displaying a reduced sensitivity to ganetespib. However, the difference is small (around 3-fold), plus cell viability reduced to only around 40% for each line. Alternative viability assays with a greater dynamic range may have aided this, in conjunction with detailed flow cytometry analysis to assess cell cycle arrest. Clearly there was no huge difference in sensitivity observed. The cell lines were also not characterised fully (doubling times etc) and so differences in IC50 value are difficult to compare.

Furthermore, transient variant 3 overexpression was unable to rescue H3122 cells from apoptosis or improve clonogenic survival. This suggests that whilst there is a difference in stability, it likely only has a small effect on sensitivity: perhaps other

mechanisms are at work, or perhaps the stress of the transfection was too much of a burden on the cell line. An inducible expression model of variant 3 in H3122 cells in *in vitro* and *in vivo* would likely solve this problem. Still, it seems unlikely that it would make a large difference in terms of clinical response, due to the markedly higher dose of ganetespib found in the blood of patients treated with the standard 200mg/m^2 of gantespib [225]. These studies should perhaps be altered to test the effect of a high dose of ganetespib for an hour, then removal of the drug to better reflect the fast rate of removal of ganetespib seen in the blood of patients [225]. This small difference in sensitivity may additionally be masked by resistant processes such as HSP72 upregulation as part of the stress response upon HSP90 inhibition or upregulation of antiapoptotic proteins such as BCL-xL. Drug removal via UGT1A metabolism and transport out of cells via P-gp may also be more important than EML4-ALK status [225]. In isogenic Ba/F3 models, again a small difference in response to increasing doses of ganetespib was observed between variants 1 and 3, with 3 proving less sensitive to the drug. The data also suggest a reduced apoptotic sensitivity. However again this is unlikely to be clinically relevant due to the comparatively low dose the cells receive. It may be worthwhile repeating these experiments in the context of HSP70 or UGT1A knockdown.

Whilst the attempt to produce ganetespib resistant Ba/F3 cells expressing EML4-ALK variant 1 was not successful in producing a logfold resistant cell line, minor interesting differences were observed in the less sensitive V1GD8 line including a reduced apoptotic activity and EML4-ALK protein persistence in response to ganetespib. However, these observations may be limited by possible differences in growth kinetics, and should be accounted for by simple growth curve assessment with trypan blue counts and cell cycle analysis to assess any differences in growth cycle. Further, assessment of known sensitivity mechanisms such as HSP72 and CUL5 should conducted. All these data have recently been confirmed in a paper by Heuckmann *et al.* [226]. This paper also demonstrates differential stability of EML4-ALK variants, with variants 1 and 2 classed as more sensitive, and variant 3 being less so. In addition, they go on to show by cyclohexamide-inhibited protein synthesis (cyclohexamide chase) experiments that EML4-ALK variant 3 is the most stable and further, that removal of

parts of the TAPE domain in variant 2 increases stability of these fusion proteins. Together these data support the hypothesis that EML4-ALK variants exhibit differential stabilities but not necessarily sensitivities to HSP90 inhibition, at least not to a clinically significant level. In addition, knockdown of BAX and BAK, the key proteins involved in mitochondrial outer membrane permeablisation in the EML4-ALK variant 1-dependent cell line H3122 did result in some reduction in apoptosis and subg1 cells after ganetespib exposure, suggesting some use of the intrinsic apoptotic pathway in this context, however many more cell lines dependent on EML4-ALK need to be tested for this. A further problem with some of these results is the lack of prove the effects observed is due to HSP90 inhibition: commonly HSP72 and known clients such as CDK4 are shown on blots to establish HSP90 inhibition. This would be done if the study was repeated.

There are additional experiments which would be valuable to furthering this story and provide more insight into how EML4-ALK variants behave with regards to HSP90 and HSP90 inhibitors. First, expanding the cell line set to include more lines expressing EML4-ALK endogenously would be valuable: if the effect described above is more pronounced in tumour xenografts, then it would be more convincing. Further, it would be useful to examine the stability of EML4-ALK variants without HSP90 inhibition, possibly by thermal denaturation studies. Moreover, studying the direct interaction of EML4-ALK variants with HSP90, perhaps by immunoprecipitation, could shed more light on the dynamics of the interaction, and site-directed mutagenesis could further pinpoint key residues responsible. However, these data, combined with the crystal structural studies with which this data has now been published, do give credence to the idea that structural disruption and protein instability are key criteria for HSP90 client selection.

Nevertheless, this reasoning is academic until tested in the clinical context. In an attempt to address this, a multiplexed real-time PCR approach was developed to specifically identify the EML4-ALK variant present in FFPE tissues from the CHIARA trial of ganetespib monotherapy in NSCLC samples. This approach has been trialled before with some success, though normally on flash-frozen tumour samples [124]. When tested with CHIARA patient FFPE samples, only 4 out of 10 produced a successful

phenotyping result. However, for many of these, the amount of tissue available was very small, and of poor quality as demonstrated by poor C_T values for housekeeping genes 18S and HPRT1. However, samples 1, 2 and 3 achieved good scores for these genes. Although all these patient samples had confirmed ALK translocation by FISH, it was worthwhile checking the ALK positivity of these samples by RT-PCR. Primers were designed against the cytoplasmic portion of ALK only, and all three of these samples tested positive, suggesting that it was indeed tumour tissue being used, rather than normal sample contamination (data not shown). In order to identify the EML4-ALK variants present, one option would be to use 5' Rapid Identification of cDNA Ends (5'RACE) to determine the nucleic acid sequence before the cytoplasmic ALK portion, thus determining the fusion partner: a precedent for this was set with the discovery of the KLC1-ALK fusion [227].

The assay is suitable for further development to enable higher detection rates: this could be achieved on older FFPE samples of patients confirmed to have ALK translocations by FISH. To improve RNA retrieval and detection, a tRNA or glycogen carrier could be employed. The assay should be expanded to include other variants of EML4-ALK and other ALK translocations such as KIF5b-ALK. Still, the amount of tumour tissue available and its quality is key to success, and should be consider as a priority rather than an afterthought when designing clinical trials. Often biopsies can be difficult to obtain or involve a significant amount of unpleasantness for the patient. Biopsies were required for this trial, however samples were needed for other research, limiting the amount available for this project. There are also issues surrounding contamination, quality control and administrative support, however establishing SOPs should circumvent these problems [228]. It would also be useful to obtain multiple sites of the tumour if possible to assess for heterogeneity of EML4-ALK expression, as such as study is yet to be conducted. However, the limiting factor may be the amount of clinical trial tissue available from HSP90 inhibitor monotherapy studies, so it might be worthwhile trialling the technique further on xenografts. If possible, it would be useful to see if EML4-ALK variant status can be reliably called from circulating tumour DNA (ctDNA). This would allow for a rapid, less invasive diagnostic test. The clinical data available for this study was limited to best response, and while the variant 3

expressing patient had progressive disease as may be expected, and a variant 1 and one variant 2 patient had stable disease, paradoxically another variant 2 patient had progressive disease. Ultimately this does not provide enough data to link EML4-ALK variant status to clinical response of patients treated with HSP90 inhibitors, despite the interesting pre-clinical data.

Chapter 4 – Investigating intrinsic resistance to HSP90 inhibition in a NSCLC cell line

4 Investigating intrinsic resistance to HSP90 inhibition in a NSCLC cell line

4.1 Introduction

Efforts to understand mechanisms of sensitivity and resistance to HSP90 inhibitors began with some of the first inhibitors to enter the clinic: 17-AAG and 17-DMAG, which appeared to show little efficacy in clinical trials and were ultimately unsuccessful, in part due to increased liver toxicity [30]. Hyperacetylation of HSP90 leads to a higher affinity for 17-AAG: greater degradation of HSP90 clients and reduced clonogenic survival [160]. Overexpression of the drug efflux pump P-gp leads to resistance to 17-AAG and 17-DMAG due to rapid elimination of the drug from cancer cells [163-165]. NQO1 metabolises 17-AAG and 17-DMAG into more potent hydroquinone forms: cancer cells with reduced expression of this key drug metaboliser reduces sensitivity [167, 168]. Further still AHA1 knockdown has been shown to increase sensitivity to HSP90 inhibitors: AHA1 boosts HSP90 ATPase function, and reduction of AHA1 decreased the phosphorylation important signalling proteins like MEK and ERK. It's possible that knockdown of AHA1 isolates HSP90's activation and stabilization roles [75].

Knowledge of mechanisms of resistance to the latest HSP90 inhibitors in development is more limited. PTEN expression has been shown to modulate the ability of AUY922 to inhibit proliferation and AKT and ERK activity in oesophageal cancer cell lines [229]. A recent study demonstrated that sensitivity to ganetespib is linked to MCL-1 addiction: cells which downregulate MCL-1 in response to HSP90 inhibition are sensitive whilst those that do not are resistant [230]. Upon the acquisition of resistance after multiple rounds of ganetespib treatment, a switch in BCL-2 protein dependence occurs which is vulnerable to a synergistic combination of HSP90 inhibitor and BH3-peptidomimetics such as ABT-737. UGT1A catalyses the addition of UDP-glucuronic acid to small molecules which increases their solubility and aids excretion [169]. Ganetespib has two glucuronide metabolites (STA-12-0671 and STA-12-0672) with half-lives ranging from 6.32 to 27 hours [225]. UGT1A expression levels are correlated with sensitivity to ganetespib in a panel of colorectal cancer cells, with higher levels leading to increased resistance, and inhibition of UGT1A activity led to increased sensitivity to ganetespib in

intrinsically resistant colorectal and FGFR3-fusion positive bladder cancer cells [170, 171].

The aim of this chapter is to determine potential intrinsic resistance mechanisms in the NSCLC setting. First, resistant and sensitive cell lines must be identified and characterised: resistant cell lines with intrinsic resistance may be difficult due to the potency and high affinity of ganetespib for HSP90. However, this will be a pilot project to compare a resistant and sensitive cell line which can later be expanded into a large panel of fully validated cell lines. This is followed by examining known resistant mechanisms to ganetespib and determining if they apply in this cancer subtype.

Aims and rationale

- Identify at least two cell lines with logfold IC_{50} differences in sensitivity to ganetespib (any cell line with IC_{50} over 500nM will be considered resistant as for bladder cancer cell lines in a previous study [171]) in order to illuminate potential intrinsic resistance mechanisms
- Profile oncogenic signalling pathways and assess addiction to MCL-1 to see if the effects our lab has observed in mesothelioma-derived cell lines with acquired resistance appear in this new context
- Probe potential mechanisms of resistance and attempt rescue of sensitivity, starting with the previously reported UGT1A metabolic mechanism

4.2 Results

4.2.1 Calu-3 cells are resistant to HSP90 inhibition

To assess potential mechanisms of intrinsic resistance to HSP90 inhibitors, a resistant cell line must first be identified and characterised. To address this, 72-hour dose response viability assays were conducted for four HSP90 inhibitors including a geldanamycin derivative (17-AAG), a novel purine-based drug (PU-H71), the natural HSP90 inhibitor radicicol and the drug under study, ganetespib, to provide a range of drug potencies and structural characteristics. This will be in the lung adenocarcinoma cell lines Calu-3 and NCI-H460, which are two non-small cell cancer lines readily available in the lab (figure 4.2-1). Calu-3 IC_{50} values were consistently over 1μM for all drugs tested: ganetespib IC_{50} – 2640nM (95%CI 2322-3001nM); PU-H71 IC_{50} – 1905nM (95%CI 1633-2221nM); 17-AAG IC_{50} – 1165 (95%CI 1066-1274nM); radicicol IC_{50} – 24545nM (95%CI 17240-34946nM). Conversely, NCI-H460 cells consistently reported much lower IC_{50} values: ganetespib IC_{50} – 49.61nM (95%CI 44.53nM – 55.26nM); PU-H71 IC_{50} – 295.4nM (95%CI 271.0-321.9nM); 17-AAG IC_{50} – 16.57nM (95%CI 13.86-19.81nM); radicicol IC_{50} – 1532nM (95%CI 1323-1775nM). There appears to be a broadly similar pattern for all the drugs used. As a consequence, Calu-3 and H460 cell lines were determined to be resistant and sensitive to HSP90 inhibition respectively for the purpose of this study.

HSP90 inhibition is known to downregulate multiple oncogenic pathways and in some cases induce apoptosis. This was assessed in Calu-3 and H460 cell lines by drugging them with logfold doses of ganetespib and assessing the effect on apoptosis and downstream signalling by western blot (figure 4.2-2)(A). PARP cleavage as an apoptotic marker is observed in H460 cells at 200nM and above, whereas no PARP cleavage is seen in Calu-3 cells even at 2000nM. There is also clear dephosphorylation of AKT at serine 473, ERK and STAT3 and degradation of AKT and STAT3 in H460 cells from 200nM, which is not seen in Calu-3 cells at all. Additionally, at this concentration downregulation of the key antiapoptotic protein MCL-1 is only seen in H460 cells, not Calu-3 cells. The effect of these doses of ganetespib on the cell cycle was also assessed (figure 4.2-2). **(B)**). The fraction Calu-3 cells in subG1 increased slightly from 2.96% for

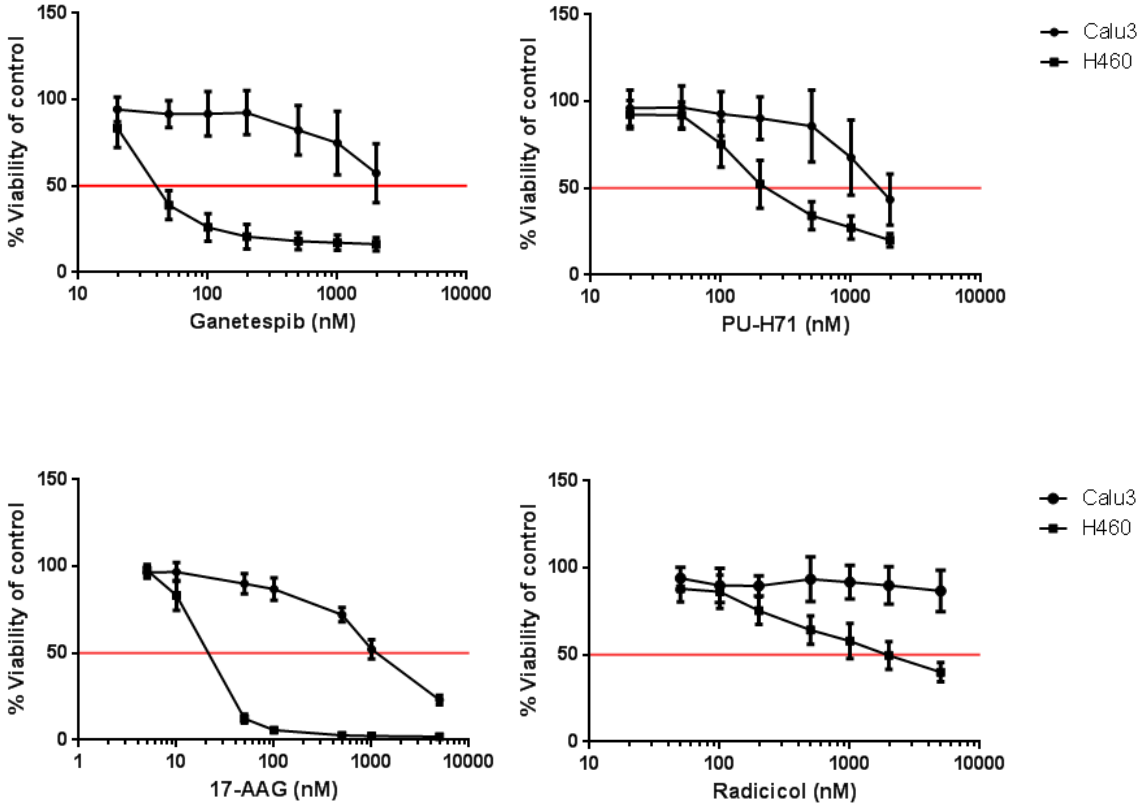

IC50s (nM)		
Drug	**Calu3 (95% CI)**	**H460 (95% CI)**
Ganetespib	2640 (2322-3001)	49.61 (44.53-55.26)
PU-H71	1905 (1633-2221)	295.4 (271.0-321.9)
17-AAG	1165 (1066-1274)	16.57 (13.86-19.81)
Radicicol	24550 (17240-34950)	1532 (1323-1775)

Figure 4.2-1 *Calu3 cells are resistant to various HSP90 inhibitors. 72h dose-response viability assays were conducted for Calu3 against the HSP90 inhibitor-sensitive line H460 for ganetespib, PU-H71, 17-AAG and radicicol and IC_{50} values calculated with non-linear regression. Error bars represent standard deviation. N=3 biological replicates for all drugs*

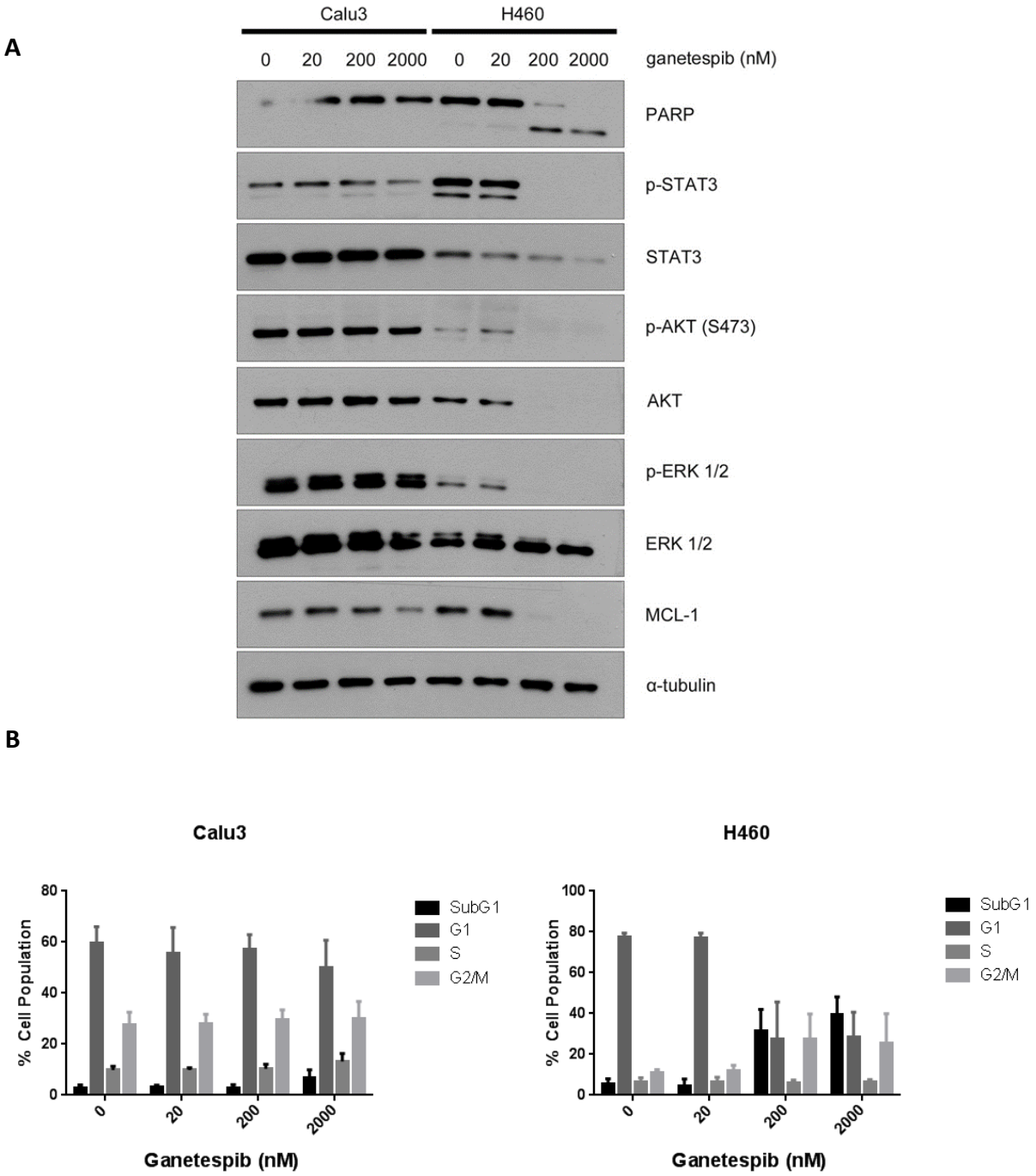

Figure 4.2-2 *Calu3 cells are less susceptible to ganetespib-induced apoptosis. (A) Calu3 and H460 cells were subjected to 0, 20, 200 or 2000nM ganetespib for 48h and assessed for apoptosis and downstream signalling by western blot. (B) The effect on cell cycle was assessed by propidium iodide staining and flow cytometry analysis. N=3 biological replicates*

untreated cells to 6.96% at 2000nM ganetespib. By contrast, H460 cells increased this fraction from 5.47% to 31.7% at only 200nM, and increased further to 39.7% at 2000nM ganetespib. There was a concurrent reduction of cells in G1 phase (0nM - 77.4%, 200nM – 27.6%) and increase in G2/M phase cells (0nM – 10.8%, 200nM – 25.6%) for H460 cells, all suggestive of increased cell cycle arrest and cell death. Calu-3 cells displayed a much smaller drop of cells in G1 (0nM – 59.5%, 2000nM – 49.9%) and a very slight increase in cells in G2/M phase (0nM - 27.7%, 2000nM - 29.9%) suggesting ganetespib has little effect on the cell cycle in this line.

4.2.2 Calu-3 cells display high levels of HSP72 and do not downregulate key antiapoptotic proteins

In order to understand why Calu-3 cells appear resistant to HSP90-induced apoptosis, both Clau-3 and H460 cells were drugged with an intermediate concentration (200nM) of ganetespib for 48h and analysed by western blot (figure 4.2-3)(A). Again, PARP cleavage and downregulation of key oncogenic signalling was observed in H460 cells but not Calu-3 cells. Further, as has been previously reported, levels of the chaperone HSP72 were upregulated in response to HSP90 inhibition in H460 cells, however the level of HSP72 is already notably higher in untreated Calu-3 cells than untreated H460 cells. Furthermore, whilst MCL-1 and BCL-xL are downregulated in response to HSP90 inhibition in H460 cells, this is not observed in the Calu-3 cell line. Previous work has shown that MCL-1 addicted cells undergo apoptosis in response to HSP90 inhibition via downregulation of MCL-1 mediated by STAT5A [230]. To assess the role of BCL-2 family antiapoptotic proteins in sensitivity to HSP90 inhibition, Calu-3 cells were dosed with 200nM ganetespib and 1µM ABT-737 (a small molecule inhibitor of BCL-2, BCL-xL and BCL-w) independently or together, for 48h and compared to the MCL-1 addicted cell line MSTO (figure 4.2-3)(B). No PARP cleavage was observed after this combination treatment. Furthermore, MCL-1 silencing in Calu-3 cells did not induce PARP cleavage, additionally confirming that the Calu-3 cell line is not addicted to MCL-1 (figure 4.2-3)(C).

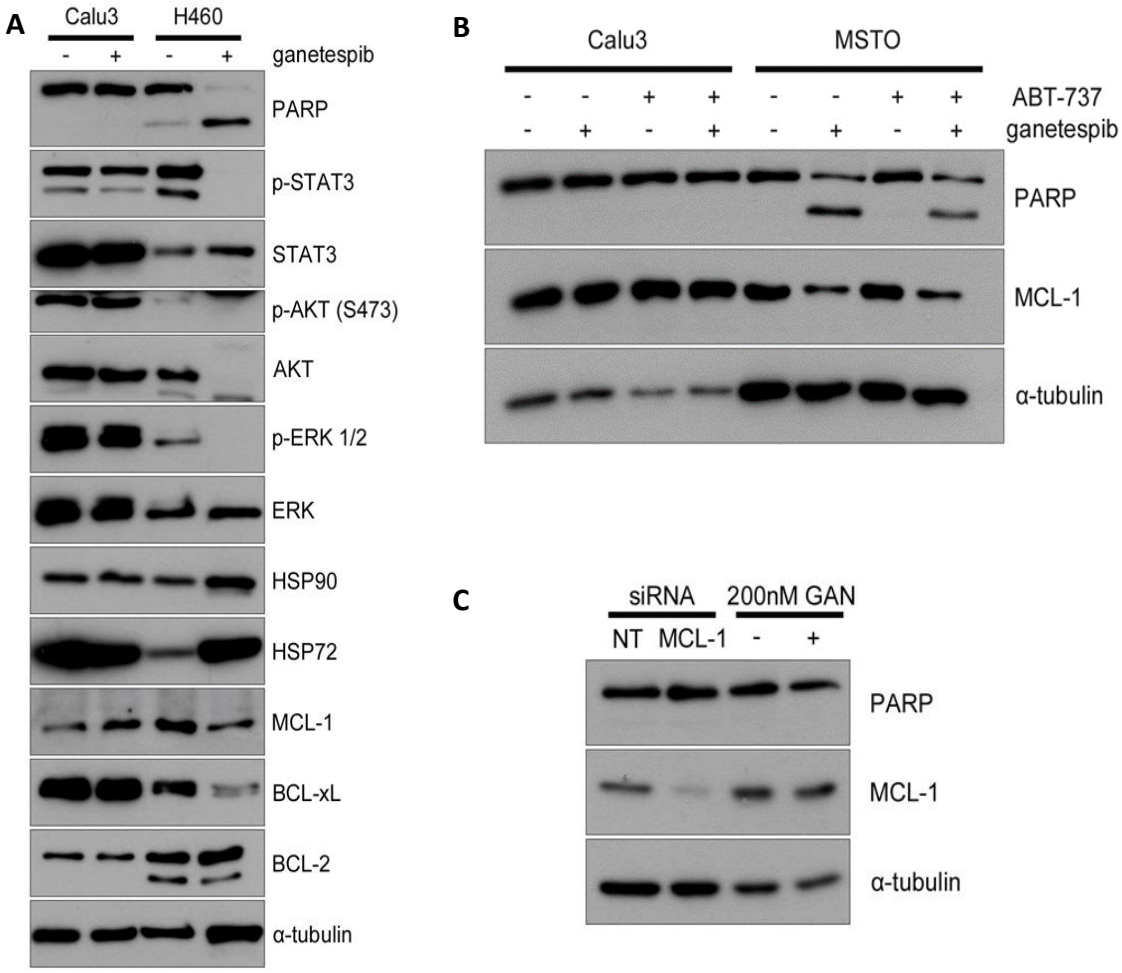

Figure 4.2-3 *Profiling of Calu-3 cells with and without ganetespib treatment* ***(A)*** *Calu-3 and H460 cells were treated with or without 200nM ganetespib for 48h and analysed by western blot.* ***(B)*** *Calu-3 and MSTO cells were treated with or without 200nM ganetespib and 1μM ABT-737 independently and together for 48h and assessed for PARP cleavage and MCL-1 expression by western blot* ***(C)*** *Calu-3 cells were transfected with siRNA against MCL-1 or treated with 200nM ganetespib for 48h and assessed for PARP cleavage and MCL-1 expression by western blot. All blots are representative of n=3 experiments.*

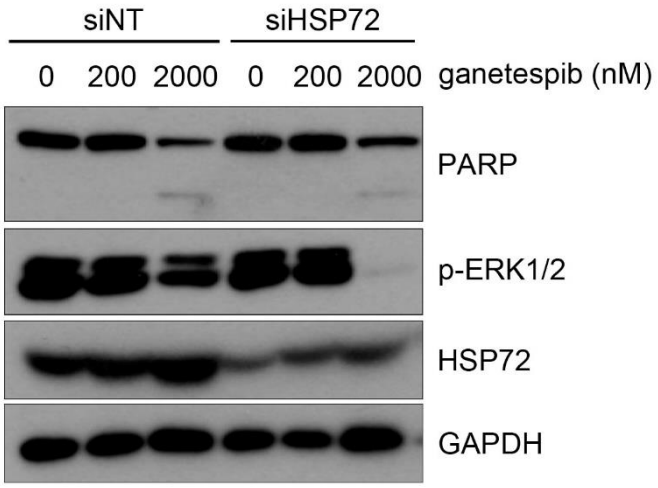

Figure 4.2-4 *Knockdown of HSP72 in Calu-3 cells does not affect sensitivity to ganetespib in Calu-3 cells. Calu-3 cells were transfected with scrambled negative control siRNA and siRNA against HSP72 and subsequently treated with 200 or 2000nM ganetespib and analysed by western blot. Representative of n=3 experiments*

4.2.3 Downregulation of HSP72 does not induce apoptosis in response to ganetespib in Calu-3 cells

It has been previously reported that HSP72 is a key mediator of HSP90 inhibitor sensitivity, and downregulation of this protein sensitises cells to 17-AAG [83]. In order to examine if HSP72 mediates Calu-3 resistance to ganetespib, cells were subjected to 100nM siRNA targeted against HSP72 for 48h followed immediately with 200 or 2000nM ganetespib for a further 48h (figure 4.2-4). Western blot revealed no increase in PARP cleavage in treated cells compared with cells transfected with negative control siRNA. HSP72 appeared to be knocked down considerably, although not completely after RNAi. Interestingly, ERK seems to be dephosphorylated when HSP72-downregulated cells were treated with 2000nM ganetespib.

4.2.4 Calu-3 cells recover oncogenic signalling pathways after early inhibition by ganetespib

Given that an HSP90 inhibitor such as ganetespib has pleiotropic effects on cancer cells it is surprising curious that no perturbation in any signalling pathways was observed. To understand this in more detail, Calu-3 and H460 cells were subjected to 200nM ganetespib for a time course of 0, 4, 8, 16, 24 and 48 hours (figure 4.2-5). ERK is dephosphorylated in H460 cells by 16h and concurrent PARP cleavage is observed. MCL-1 is additionally downregulated by 24h. Conversely, by only 4 hours, Calu-3 cells appear to reduce phosphorylation of ERK, though not completely, which is then rescued at 8 hours and stronger ERK phosphorylation is seen after this time point. No PARP cleavage or MCL-1 downregulation was observed in Calu-3 cells.

4.2.5 Calu-3 cells convert ganetespib to a glucuronidated metabolites

The initial downregulation and subsequent recovery of oncogenic signalling pathways in Calu-3 cells is suggestive of drug excretion, inactivation and/or metabolism. A precedent has been noted for ganetespib to be converted to a glucuronidated metabolite [170, 171]. To assess if this is the case in Calu-3 cells, LC-ESI-MS/MS mass spectrometry experiments were performed on the cell media of Calu-3 and H460 cells treated with ganetespib for 48 hours (note samples were prepared by myself and kindly run by Dr. Rajinder Singh, University of Leicester) (figure 4.2-6)). Ganetespib was detected at all time points in both cell lines in the cell media between 13.50 and 13.92

minutes. Conversely, two stereoisomer forms of glucuronidated ganetespib were detected at 48 hours in Calu-3 cell lysate and cell media between 11.91 and 12.83 minutes, and no glucuronidated peaks were detected in H460 cells. No sulphated metabolites of ganetespib were detected in either cell line.

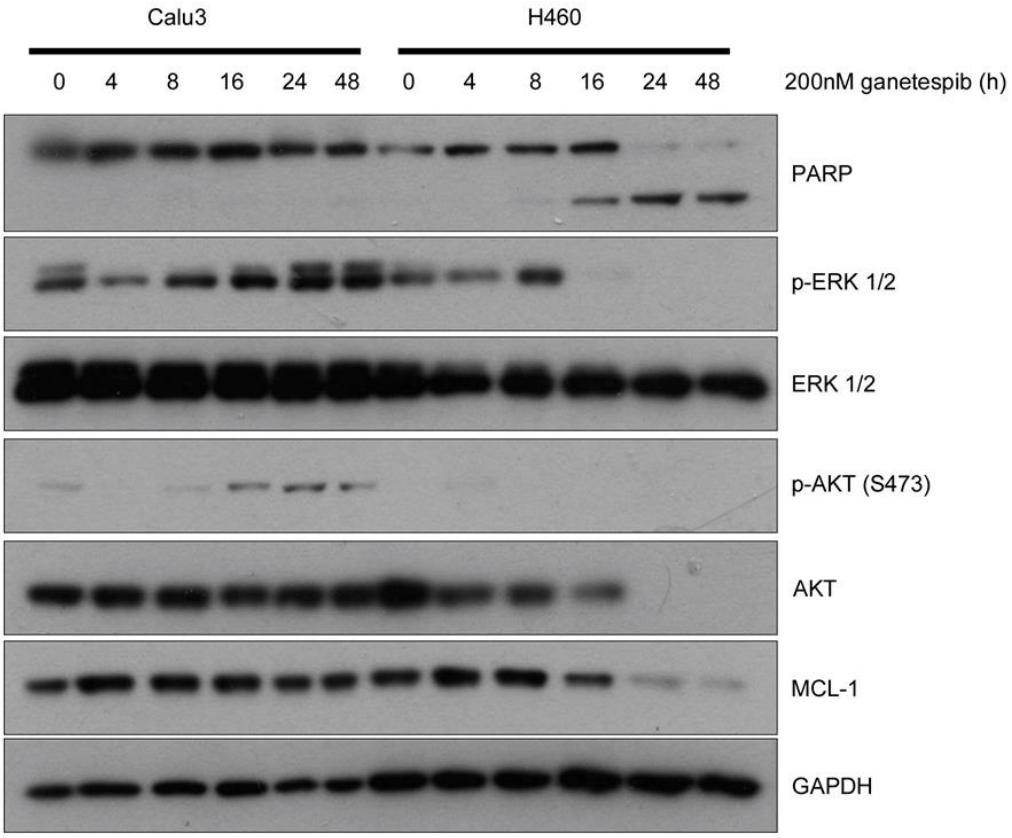

Figure 4.2-5 *Calu-3 cells recover oncogenic signalling pathways over time. Calu-3 and H460 cells were treated with 200nM ganetespib for 0, 4, 8, 16, 24 and 48h timepoints and assessed for apoptosis and oncogenic signalling pathways by western blot. Representative of n=3 experiments*

Calu-3

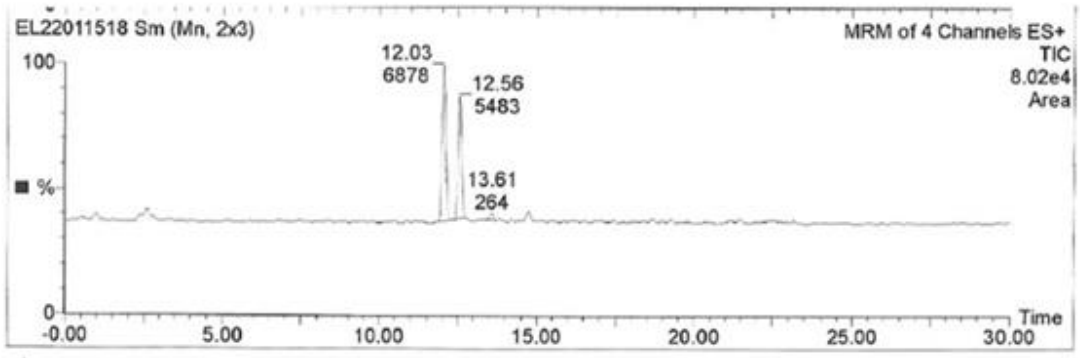

H460

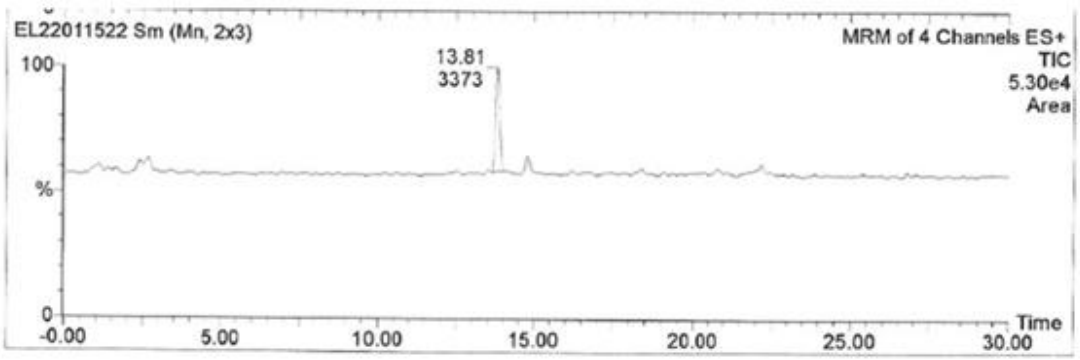

Figure 4.2-6 *LC-ESI-MS/MS summary profiles of Calu-3 and H460 cell media treated with 200nM ganetespib for 48h. Time is inidicated in minutes for each peak followed by the m/z value. Peaks between 13.50 and 13.92 minutes represent unmetabolised ganetespib, whilst peaks between 11.91 and 12.83 minutes indicate glucuronidated ganetespib metabolites. Representative of n=3 experiments*

4.2.6 Calu-3 cells display high levels of UGT1A, but knockdown has no effect on signalling or apoptosis with concurrent ganetespib treatment

It has been reported in previous studies of colorectal and bladder cancer that UGT1A expression is linked with resistance to ganetespib, as it catalyses the addition of glucuronic acid to small molecules, making them more hydrophilic thus aiding excretion from cells [169-171]. Western blot analysis indeed reveals a high expression level of UGT1A in Calu-3 cells, but was undetectable in H460 cells (figure 4.2-7)(A). To assess if expression of UGT1A was responsible for resistance to ganetespib, Calu-3 cells were transfected with siRNA targeted against all UGT1A variants with or without 48h ganetespib treatment (figure 4.2-7)(B). Although UGT1A was efficiently knocked down, no PARP cleavage nor perturbation of signalling pathways after ganetespib treatment was observed. Furthermore, no evidence of apoptosis was observed by caspase 3/7 assay in cells transfected with UGT1A siRNA after ganetespib was added (figure 4.2-7)(C).

4.2.7 Addition of curcumin to ganetespib treatment of Calu-3 cells does not affect oncogenic signalling pathways nor apoptosis

It has been demonstrated that curcumin directly inhibits UGT1A activity in HEK293 and LS180 cells [231]. To confirm that inhibition of UGT1A does not cooperate with ganetespib to downregulate oncogenic signalling, first a maximum tolerated dose (MTD) of curcumin was calculated (figure 4.2-8)(A)**.** The dose response viability curve for curcumin reveals an IC50 value of 8.22µM, (95%CI 7.043-9.593µM). The concentration at which no effect on viability is observed is 1µM for Calu-3 cells. Combining 1µM curcumin with 200nM ganetespib for 48h did not have any noticeable effect on downstream signalling or apoptosis for these cells as seen by western blot (figure 4.2-8)(B).

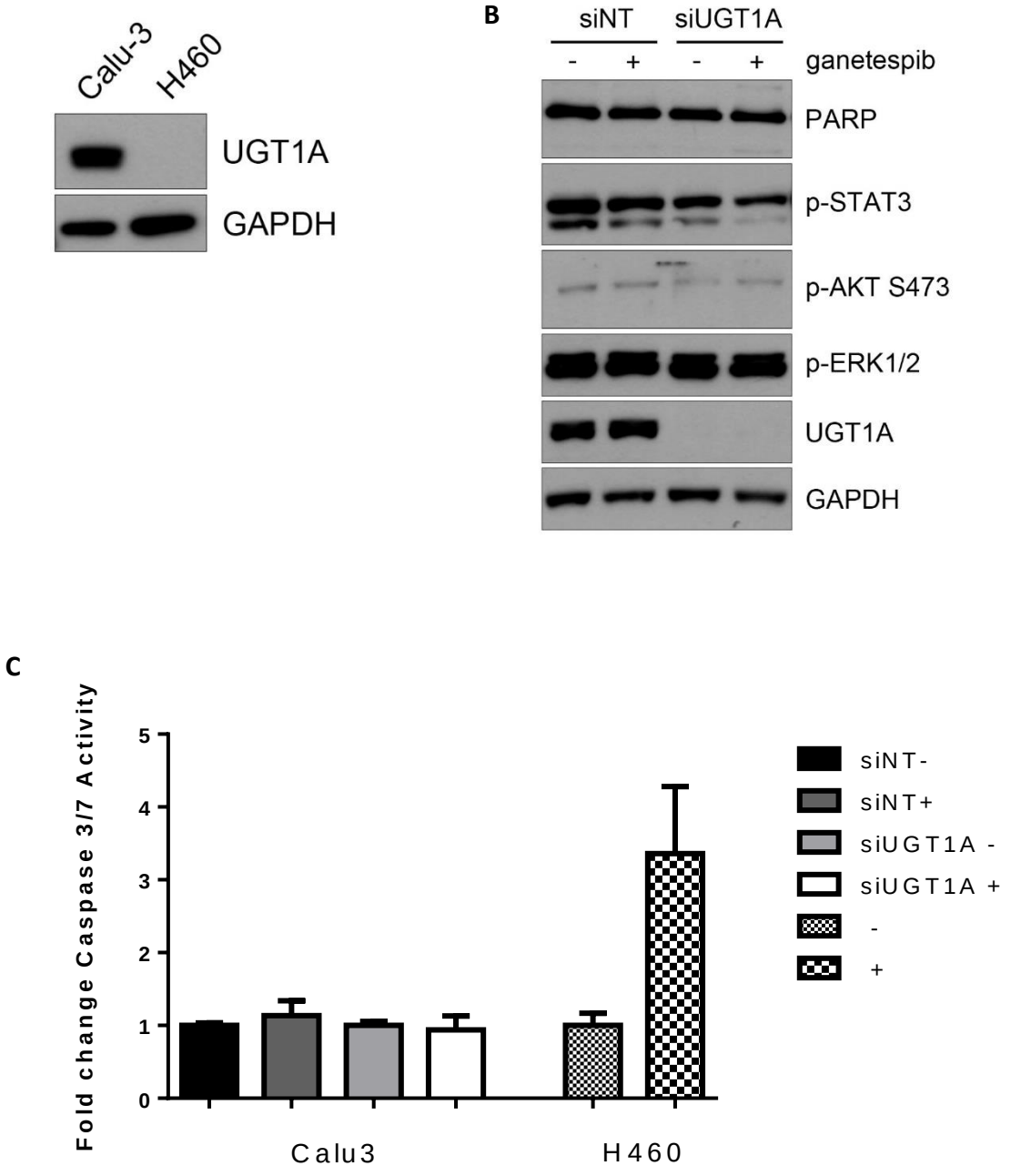

Figure 4.2-7 *The role of UGT1A in resistance to HSP90 inhibition in Calu3 cells* ***(A)*** *Western blot of UGT1A expression in Calu3 and H460 cells (n=3)* ***(B)*** *Western blot of Calu-3 cells transfected with negative control (NT) or UGT1A-targeted siRNA with or without 48h 200nM ganetespib (n=2).* ***(C)*** *Caspase3/7 assay of Calu-3 cells transfected with negative control (NT) or UGT1A-targeted siRNA with or without 48h 200nM ganetespib exposure. H460 cells with or without 200nM ganetespib were used as a positive control for apoptosis (n=2)*

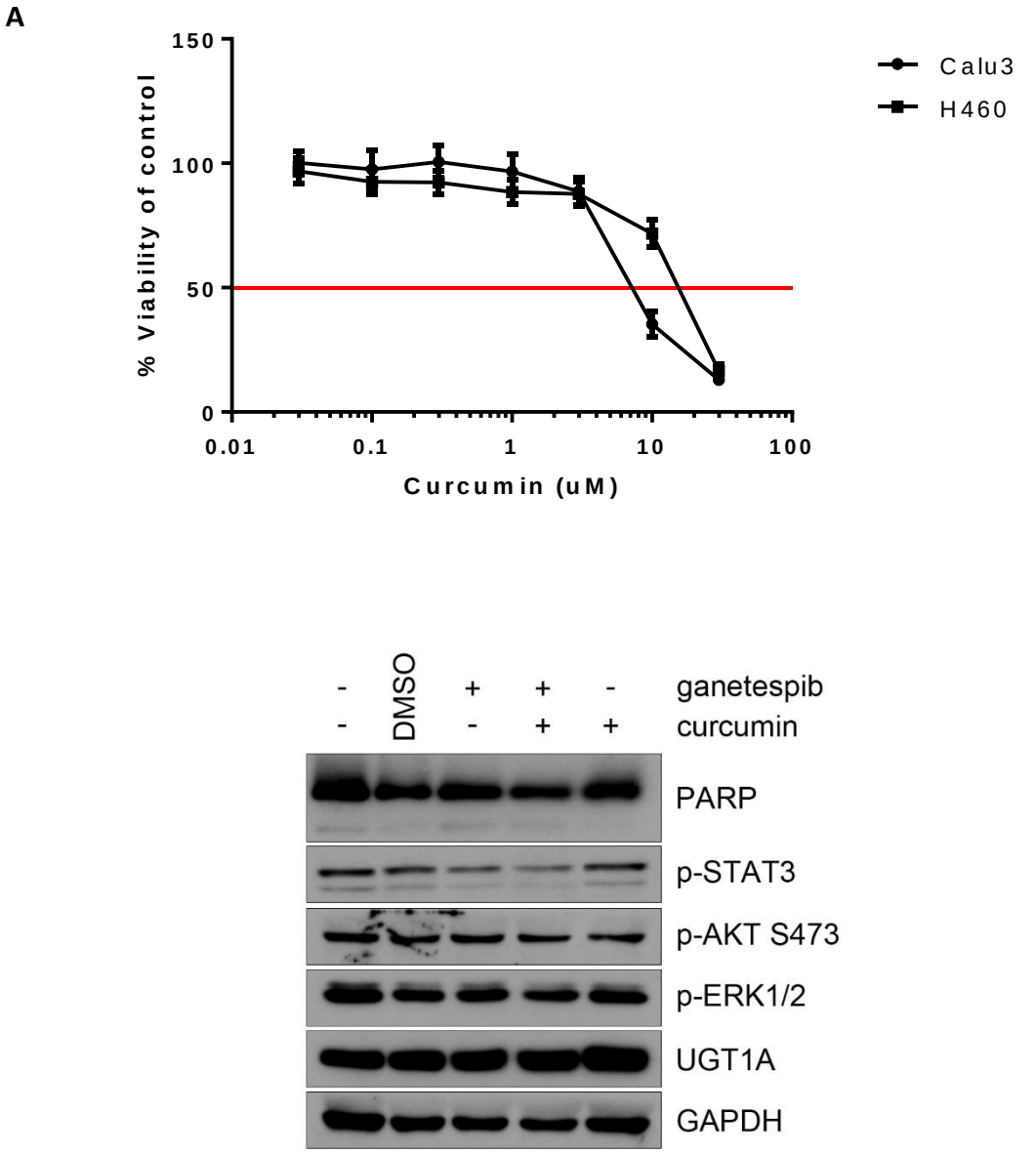

Figure 4.2-8 *The effect of combination treatment of ganetespib plus curcumin in Calu-3 cells.* ***(A)*** *72h dose response viability assay in Calu3 (IC50 8.22µM, 95%CI 7.043-9.593µM) and H460 (IC50 14.24µM, 95% CI 12.15-16.69µM) cells for curcumin.* ***(B)*** *Western blot of Calu3 cells treated for 48h with or without 200nM ganetespib and 1µM curcumin. Represents n=3 replicates*

4.2.8 Discussion

Utilising HSP90 inhibition to negatively regulate multiple oncogenic signalling pathways simultaneously in cancer has been a key goal for some time. HSP90 inhibitors selectively target cancer cells, likely due to the increased burden of mutated proteins and a high affinity conformation of HSP90 in tumour cells [90]. Despite the development of many second generation HSP90 inhibitors such as AUY922 and ganetespib, to date clinical trials have produced mixed results. Therefore, efforts to understand mechanisms of sensitivity and resistance to the latest HSP90 inhibitors is an ongoing task. In this chapter, two NSCLC cell lines were tested for sensitivity to a range of HSP90 inhibitors: Calu-3 cells were determined to have logfold higher IC_{50} values for ganetespib, 17-AAG and radicicol and a six times higher IC_{50} value for PU-H71 than H460 cells. Calu-3 and H460 cells were subsequently taken forward as representative resistant and sensitive lines for study. Though reasonable for a pilot study such as this, many more resistant and sensitive NSCLC lines should be tested for the results to be more robust. These cell lines should also be better characterised with knowledge of cell doubling times and drug accumulation in order to achieve a better comparison. A panel of NSCLC should be tested for sensitivity to a range of HSP90 inhibitors inclusive of second generation in-trial inhibitors such as AUY922. Once a range of IC_{50} values were produced, bioinformatics analysis using the Catalogue of Somatic Mutations in Cancer would be useful to attempt groupings and look for common mutations. Failing that, microarrays could be conducted to assess mRNA expression levels and pathway analysis may identify key signalling networks in sensitive and resistant cell line sets. Furthers, drugs which are known to be affected by transporters such as cisplatin, or by UGT1A such as curcumin could be utilised to rule out potential mechanisms of resistance in the panel of cell lines. It would then be interesting to look at xenografts of some of these cells lines, and assess ganetespib metabolites in the plasma in a quantitative fashion.

HSP90 inhibitors have been shown to downregulate several oncogenic signalling pathways simultaneously and induce apoptosis in some contexts. No such effect was observed in Calu-3 cells at even 2000nM ganetespib, and there was little perturbation on the cell cycle, suggesting these cells are rapidly eliminating the drug from the cell or

the drug is unable to inhibit HSP90 within the cell. Ganetespib is known to be a soluble drug, however use of fluorescently tagged ganetespib could be useful in assessing the speed of the drug entering and exiting the cell lines. No HSP90 mutations have been reported to date as a mechanism of drug resistance, so this seems unlikely. Recent work from our lab demonstrated that MCL-1 addiction is key to apoptotic response after HSP90 inhibition [230]. Calu-3 cells fit this model as they represent a resistant cell line which does not undergo cell death after MCL-1 downregulation. Further, there is no perturbation of key anti-apoptotic BCL-2 family members, nor is there synergism of ganetespib with the BCL-2 family inhibitor ABT-737. It might be useful to complete this work by dynamically profiling BH3 proteins in response to HSP90 inhibition at earlier time points, as previously demonstrated in [232, 233]. These Calu-3 cells may be resistant to a broader panel of drugs rather than just HSP90 inhibitors, and this may give a clue to their underlying resistance, for example high levels of p-gp.

Normally in after HSP90 inhibition, HSP72 is upregulated as part of the heat-shock response, and knockdown of this chaperone has been demonstrated to improve sensitivity to 17-AAG [83]. In this case, no increase in PARP cleavage was observed after HSP72 knockdown and ganetespib treatment, although ERK dephosphorylation occurred at the highest concentration, suggesting HSP72 does have some role in maintaining oncogenic signalling. It is possible HSC70, another HSP70 family member demonstrated to be important in response to HSP90 inhibition, can compensate for loss of HSP72. HSP72 in Calu3 cells was found to be at a very high level and did not appear to be induced in response to HSP90 treatment as may normally be expected via HSF1 activation. However, this does not appear to be the case, although it is possible that the exposure time and/or antibody optimisation may need to be improved.

Drug metabolism has previously been demonstrated to improve efficacy of 17-AAG via conversion to a more active form via NQO1 [167, 168]. For ganetespib, UGT1A has been identified as a group of proteins which glucuronidated ganetespib and aid its excretion from the cell, preventing inhibition of HSP90: furthermore, UGT1A has been shown to be directly responsible for resistance in bladder and colorectal cancer cells [170, 171]. Addition of HSP90 inhibitors to Calu-3 cells at 4 hours demonstrates slight

perturbation in oncogenic signalling, which recovers over time and this fits the narrative of a metabolic process and/or drug excretion taking place. Mass spectrometry analysis confirms the presence of glucuronidated metabolites of ganetespib in Calu-3 cells and media at 48 hours: this is not seen at all in H460 cells. It would be useful to use a labelled form of ganetespib in order to assess ganetespib and glucuronidated ganetespib at multiple time points to understand the dynamics of ganetespib metabolism.

UGT1A is confirmed to be at a high level in Calu-3 cells but not H460 cells. It would be useful to confirm this at the transcriptional level with qPCR. However, whilst UGT1A has been confirmed to be solely responsible for resistance in cell lines of alternate tissue type, downregulation of UGT1A by RNAi or by curcumin did not appear to sensitise the cells to HSP90 inhibition by ganetespib. Furthermore, unlike cell lines in the bladder cancer study, Calu-3 cells are cross resistant to 17-AAG. This is suggestive of several mechanisms which are cooperating in order to prevent cell death. These could include a combination of UGT1A, apoptotic block at a number of points in the intrinsic apoptosis cascade and the actions of chaperones such as HSP72. More comprehensive analysis is required to understand the resistance mechanisms to HSP90 inhibition in this cell line: microarray analysis with or without ganetespib may prove a useful starting point. Technologies such as CRISPR-Cas9 or multiplexed RNAi could be used to remove multiple suspected genes responsible for resistance. However, like HSP90, proteins such as HSP72 interact with many other clients, and as a consequence deciphering the mechanisms of resistance could prove difficult. A more prudent strategy may be to work directly with patient samples and use large scale genetic analysis of tumour tissue to identify correlations of gene networks and survival.

Chapter 5 – DNA copy number alterations predict HSP90 inhibitor efficacy in advanced NSCLC

5 DNA copy number alterations predict HSP90 inhibitor efficacy in advanced NSCLC

5.1 Introduction

In the cancer cell, HSP90 levels are upregulated due to an increasingly stressful environment [172]. Cancer cells display a selective dependency on HSP90 compared to untransformed cells, making HSP90 an attractive target for therapeutics. HSP90 inhibitors bind with higher affinity to the complexed, active HSP90 in cancer cells [90].

To date, there is little clinical evidence to support biomarker stratification of HSP90 inhibitors. As stated in the introduction, many sensitivity and resistance mechanisms have been suggested, including MCL-1 addiction [230] and expression levels of NQO1 and P-gp [163-165], UGT1A [170, 171] CUL5 [173, 174], AHA1 [75], HSP70 and HSP27 [32, 83, 234-236]. HSP90 inhibition in yeast has been reported to lead to drug resistance associated with copy number gain on chromosome 15 via induction of aneuploidy [103]. However, none of these markers have yet been proven as biomarkers of response to HSP90 inhibitors in the clinical setting. In particular, little attention has been paid to the role of copy number alterations (CNAs) in response to HSP90 inhibition in NSCLC.

Methods to detect CNAs are diverse and all have advantages and challenges. Methods such as quantitative polymerase chain reaction (qPCR) based direct ratio testing (DRT) and fluorescence *in situ* hybridisation (FISH) have been developed to look at and verify copy number change of specific genes or regions: whilst high accuracy and specificity is obtainable, these methods are unable to look at entire genomes in a high-throughput manner. Array comparative genomic hybridisation (aCGH) was developed for this, but what is gained in throughput is lost in specificity, potentially leading to incorrectly calling a region with copy number change. More recently, SNP-array based and next-generation sequencing (NGS) technologies have come to the fore for CNA detection. NGS methods including whole genome sequencing (WGS) and whole exome sequencing (WES) provide high accuracy across large swathes of the genome and

represent the most powerful CNA detection strategies, however the price remains relatively high for both data collection and processing [237]. If routine CNA testing of cancer samples is to be conducted, a methodology with quick turnaround, high throughput, high accuracy and low cost is required. This is where a cancer-focused, SNP-based technology like Oncoscan® by Affymetrix may be useful. This methodology can utilise less than 75ng of genomic DNA from formalin-fixed paraffin-embedded tissue, which is subsequently hybridised to hundreds of thousands of molecular inversion probes (MIPs): probes which contain two regions of genetic homology at each end and invert to flank the SNP site of interest (). These probes anneal to the site of interest, the SNP gap is filled by a complementary base and ligated to the rest of the probe, which becomes circularised and is released from the genomic DNA. The probe is now inverted and is amplified using the PCR primer sites before being hybridised to an array for detection [238]. This technology has now been successfully employed to detect CNVs in several cancer subtypes including ovarian, breast cancer and lung cancer [239-241].

Two types of data are obtained from this process: the $\log_2$ ratio, which is the ratio between the tumour sample and either a matched normal sample, or in this case a reference genome for each probe; and B-allele frequency (BAF), which is the estimated allelic fraction for a particular SNP position (normally “AA”, “AB”, “BA” or “BB” with “A” representing the nucleotide found in the reference genome) [237]. B-allele frequency is used to determine allelic imbalance and loss of heterozygosity, however for simplicity this dataset will not be analysed in this analysis. In order to reliably determine whether a region has undergone copy number change, several probes and associated $\log_2$ ratios must be combined to form a “segment” which is called as a “gain”, “loss” or no change in copy number. There are multiple algorithms available to segment the data into distinct regions of copy number, such as circular binary segmentation (CBS), gain and loss analysis of DNA (GLAD) and QuantiSNP, many of which are summarised in a paper by Dellinger *et al.*: of these, QuantiSNP seemed to perform best, however CBS was determined to be one of the best for accurately determining CNV boundaries and was suited to Affymetrix arrays, so this algorithm was used for the analysis below [242].

In order to determine if the segmented regions of copy number are important, further refinement is conducted using algorithms to identify significant “driver” CNAs amongst multiple tumour specimens rather than minor “passenger” CNAs. This is known as recurrence detection, and a summary of algorithms for this purpose are shown (**Table 5.1-1**) [243]. For this analysis, it was decided to use the GISTIC2 algorithm, which looks at CNA

Figure 5.1-1 Molecular inversion probe technology for CNV detection. The probe is flanked each end by two regions of genomic homology which when annealed around the SNP site span around 40bp, making the probes better for FFPE and highly degraded DNA. DNA polymerase fills the gap with a complementary base, which is then ligated to the probe. Exonuclease digestion removes single stranded DNA and linearises the probe ready for hybridisation to an array. These images were obtained from the Affymetrix Oncoscan website

Name	Input	Output (significance)	Null model (For significance)
CGHregions	Gains/Losses	None	None
Master HMMs	log2 ratios	Probabilities of alteration for each probe	Homogenous Hidden Markov Model
cghMCR	Smoothed log2 ratios	None	None
MAR/CMAR	Gains/Losses	None	None
GEAR	log2 ratios	p-values	Permutation of the alterations over the entire genome
KC-SMART	log2 ratios	p-values	Permutation of the log-ratios over the entire genome
STAC	Gains/Losses	Confidence for regions	Permutation of the regions within chromosomes
MSA	log2 ratios	p-values	Permutation of the regions within chromosomes
GISTIC/GISTIC2	Gains/Losses	p-values	Permutation of the probes over the entire genome
RAE	log2 ratios	p-values	Permutation of the copy number values using hotspots information
Interval scores	log2 ratios	Scores for each interval	Large deviation bound for iid Gaussian data
CoCoA	Gains/Losses	Scores for each interval	Binomial distribution on probes and intervals
BSA	log2 ratios	Bayes factors	Bayesian hierarchical model
pREC-A	log2 ratios	Probabilities of alteration for each region	Non-Homogenous Hidden Markov Model
pREC-S	log2 ratios	Probabilities of alteration for each region	Non-Homogenous Hidden Markov Model

Table 5.1-1 *Summary of recurrence detection algorithms. Modified from Rueda et. al (2010)*

amplitude and frequency for recurrence detection due to its optimisation for cancer samples and because it has been used in significant publications, which will allow for easier comparison of results [196, 221].

Whilst genomic regions can be identified which are important to cancer development and patient prognosis, understanding which regions contribute to sensitivity or resistance to chemotherapy and targeted agents is not so clear. Elucidation of these key CNAs and the groups of genes within them requires combination with survival data from clinical trials. CNA regions identified as recurrent in this study can therefore be combined with survival metrics in order to find potential biomarkers.

Here a translational study is described linked to the GALAXY-1 phase II trial (NCT01348126, see Ramalingam *et al., Annals of Oncology,* 2015) which randomized patients to docetaxel with or without ganetespib (referred to as "D" and "G-D" arms hereafter) in patients with advanced non-small cell lung adenocarcinoma in the second line setting [39]. In a retrospective analysis, patients previously treated with platinum or pemetrexed- based regimen, and subsequently diagnosed with advanced disease greater than 6 months before trial randomization (chemosensitive patients), had longer survival on the G-D arm (N = 177): PFS (adjusted HR = 0.74, P = 0.0417); OS (adjusted HR = 0.69, P = 0.0191) [39]. To establish whether genomic interrogation could be used to identify a subgroup of patients likely to benefit from G-D, we conducted genome-wide analysis of copy number alterations (CNA) detection, using the Oncoscan® array and bioinformatics workflow.

Aims

- Utilise SNP-based array technology Oncoscan® in combination with bioinformatics analysis to identify recurrent regions of CNA in the GALAXY-1 trial
- Combine recurrent regions with survival data to produce Kaplan-Meier curves and log-rank analysis of survival to find regions which significantly separate survival curves, thus potential predictive/prognostic markers
- Look at the effect of having multiple CNAs on survival, as genomic instability has been linked before with drug responses

5.2 Results

5.2.1 Study cohort for array based CNA analysis

Figure 5.2.1(A) presents an overview of the GALAXY-1 trial [39]. Patients were included with advanced NSCLC with adenocarcinoma histology and 1 prior chemotherapy regimen and ECOG status of 0 or 1. Of 253 adenocarcinoma patients enrolled, 212 were analysed with Oncoscan 2.0. A simplified bioinformatics workflow is shown in figure 5.2.1(B). Only 165 samples passed quality control. Clinical characteristic analysis of this subgroup (table 5.2-1) reveals a balanced sample size for each trial arm. Approximately three quarters of patients analysed were from Eastern Europe. Chemosensitive (diagnosed >6 months since diagnosis) and chemoresistant (diagnosed with advanced disease <=6 months since diagnosis) patients represented 70.3% and 29.7% of this cohort respectively. All clinical variables were balanced between the two treatment arms.

No difference in survival was observed between the experimental and control arms for the 165 patients investigated for this study (figure 5.2-2) (A); HR = 0.943, p-value = 0.742). Patients were separated into those chemoresistant (figure 5.2-2) (B);(n=49) and chemosensitive (figure 5.2-2) (C) n=116) subgroups. There was a trend for the chemoresistant patients to perform badly in this study (HR = 1.805, p-value = 0.059), whereas chemosensitive patients appeared to benefit from the combination treatment, though this was not significant (HR = 0.724, p-value = 0.1283). These results are in line with the overall trial of 253 patients [39]. Chemosensitive patients (n=116) were taken forward to identify predictive CNAs for this subgroup only.

5.2.2 Identification of predictive CNAs

GISTIC2 identified 44 CNAs as recurrent in this cohort with residual q-values <0.01: 18 chromosomal regions with copy number gain and 26 with copy number loss (figure 5.2-3) The median number of CNAs per patient was 22 (range 0-33 CNAs).

A non-uniform distribution of *p*-values was identified in our dataset, therefore we utilised the Sliding Linear Model (SLIM) for false discovery rate multiple comparison correction in addition to simple Bonferroni analysis (figure 5.2-4). A pi0 value of 0.64 was calculated for p-value adjustment of the 44 CNA patient groups. Randomly sampling the dataset for 10-70 patient overall survival scores and conducting log-rank survival analysis 10,000 times reveals a non-normal distribution, however there is a low proportion of p-values supporting the alternative hypothesis and the pi0 value for FDR adjustment was 0.98, suggesting the dataset as a whole is relatively unbiased. Three recurrent CNAs were discovered associated with significantly reduced HR for overall survival with FDR (slim), with adjusted $p<0.05$ (figure 5.2-5): one region of copy number loss was identified in cytoband 18q23 ($p=0.0186$, HR = 0.2802) and two regions of copy number gain were found in cytobands 11q13.3 ($p=0.0324$, HR = 0.2130) and 16q22.3 ($p=0.0331$, HR = 0.3790). Only the region of loss at 18q23 had an adjusted *p*-value below 0.05 after Bonferroni correction ($p=0.0271$). 12 further regions held *p*-values <0.05 by univariate analysis but did not pass multiple correction (not shown).The top 3 CNAs which passed FDR correction were not mutually exclusive (figure 5.2-5)(C); of the 116 chemosensitive patients analysed, 17 patients had none (14.7%), 41 had 1 CNA (35.3%), 42 had 2 CNAs (36.2%) and 16 had all 3 CNAs (13.8%). These CNAs were evenly distributed between the treatment arms, with the exception that the docetaxel arm had more patients with 1 of the top 3 CNAs (21.6%) and the docetaxel plus ganetespib arm had more patients with 2 of the top 3 CNAs (23.3%).

5.2.3 Concurrent 18q23 loss, 11q13.3 gain and 16q22.2 gain predicts shorter survival following docetaxel alone

Patients were next selected based on the presence of these top three CNAs (**figure 5.2-6**). Interestingly, whilst overall survival increases sequentially up to two of the top three CNAs (409.5 days), a sudden drop in survival can be seen in patients with all three CNAs (186.5 days). When separated by treatment arm, a significant difference in survival was observed in patients with all three CNAs ($p=0.0035$, HR=0.212 (95%CI 0.0705-0.6375)): median overall survival in patients treated with docetaxel was only 123.5 days (range 33-243 days), much worse than the median 239 days for the overall

population in this treatment arm. Furthermore, patients treated with docetaxel plus ganetespib fared much better if positive for all three CNAs, with a median overall survival of 603.5 days (range 181-883 days). Further still, removal of patients positive for all three CNAs from the population ablated any positive signal (*p*=0.8091, HR=0.9214 (95%CI 0.5792-1.466).Analysis of the treatment arms in isolation (figure 5.2-7) reveals patients with 18q23 loss, 11q13.3 gain and 16q22.2 gain lung adenocarcinoma exhibited significantly worse outcome for docetaxel alone compared with all docetaxel-treated tumours (HR= 2.766 (95%CI 1.01-7.569), *p*=0.0057), whereas no significant trend was seen in patients with these CNAs favouring longer survival in the combination arm (HR = 0.7062 (95%CI 0.2891-1.725), p-value = 0.4198). Nevertheless, a forest plot comparing clinical factors with 18q23 loss plus 11q13.3 gain patients indicated that only CNA status could be used as a potential predictive marker for ganetespib in combination with docetaxel (HR 95% CI 0.05205-0.3001) (figure 5.2-8).

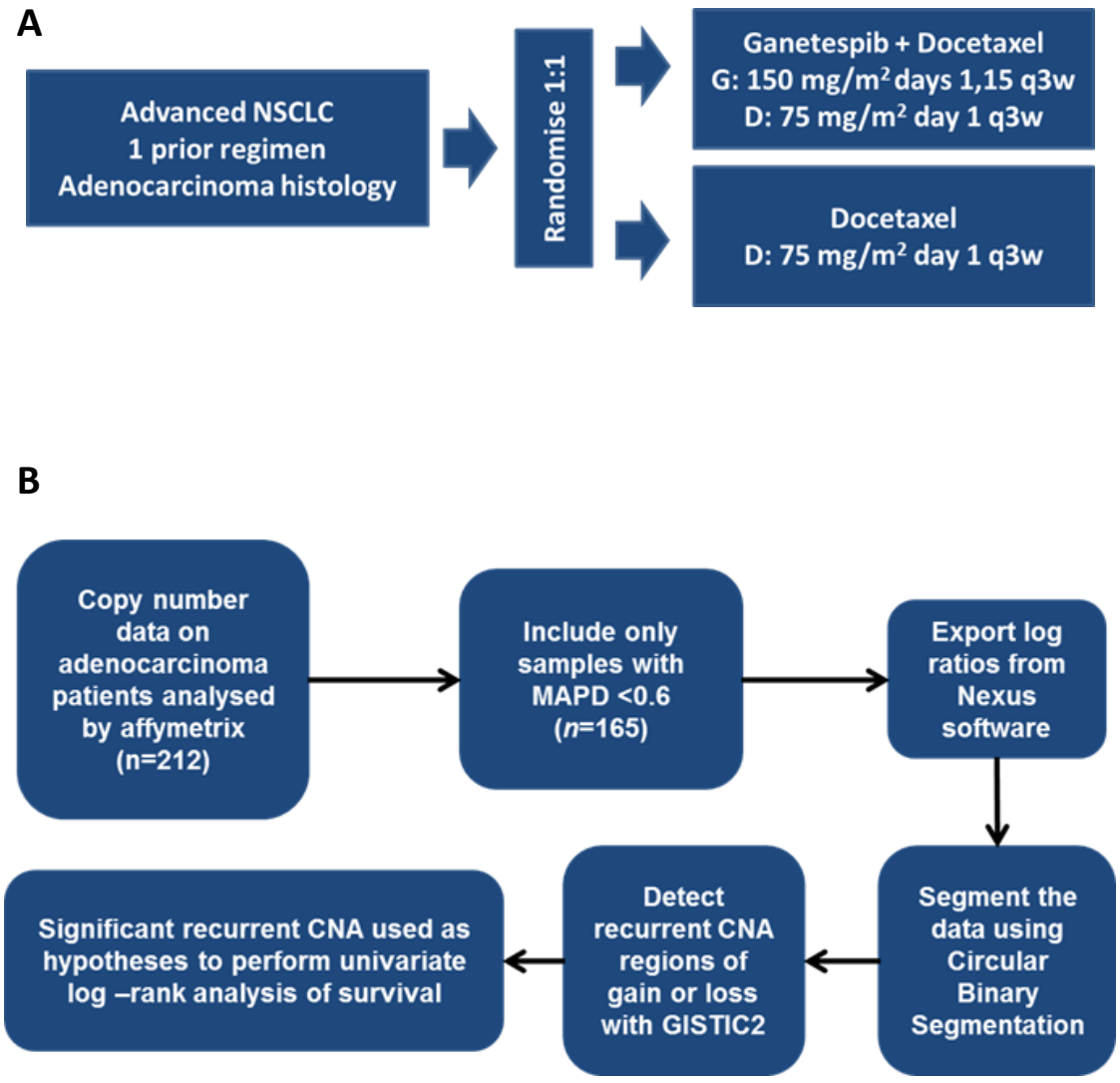

Figure 5.2-1 (A) *Patient selection and randomisation* ***(B)*** *Patient subgroup, quality control and bioinformatics workflow*

>6mon only		D (n=57)	D + G (n=59)
Median Age (Range)		60 (41-77)	60 (42-75)
Sex	Male	35	30
	Female	22	29
ECOG Status	0	20	27
	1	37	32
Stage at Initial Diagnosis	I/II	8	2
	IIIA	1	8
	IIIB/IV	48	49
Smoking status	Ever	42	39
	Never	15	20
LDH	Normal	35	41
	Elevated	22	18
Prior Therapy	Platinum-based regimen	55	56
	Pemetrexed	10	12
Geographic Region	North America	6	9
	Eastern Europe	45	41
	Western Europe	6	9
mKRAS	No mutation	39	40
	G12A	1	1
	G12C	12	8
	G12D	1	4
	G12V	4	5
	Q61L	0	1
	Mut +ve	18	19

Table 5.2-1 *Clinical characteristics of the chemosensitive subgroup (patients diagnosed with advanced disease >6 months since initial diagnosis, n=116)*

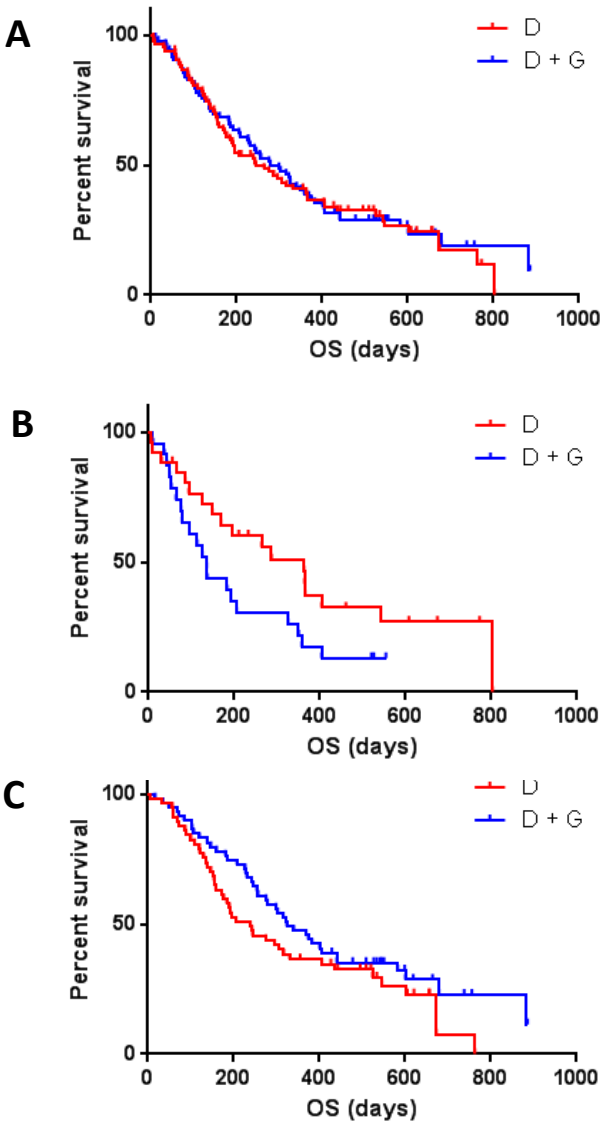

D

	All	<=6 months	>6 months
N	165	49	116
D	83	26	57
D + G	82	23	59
Median OS			
D	244	363	239
D + G	289	136	324
HR	0.943	1.805	0.724
p-value	0.742	0.059	0.1283

Figure 5.2-2 *Kaplan-Meier curves of overall survival (days) for patient subgroups.* ***(A)*** *All analysed patients (n=165)* ***(B)*** *Patients diagnosed with advanced disease less than 6-months since diagnosis (n=49)* ***(C)*** *Patient greater than six months since diagnosis (n=116)* ***(D)*** *Summary table. HR and p-value calculated by log-rank*

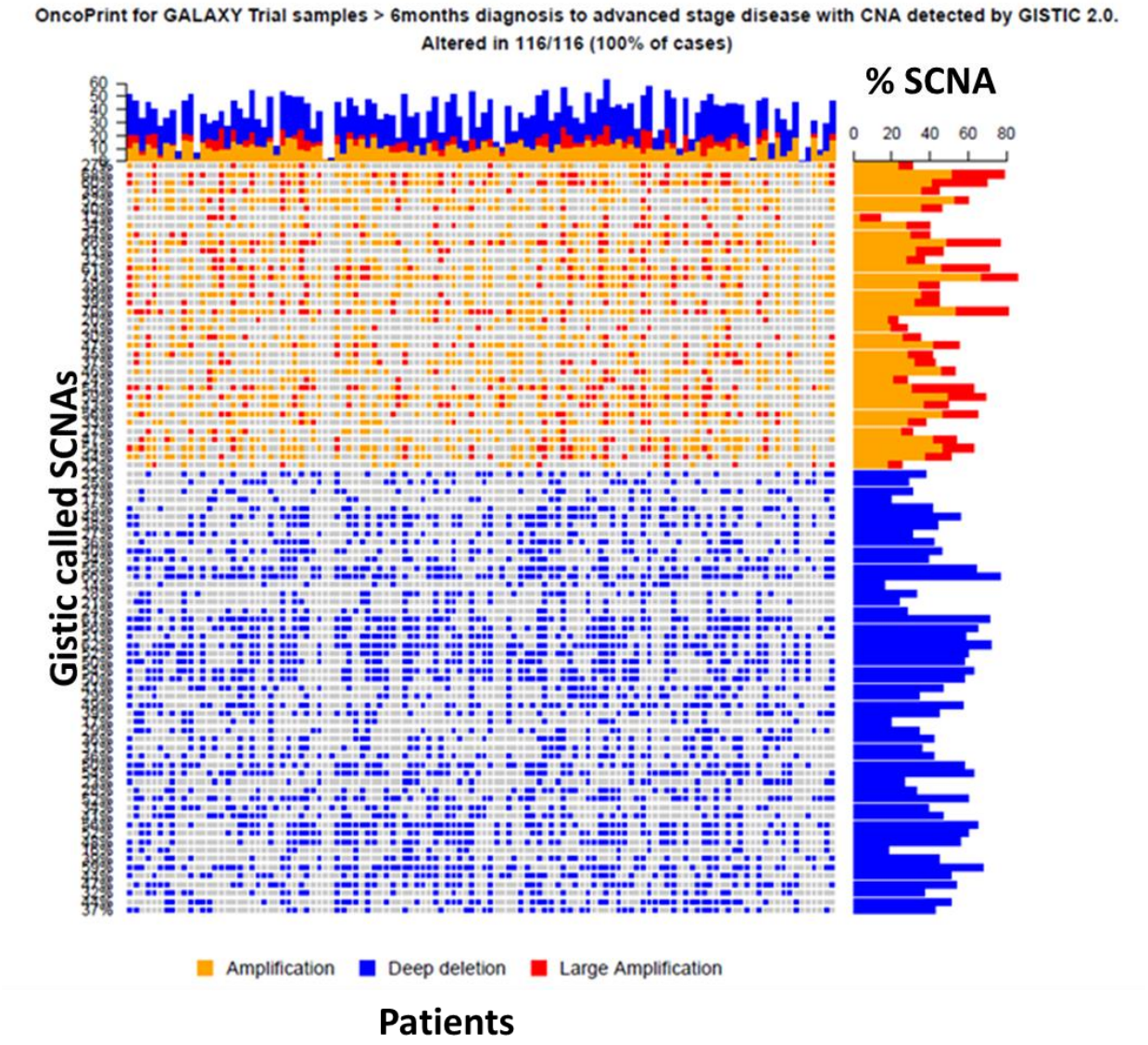

Figure 5.2-3 *The landscape of recurrent copy number alterations in chemosensitive patients (n=116). Patients run along the x-axis and each recurrent CNA is labelled on the y-axis. Red dots represent large gains, orange dots are gains and blue dots are losses as defined in the methodology.*

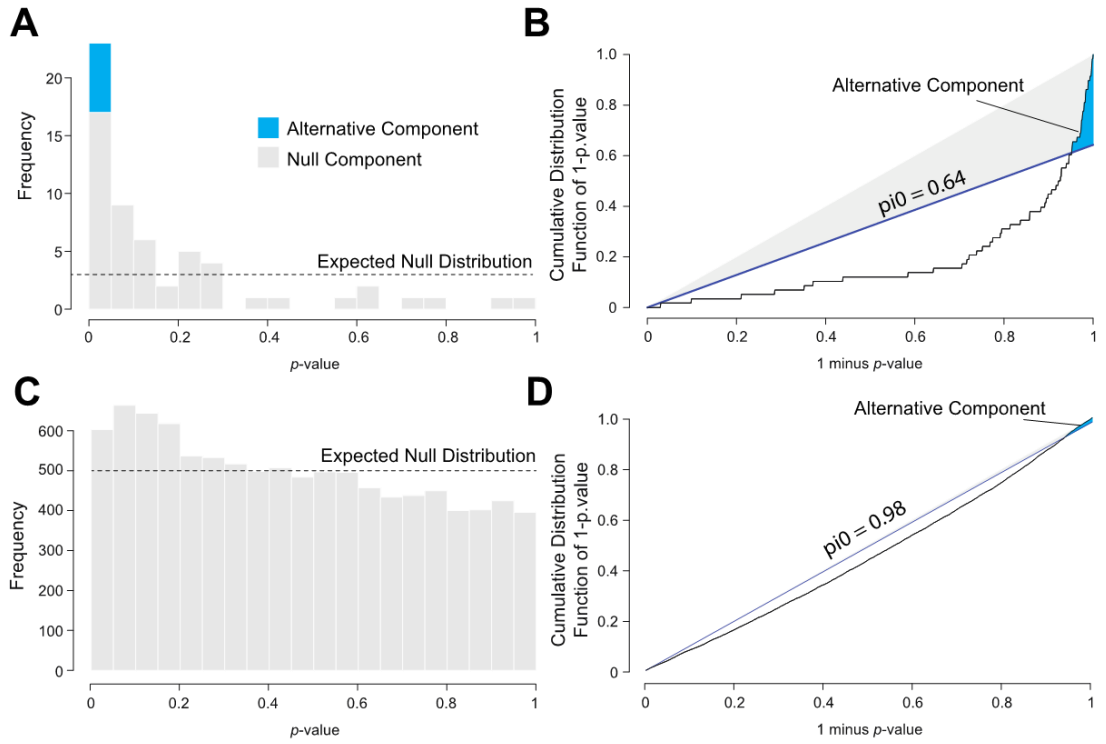

Figure 5.2-4 Comparison of log rank survival p-values in patient groups determined by significant CNAs or at random *Note this figure was produced in conjunction with Callum Rakhit* ***(A)*** *p-values for log rank survival tests comparing overall survival in each of the two treatment arms for the 44 CNAs determined patient groups There are a high proportion of p-values supporting the alternative hypothesis* ***(B)*** *Calculation of the pi0 value for FDR adjustment of the 44 p-values. The minimum value for the adjusted p-values was 0.023* ***(C)*** *p-values for log rank survival tests comparing overall survival in each of the two treatment arms for 10,000 randomly determined patient groups of a random size from 10-70 patients. The p-values are non-normally distributed and there are a low proportion of p-values supporting the alternative hypothesis* ***(D)*** *Calculation of the pi0 value for FDR adjustment of the 10,000 p-values. The minimum value for the adjusted p-values was 0.56*

A

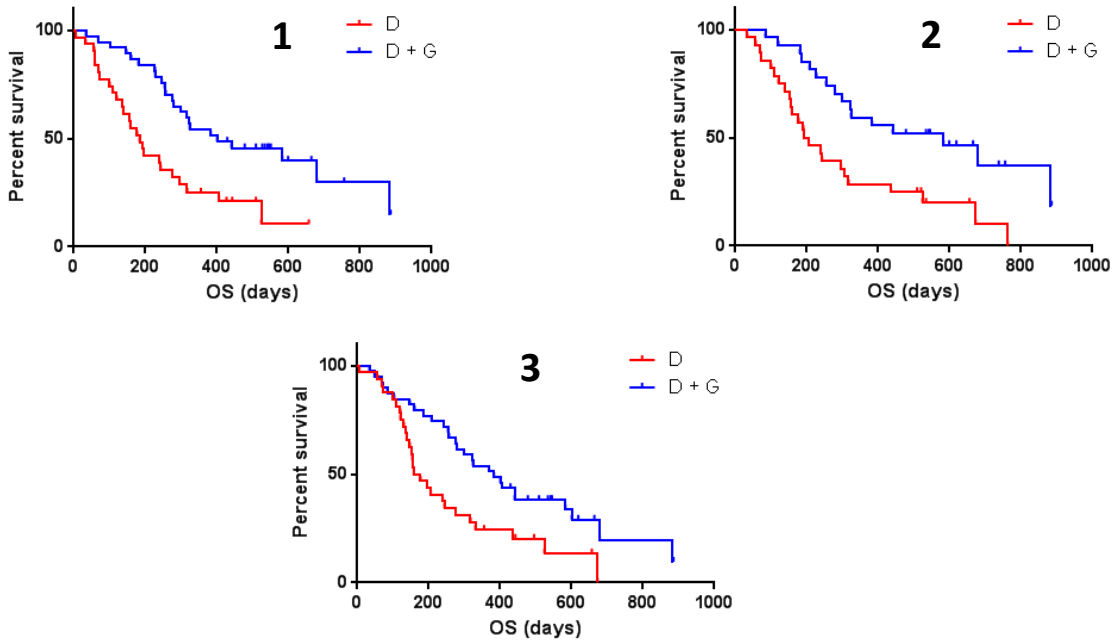

B

ID	1	2	3
Event	del	amp	amp
Cytoband	18q23	11q13.3	16q22.2
Start	76630415	68853034	71646526
Stop	77450636	69935446	71690029
Gehan-Breslow-Wilcoxon Test	0.000615119	0.002143046	0.003289238
GBW HR	0.280221306	0.213023588	0.379036697
Log-Rank Test	0.001333514	0.002574471	0.0071314
Log Rank HR	0.391668996	0.379036697	0.38376208
Bonferroni	0.027065245	0.094294017	0.14472648
FDR (Slim)	0.01857162	0.03235134	0.0331028
Genes	NFATC1, SALL3, ATP9B	CCND1, FGF3, FGF19, MYEOV, ANO1, TPCN2, ORAOV1	PHLPP2, MARVELD3

C

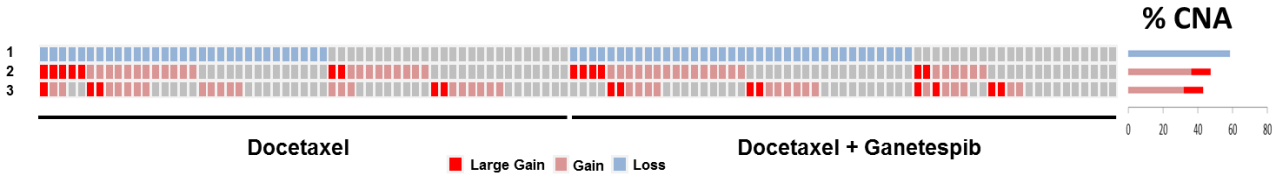

Figure 5.2-5 *Three CNA regions identified by GISTIC as recurrent, which produced survival curves with p-value <0.05 after correction with FDR (slim)* ***(A)*** *Kaplan-Meier survival curves for patients with a candidate CNA* ***(B)*** *Summary table and genetic annotations* ***(C)*** *Oncoprint of top 3 CNAs separated by treatment. Blue represents loss, pink gain and red large gain.*

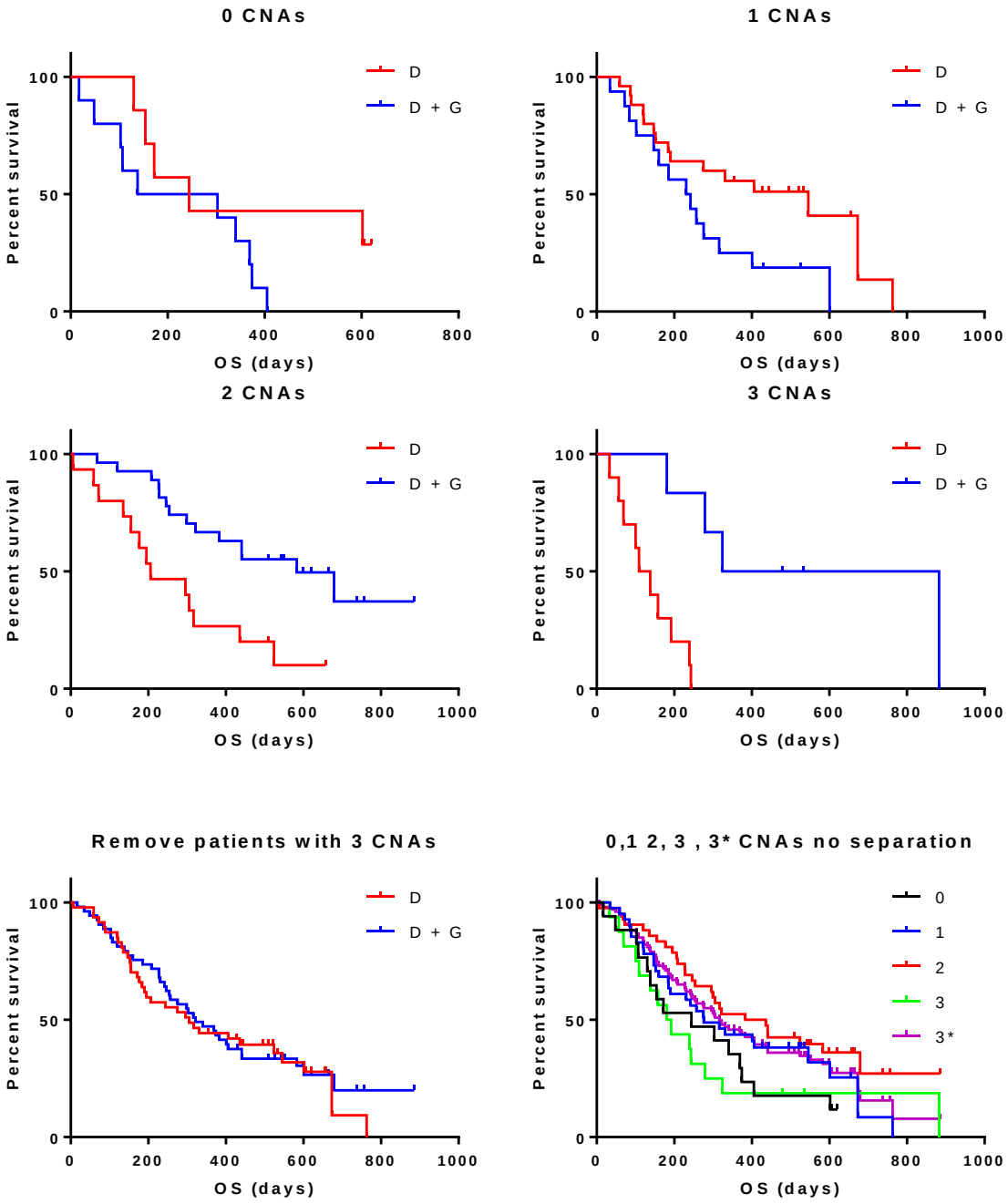

Figure 5.2-6 *Effect on overall survival when grouping patients with multiple top CNAs. Kaplan-Meier survival curves demonstrate survival time for patients with docetaxel alone or in combination with ganetespib.*

Top 3 CNAs	0	1	2	3	3*
N (%)	17 (14.7)	41 (35.3)	42 (36.2)	16 (13.8)	100 (86.2)
D (%)	7 (6.0)	25 (21.6)	15 (12.9)	10 (8.6)	47 (40.5)
D+G (%)	10 (8.6)	16 (13.8)	27 (23.3)	6 (5.2)	53 (45.7)
Median OS (days)	244	276	409.5	186.5	316
D	244	546	206	123.5	305
D+G	220.5	236.5	583	603.5	322
HR (95% CI)	2.284 (0.8284 to 6.3)	2.126 (0.9675 to 4.673)	0.3277 (0.1343 to 0.7995)	0.212 (0.07052 to 0.6375)	0.9214 (0.5792 to 1.466)
GBW p-value	0.1799	0.0859	0.002	0.0035	0.8091

Table 5.2-3 *Survival metrics table for figure 5.2-6*

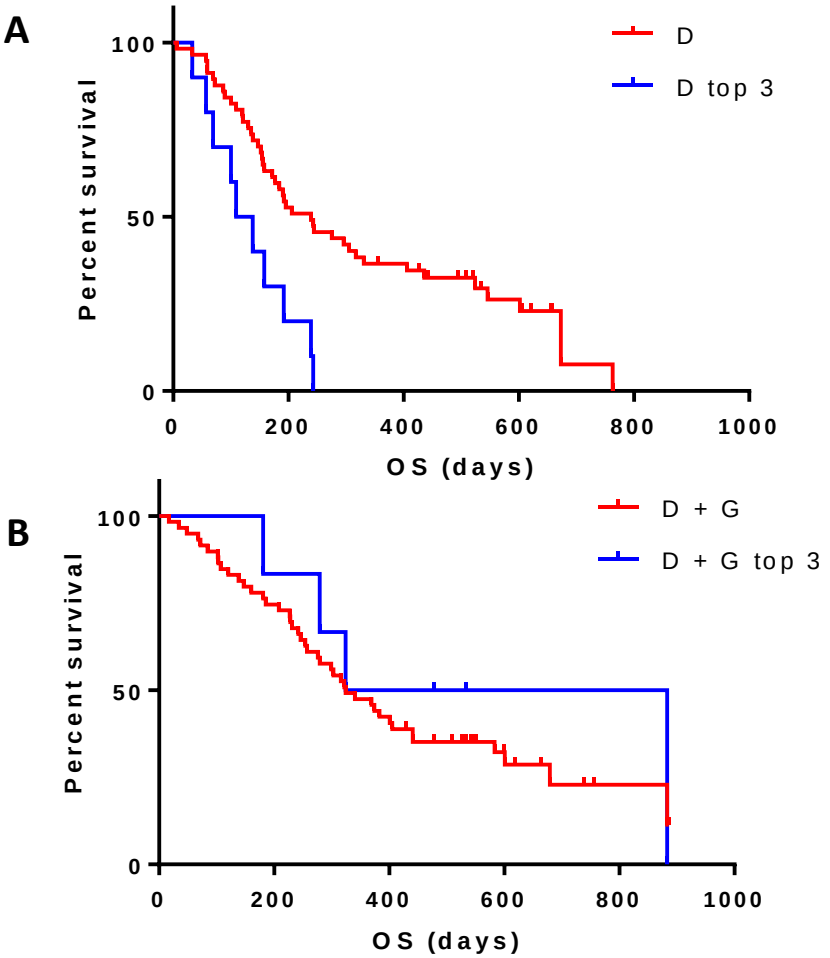

C

	D vs D top 3 CNAs	D + G vs D + G top 3 CNAs
N		
All pts in arm	57	59
Top 3 CNA +ve	10	6
Median OS		
All pts in arm	239	324
Top 3 CNA +ve	123.5	603.5
HR (95% CI)	2.766 (1.01 to 7.569)	0.7062 (0.2891 to 1.725)
GBW p-value	0.0057	0.4198

Figure 5.2-7 *Analysis of treatment arms in insolation for patients with 18q23 loss, 11q13.3 gain and 16q22.3 gain.* ***(A)*** *Kaplan-Meier analysis for patients with 18q23 loss, 11q13.3 gain and 16q22.3 gain for docetaxel only vs all docetaxel treated patients* ***(B)*** *Kaplan-Meier analysis for patients with 18q23 loss, 11q13.3 gain and 16q22.3 gain for docetaxel plus ganetespib vs all docetaxel plus ganetespib treated patients.* ***(C)*** *Summary table of log-rank survival analysis. HR = hazard ratio*

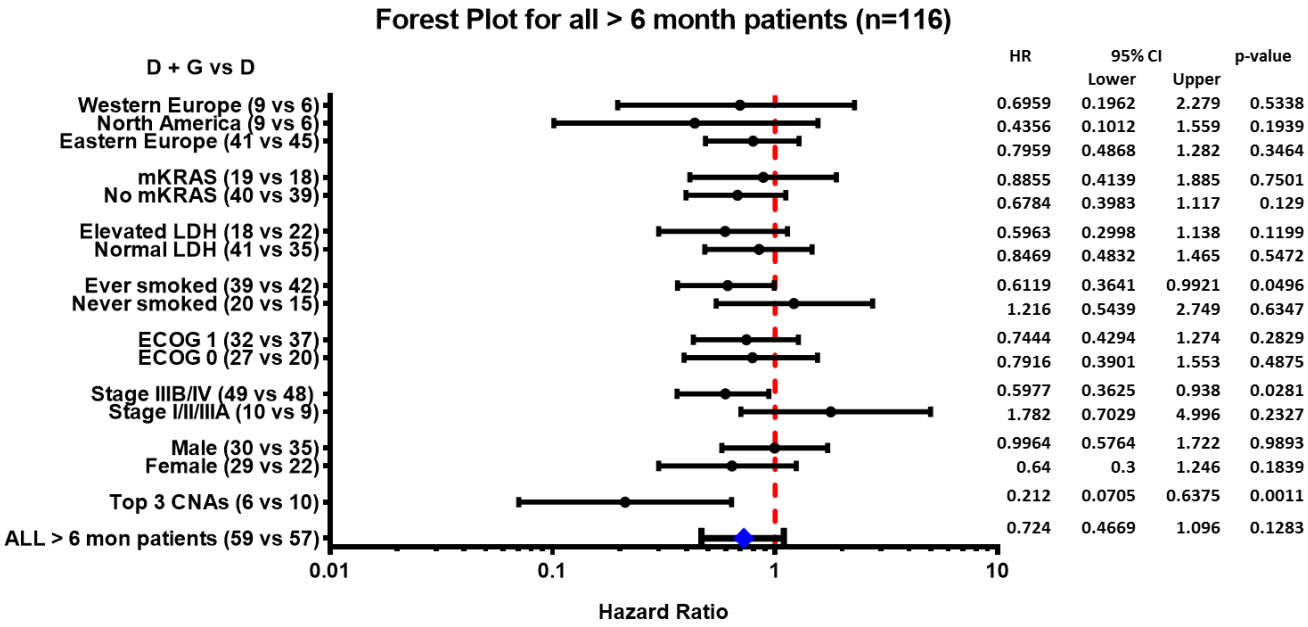

Figure 5.2-8 *Forest plot of clinical characteristics for all chemosensitive patients vs patients with concurrent 18q23 loss, 11q13.3 gain and 16q22.3 gain. Y-axis labels are followed by (N) for each treatment arm. Spots represent hazard ratio (HR) and bars represent the 95% confidence interval. Hazard ratios less than one are representative of patient subgroups who perform better when treated with docetaxel plus ganetespib*

5.2.4 Mutational burden and survival outcome

To understand how mutational burden affects survival outcome, the number of CNAs per patient was compared with overall survival of every individual for each treatment arm, then subjected to linear regression (figure 5.2-9). Patients treated with docetaxel did not appear to display a trend for shorter overall survival with a greater number of CNAs (R^2=0.05, p-value=0.09), and neither did patients with all top 3 CNAs, though these patients did tend to have a higher number of CNAs overall. Patients on the G-D arm did not significantly achieve a longer overall survival when harbouring a greater number of CNAs, (R^2=0.04, p-value=0.13) however, patients who simultaneously harboured all three top CNAs 11q13.3 gain, 16q22.3 gain and 18q23 loss did appear to show a trend towards greater survival, with more CNAs overall, however this did not reach significance (R^2=0.55, p-value=0.09).

5.2.5 Putative biomarkers and preclinical drug response

To determine whether the identified CNAs were associated with preclinical drug response, copy number data from the Cancer Cell Line Encyclopedia (CCLE) was interrogated in combination with lung cancer cell line IC_{50} data from the Catalogue of Somatic Mutations in Cancer (COSMIC) database, or in the case of ganetespib data was kindly provided by Synta. No link between the number of top 3 CNAs and lung cancer cell line IC_{50} values was found for any of the drugs assessed including docetaxel, ganetespib, 17-AAG and AUY922 (figure 5.2-10).

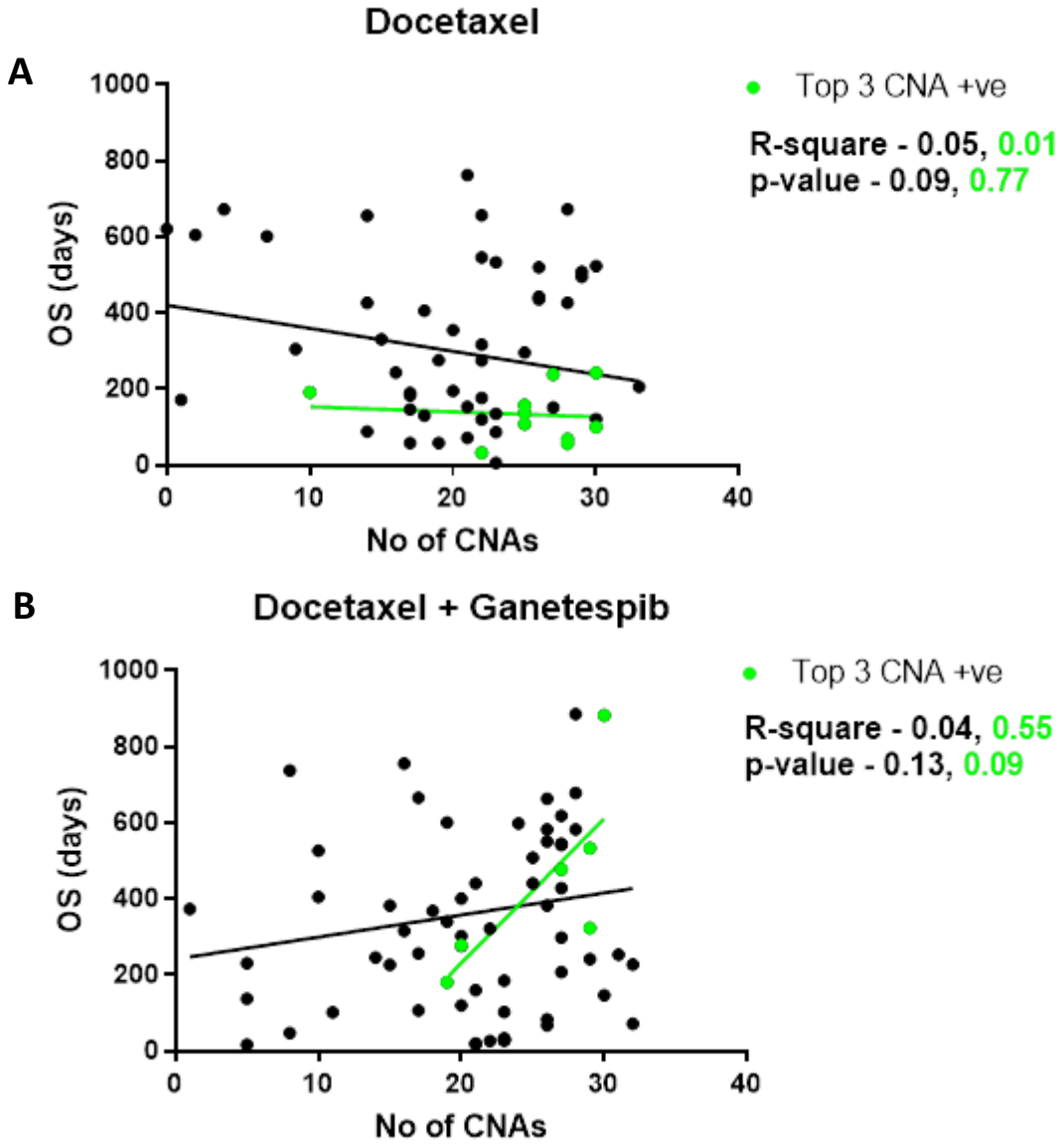

Figure 5.2-9 *Correlation of no of CNAs per patient and overall survival. Patients with all 3 top CNAs are labelled in green* ***(A)*** *Scatter plot of patients treated with docetaxel comparing number of CNAs versus overall survival. Linear regression correlation R-square and p-values are shown for all patients (black) and patients with top 3 CNAs (green)* ***(B)*** *Scatter plot of patients treated with docetaxel and ganetespib comparing number of CNAs versus overall survival. Linear regression correlation R-square and p-values are shown for all patients (black) and patients with top 3 CNAs (green)*

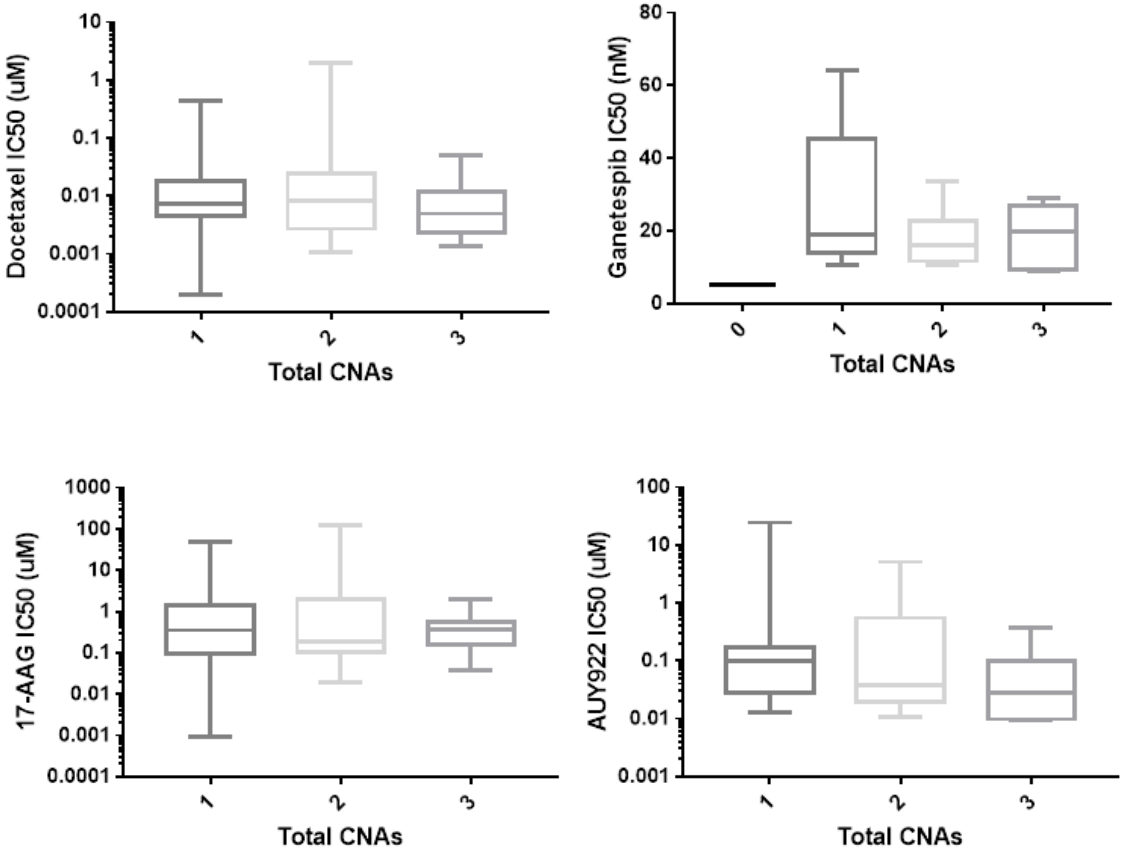

Figure 5.2-10 *Box and whisker plots of lung cancer cell lines IC_{50} data for docetaxel and 3 HSP90 inhibitors, correlated with the presence of the top 3 significant CNAs found in this study. Cell line numbers as follows: N=59 (docetaxel), 36 (ganetespib), 58 (17-AAG) and 59 (AUY922)*

5.3 Discussion

HSP90 inhibitors exhibit pleiotropic effects across pro-oncogenic signalling networks in cancer cells, potentially interacting with several pathways concurrently. To date there has been a limited understanding of how to stratify therapy with this class of agent. Our recent data suggests EML4-ALK variant status may be a consideration in determining response to ganetespib monotherapy [224]. However, the GALAXY-1 trial did not look at ALK positivity as a potential biomarker, so the effect of ALK status on ganetespib plus docetaxel therapy remains unknown. KRAS mutation status was assessed but appeared to have no effect on response (figure 5.2-8).

DNA damage is known to lead to copy number alteration, for example: DNA breaks have been shown to aid missegregation of centromeric chromosomal fragments and increase loss of heterozygosity [244]. Yet, whilst many mechanisms of copy number alteration are known, copy number alterations have been under-explored in relation to clinical drug response. Using an array based platform, an unbiased genome wide scan of copy number alterations has been conducted to interrogate potential determinants of efficacy in the GALAXY-1 trial. We have shown that patients who have lung adenocarcinomas harbouring copy number alterations in 18q23, 11q13.3 and 16q22.3 had shorter survival with docetaxel alone, but not with the combination of docetaxel with ganetespib for whom overall survival nearly doubled. However significance was only achieved when looking at the effect of these CNAs on the docetaxel population alone, suggesting they represent a group of patients who respond poorly to docetaxel (negatively prognostic), but gain a survival advantage with the addition of ganetespib.

18q23, 11q13.3 and 16q22.3 alterations did not predict resistance to docetaxel in cell lines as might be expected from the trial data. However, the sample sizes were quite small and these 2-dimensional cell line studies may not be representative of the tumour microenvironment. It is also possible that the reduced sensitivity to docetaxel is not due to 18q23, 11q13.3 and 16q22.3, but rather these CNAs represent labels of

increased genomic instability in the tumour leading to increased resistance from a variety of mechanisms.

Although no significant trend was found in terms of number of CNAs and overall survival, there is a possibility that patients with concurrent 18q23 loss, 11q13.3 gain and 16q22.3 gain may do better on ganetespib plus docetaxel if they have more CNAs in the background. It's possible that this suggest that patients who have all three CNAs and have more genomic instability overall may benefit from a survival advantage, however many more patients would be required to understand this effect.

Whilst the methodology used for this study is viable, it may not capture all possible CNAs. As discussed previously, the algorithms used for segmentation and recurrence detection could change the called CNAs. For example, the CBS algorithm has been shown to miss CNVs successfully called with other methods with simulated datasets [242]. The parameter settings for these algorithms may also affect segment length and recurrence calls. It may be worth utilising several algorithms such as GLAD and QuantiSNP for CNA detection and STAC for recurrence detection and comparing results, in addition to parameter optimisation.

Of the top three CNAs detected, only 11q13.3 gain has been previously shown to be associated with lung cancer [245]. In fact, 11q13.3 appears to be a frequent amplification in lung adenocarcinomas [245]. It would be interesting to look again at the tumour specimens for this study and conduct immunohistochemistry analysis for proteins of genes found within this region to see if it is suggestive of a gene dosage effect, and potential candidate genes responsible for sensitivity docetaxel and/or ganetespib. Cyclin D1 overexpression has been detected in hepatocellular cancer (HCC) and may perturb normal cell cycle control, whilst fibroblast growth factor 3 (FGF3) amplification, also in HCC, has been shown to be linked to responders to sorafenib [246]. A study in head and neck cancer found cyclin D1 to be negatively prognostic in patients treated with docetaxel and radiotherapy (p=0.0004), however a meta-analysis of 24 studies did not find cyclin D1 overexpression to be prognostic in NSCLC (HR 1.08 [95% CI, 0.80-1.45]) [247, 248]. Fibroblast growth factor receptor (FGFR) signalling is involved with proliferation, survival and angiogenesis [249]. It is

possible to postulate a situation where increased FGFR signalling due to amplified FGF3 and FGF19 results in a poor prognosis for patients treated with docetaxel, however upon the addition of HSP90 inhibition, this pathway breaks down due to downregulation of HSP90 clients such as AKT, MAPK and FGFR1.

NFATC1, found within the 18q23 locus, is a component of the nuclear factor of activated T-cells (NFAT) transcription complex, which is involved in regulating expression of genes responsible for cell motility [250]. Loss of NFATC1 may augment the effect of amplification of the FGFR pathway as it is activated and translocates to the nucleus downstream of FGFR-PLCγ1-IP_3-Ca^{2+}-calcineurin, and therefore may result in an improved response to ganetespib plus docetaxel [250]. It is unclear why loss of NFATC1 may result in a poor response to docetaxel alone. Given the number of variables this is conjecture and the exact genetic basis for sensitivity to combination therapy for 11q13.3 gain and 18q23 loss is likely to be complex.

The region amplified in 16q22.3 encodes two genes: pleckstrin homology domain leucine-rich repeat protein phosphatase 2 (PHLPP2), and membrane-associating domain containing 3 (MARVELD3). PHLPP2 is a phosphatase involved in control of AKT activity and is normally considered a tumour suppressor, whilst MARVELD3 is a regulator of the JNK pathway via tight junctions and loss of this protein leads to increased cell proliferation and migration in Caco-2 cancer cell lines [251, 252].

Using the cBioportal website, it is possible to quickly assess CNA prevalence and association with survival for many cancer subtypes [253, 254]. Genes within the 11q13 region are altered in around 5% of lung adenocarcinomas according to the TCGA dataset from 2014 of 230 samples, including several amplifications. This figure is lower than the 47% prevalence found in our dataset, likely because only high level events are shown for the TCGA data (shallow gains and deletions are not included) (figure 5.3-1). **(A).** Furthermore, 11q13 gain does not appear to be prognostic for the TCGA dataset (**figure 5.3.1(B)**).

18q23 deletion has been previously reported in a study of pancreatic cancer samples, though a literature search did not find any presence in lung adenocarcinomas [255]. Analysis of the TCGA dataset again reveals genes in the 18q23 region underwent

homozygous deletion in 2/230 cases (<1%, figure 5.3-2**(A)**) and no effect on overall survival was observed: though given the small number of positives this is not surprising (figure 5.3-2 **(B)**). Interestingly, unlike 11q13.3 gain, 18q23 loss was detected in around 12% of normal samples in the GALAXY-1 dataset (4/34 representative normal samples, matched normals were unavailable): conversely 18q23 loss was present in 59% of tumour samples. This suggests either a possible enrichment of a CNV site found in normal tissue or possible contamination of normal samples with tumour DNA. No amplifications of 16q22.3 genes were found in this dataset (figure 5.3-3) although one deletion was noted (0.4%) of patients.

It remains unknown whether any of these patient tumours displayed high levels of active UGT1A which would confer resistance to ganetespib therapy [170, 171]. It is also unknown whether patients with CNAs at 18q23, 11q13.3 and 16q22.3 concurrently held known docetaxel resistance factors such as upregulated p-glycoprotein, β-tubulin mutations or apoptotic defects [256]. More preclinical data will be required utilising more representative model systems in order to verify the regions identified as biomarkers and to probe further into the molecular mechanisms at work.

In summary, CNAs have been identified which correlate with poorer outcome for patients treated with docetaxel in alone GALAXY-1, which may benefit from the addition of an HSP90 inhibitor such as ganetespib as a second line therapy. There is potential to support future stratification of therapy for improved patient outcomes with HSP90 inhibitors.

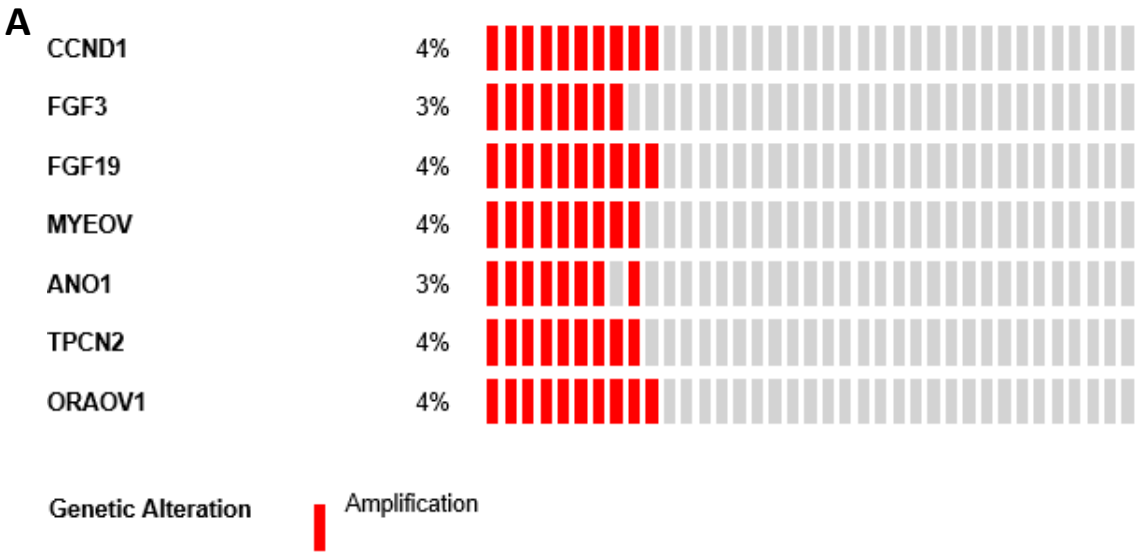

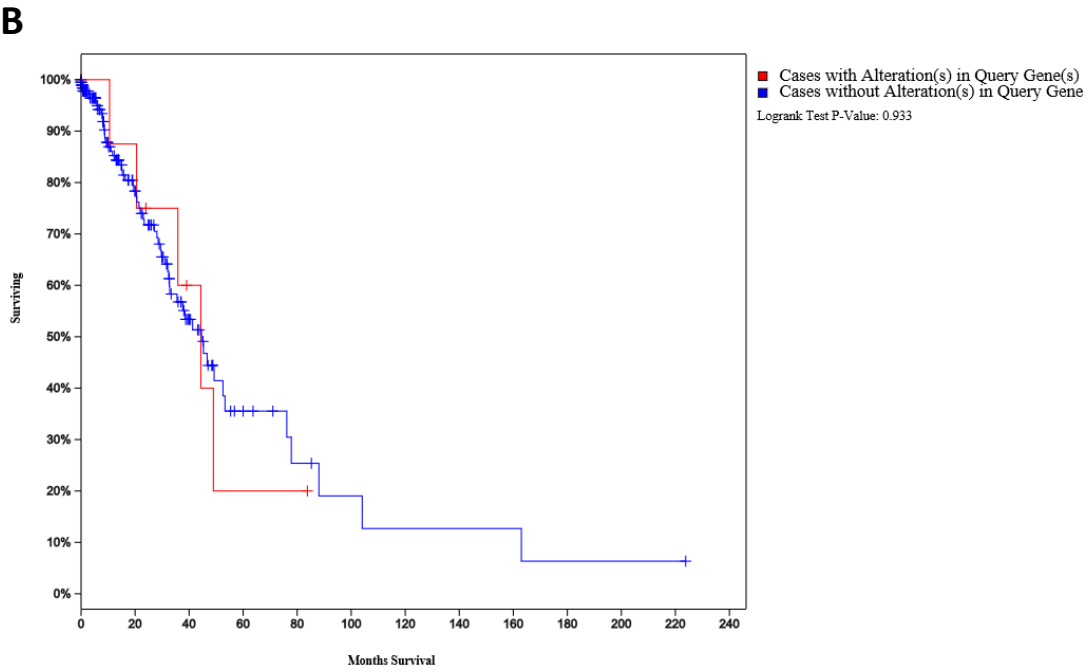

Figure 5.3-1 *Copy number and survival data from the TCGA dataset of 2014 from cBioportal (n=230) for genes within the 11q13.3 cytoband* ***(A)*** *Prevalence of CNAs within indicated genes* ***(B)*** *Effect of presence of CNAs on overall survival*

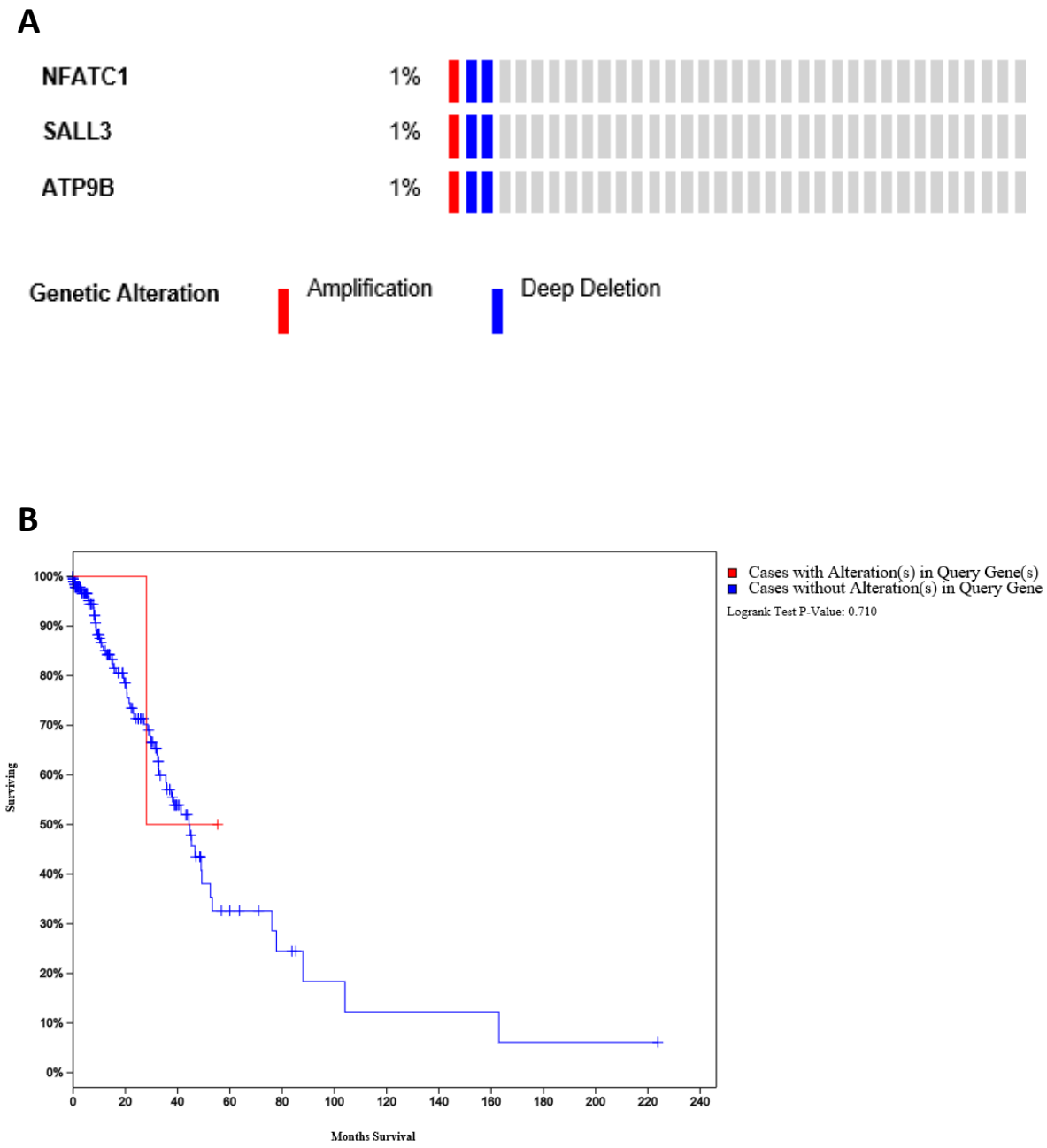

Figure 5.3-2 *Copy number and survival data from the TCGA dataset of 2014 from cBioportal (n=230) for genes within the 18q23 cytoband (A) Prevalence of CNAs within indicated genes (B) Effect of presence of CNAs on overall survival*

A

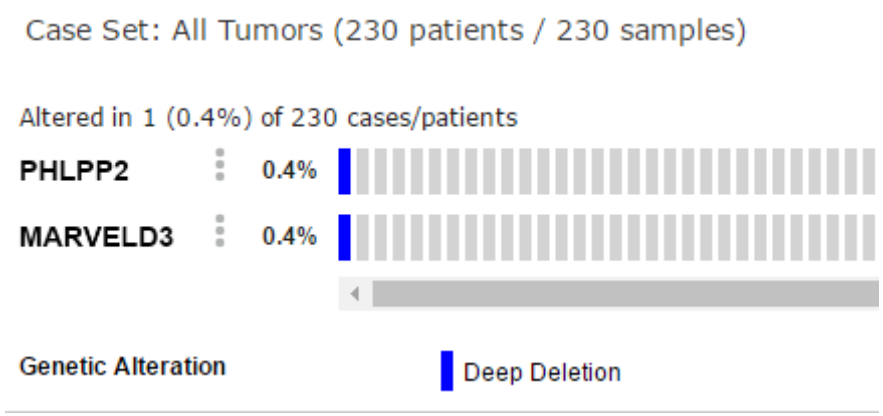

B

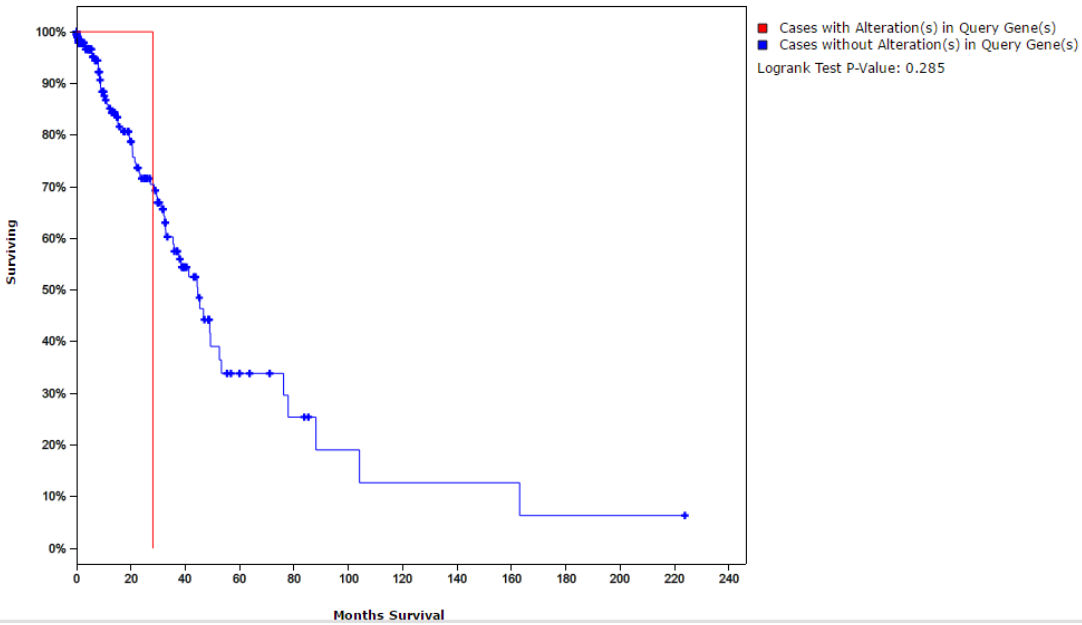

Figure 5.3-3 *Copy number and survival data from the TCGA dataset of 2014 from cBioportal (n=230) for genes within the 16q22.3 cytoband* ***(A)*** *Prevalence of CNAs within indicated genes* ***(B)*** *Effect of presence of CNAs on overall survival*

Chapter 6 – Final Discussion and future directions

6 Final discussion and future directions

6.1 Deciphering mechanisms of sensitivity and resistance to HSP90 inhibitors

Understanding mechanisms of sensitivity and resistance to small molecular inhibitors is key to deciphering treatment strategies. In order to transform NSCLC in to a long-term manageable disease, it is necessary to predict the likely copy number changes and genetic mutations that will arise, and predict sensitivity or resistance to specific therapeutics. Recent efforts to track tumour evolution in NSCLC revealed a great extent of tumour heterogeneity in terms of copy number alteration and mutation spatially and temporally, as well as mutations in APOBEC cytidine deaminises, which is involved in the tumour burden of NSCLC tumours [214]. Tumour heterogeneity evolution of NSCLC tumours in space and time is now being evaluated in an expanded study, to understand its effect on treatment outcome in the TRACERx (TRAcking non-small cell lung Cancer Evolution through therapy [Rx]) study [257]. A similar approach could be useful for all future trials of HSP90 inhibitors.

Linking clinical trials of HSP90 inhibitors with genetic data is a way to identify subpopulations which respond to treatment, and those that do not. Obtaining data at the DNA, RNA and protein level from tumour samples would be useful to make the potential biomarkers more robust. In chapter 3, a RT-PCR approach was developed to understand whether EML4-ALK variant status affects treatment outcome with ganetespib. If proved successful in a larger cohort, it would be worth expanding this research to focus on cfDNA, which would allow for a rapid, less invasive diagnostic test in order to determine correct treatment. However, the need for development of more comprehensive PK-PD work *in vitro* and *in vitro* before approaching clinical trials is clear: this includes establishing alteration of drug targets, assessing potential metabolic mechanisms or transporters and full assessment of likely solubility and safety.

However, much work remains in the field of HSP90 inhibition as a therapeutic strategy. Work in chapter 3 on EML4-ALK tentatively is interesting, but failed to produce a

useful biomarker. However, it did provide some evidence for the idea that client protein instability and disorganised protein structure is important as selection criteria for HSP90 clients, at least *in vitro*. This process is currently poorly understood, though Susan Lindquist's key study revealed that CDC37 sequestered only protein kinases, and that HSP90 bound more unstable clients [77]. It would be worthwhile to see if EML4-ALK stability and HSP90 client binding is observed *in vivo.* Comprehending HSP90-client interaction dynamics may allow for more specific drug strategies which take advantage of the client selection process, meaning a much more specific inhibition of selected client groups and possibly an improved safety profile.

Resistant mechanisms can be predicted by examining panels of cell lines, and comparing genetic profiles with drug response. Whilst the work in chapter 4 revealed an interesting mechanism of ganetespib drug metabolism in an NSCLC cell line context, no new mechanism of resistance to ganetespib was discovered, nor was it expanded to *in vivo* studies. Analysis of human NSCLC samples for UGT1A expression would benefit this project, particularly if survival data is available, in order to correlate UGT1A expression with HSP90 inhibitor response data. This work as it stands is much too small scale and is more of a "fishing" exercise in the hope that a mechanism of resistance is simple, when it could be complex involving many gene interactions. On the other hand, it has been demonstrated that acquired resistant mechanisms can be mimicked *in vitro* by rapid mutagenesis combined with multiple rounds of drug exposure; as in the case of Ba/F3 cells exposed to ENU and increasing levels of crizotinib predicted several gatekeeper mutations in ALK which render the drug ineffective [139]. Larger scale *in vitro* approaches could be used in order to improve the likelihood of detection of novel resistance mechanisms: a large scale mutagenesis approach such as ROSAFARY, which inserts into intronic genomic regions at random, utilising a "gene-trap" approach to silence genes [179]. After multiple rounds of drug exposure, surviving clones can be immediately identified using 3' RACE. However, such an approach is only able to effect heterozygous gene change. Looking forward, CRISPR (Clustered regularly-interspaced short palindromic repeats) approaches are being examined by multiple groups such as the Sanger Institute [258]. CRISPR/Cas9 (loss of function) CRISPR/SAM (gain of function) and ENU mutagenesis approaches are

combined with NGS sequencing to rapidly identify isogenic mutants which are resistant to a panel of drugs. The CRISPR/Cas9 loss of function screen approach was recently employed in models of mouse tumours to identify a set of genes responsible for metastasis [259].

In work recently published by our group, the mesothelioma-derived cell line MSTO gained acquired resistance to ganetespib via multiple rounds of drug exposure [230]. The resulting resistant MSTO STAR cell line was cross resistant to multiple HSP90 inhibitors, however apoptotic sensitivity could be restored by the addition of ABT-737: a BH3-peptidomimetic which inhibits BCL-2, BCL-xL and BCL-w**.** ABT-199 which only targets BCL-2 could not mimic this effect (**Figure 6.1-1)**. This BCL-2 family addiction switch has not been previously seen in the context of HSP90 inhibition. Dynamic BH3 profiling of NSCLC patients treated with HSP90 inhibitors may further elucidate the role of intrinsic apoptosis in response to HSP90 inhibition. Furthermore, Oncoscan analysis of the parental and resistant MSTO cell lines reveal that the MSTO STAR resistant cells have 81 regions of copy number change unique to the cell line (**Figure 6.1-2**). In addition, it's possible looking at the copy number profile that the MSTO STAR resistant cells have developed 4N hyperploidy, though this is not confirmed. It remains unclear how copy number changes affect MSTO STAR sensitivity to HSP90 inhibition, if at all. However, chromosomal instability has been previously induced by HSP90 inhibition-generated proteotoxic stress resulting in drug resistance [103].

Chapter 5 sought to identify copy number alterations as potential markers of sensitivity or resistance to ganetespib plus docetaxel in NSCLC lung adenocarcinoma patients. Three potential biomarkers were identified after FDR correction, with patients harbouring concurrent 18q23 loss, 11q13.3 gain and 16q22.3 gain appearing to represent the strongest predictive signal: however, it does seem that these CNAs are prognostic markers for poor response to docetaxel, which is somewhat rescued by the addition of ganetespib. This now needs to be verified in tumour DNA from patients enrolled in the phase III trial GALAXY-2 for verification. Further work to narrow down the genetic changes responsible for sensitivity are essential if a diagnostic test is to be produced such as a direct ratio test on plasma. The first step would be to sequentially knock out or knock in all genes within the top regions of copy number alteration across

multiple cell lines, preferably in a 3D model system, and assess changes in sensitivity to docetaxel and docetaxel plus ganetespib. Pathway analysis of genes within these regions may help to narrow this down. However, it is not known exactly what these copy number changes are doing – are they disrupting the gene, or a repressor or are they truly having a gene dosage effect? After a clear mechanism of action has been elucidated, work to see if these copy number changes can be detected reliably in blood plasma would be extremely useful in development of a diagnostic, as it would also be possible to measure copy number alterations as the disease progresses.

In summary, this work has found potentially interesting mechanisms that may play a role in ganetespib sensitivity in several different contexts, however more work is required in particular areas: firstly with regards to EML4-ALK to establish how clinically relevant the differential stability of EML4-ALK variants is, secondly to establish how important UGT1A expression is in NSCLC patients treated with HSP90 inhibitors, and finally validation of putative biomarkers in the GALAXY-1 trial, followed by elucidation of the mechanisms at work may open a door for personalising this treatment to NSCLC patients in the second line setting. As a final point of interest, it would be fascinating to see if patients with all top three CNAs discovered were mutually exclusive from the population who express PD-1/PD-L1, as if true it would represent a truly unique opportunity to finally realise the potential of HSP90 inhibition in the clinic.

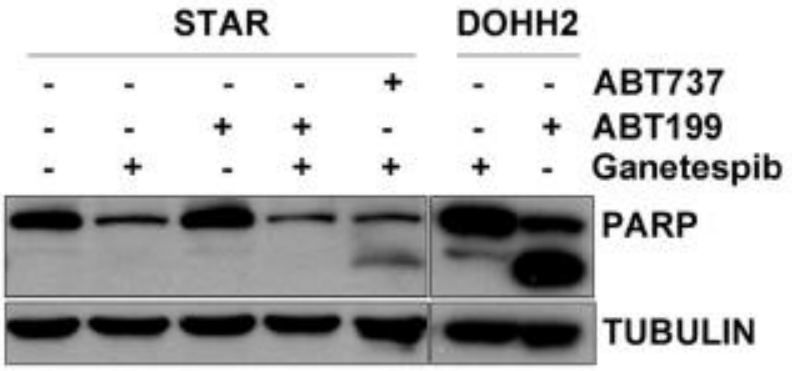

Figure 6.1-1 MSTO STAR resistant cells undergo apoptosis in response to treatment with ganetespib plus ABT-737 but not ABT-199. MSTO STAR cells were treated with 200nM ganetespib with or without 200nM ABT-737 or 200nM ABT-199 for 48h and assessed for apoptosis by western blot. DOHH2 BCL-2-dependent cells were used as a positive control for ABT-199 activity. Representative of n=3 experiments

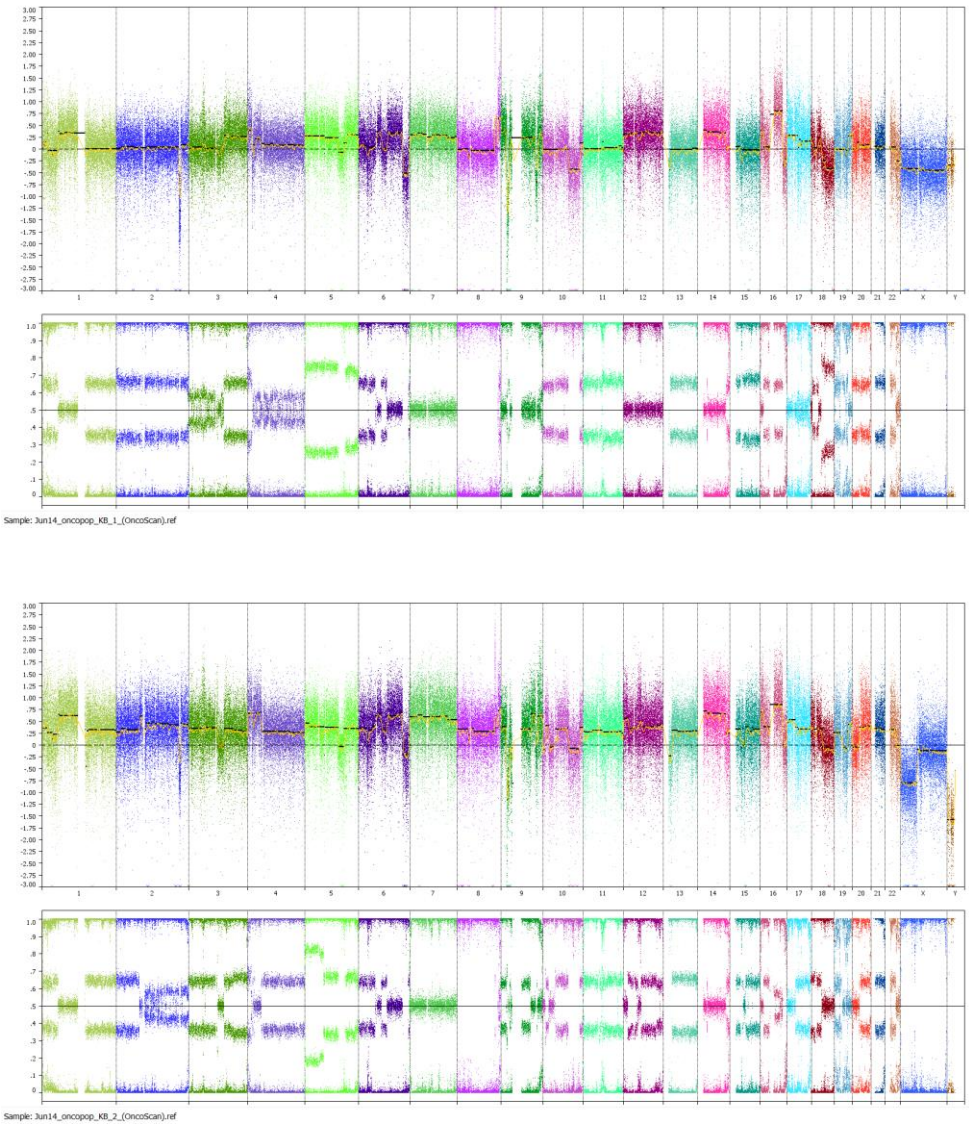

Figure 6.1-2 Global view of copy number profiles of MSTO parental (A) and MSTO STAR ganetespib resistant (B) cells. The upper panel represents the integer copy number value and the lower panel represents the B-allele frequency, obtained with the Oncoscan TuScan algorithm in Nexus.

7 References

1. Hanahan, D. and R.A. Weinberg, *Hallmarks of cancer: the next generation.* Cell, 2011. **144**(5): p. 646-74.
2. *Lung Cancer Statistics: Cancer Research UK* http://www.cancerresearchuk.org/cancer-info/cancerstats/types/lung/.
3. Kanaan, Z., et al., *Novel targeted therapies for resistant ALK-rearranged non-small-cell lung cancer: ceritinib and beyond.* Onco Targets Ther, 2015. **8**: p. 885-92.
4. Scagliotti, G.V., et al., *Phase III study comparing cisplatin plus gemcitabine with cisplatin plus pemetrexed in chemotherapy-naive patients with advanced-stage non-small-cell lung cancer.* J Clin Oncol, 2008. **26**(21): p. 3543-51.
5. Paez, J.G., et al., *EGFR mutations in lung cancer: correlation with clinical response to gefitinib therapy.* Science, 2004. **304**(5676): p. 1497-500.
6. Lynch, T.J., et al., *Activating mutations in the epidermal growth factor receptor underlying responsiveness of non-small-cell lung cancer to gefitinib.* N Engl J Med, 2004. **350**(21): p. 2129-39.
7. Han, S.W., et al., *Predictive and prognostic impact of epidermal growth factor receptor mutation in non-small-cell lung cancer patients treated with gefitinib.* J Clin Oncol, 2005. **23**(11): p. 2493-501.
8. Gridelli, C., et al., *Gefitinib as first-line treatment for patients with advanced non-small-cell lung cancer with activating epidermal growth factor receptor mutation: Review of the evidence.* Lung Cancer, 2011. **71**(3): p. 249-57.
9. Shimizu, F., et al., *The binding of insulin to mouse leucocytes during viral infections.* Diabetologia, 1983. **25**(6): p. 521-4.
10. Linardou, H., et al., *Assessment of somatic k-RAS mutations as a mechanism associated with resistance to EGFR-targeted agents: a systematic review and meta-analysis of studies in advanced non-small-cell lung cancer and metastatic colorectal cancer.* Lancet Oncol, 2008. **9**(10): p. 962-72.
11. Cox, A.D., et al., *Drugging the undruggable RAS: Mission possible?* Nat Rev Drug Discov, 2014. **13**(11): p. 828-51.
12. Blumenschein, G., et al., *A randomized phase III trial comparing ionafarnib/carboplatin/paclitaxel versus carboplatin/paclitaxel (CP) in chemotherapy-naive patients with advanced or metastatic non-small cell lung cancer (NSCLC).* Lung Cancer, 2005. **49**: p. S30-S30.
13. Janne, P.A., et al., *Selumetinib plus docetaxel for KRAS-mutant advanced non-small-cell lung cancer: a randomised, multicentre, placebo-controlled, phase 2 study.* Lancet Oncol, 2013. **14**(1): p. 38-47.
14. Heist, R.S. and J.A. Engelman, *SnapShot: non-small cell lung cancer.* Cancer Cell, 2012. **21**(3): p. 448 e2.
15. Gerber, D.E., L. Gandhi, and D.B. Costa, *Management and future directions in non-small cell lung cancer with known activating mutations.* Am Soc Clin Oncol Educ Book, 2014: p. e353-65.
16. Kobayashi, S., et al., *EGFR mutation and resistance of non-small-cell lung cancer to gefitinib.* N Engl J Med, 2005. **352**(8): p. 786-92.

17. Zou, M., et al., *Knockdown of the Bcl-2 gene increases sensitivity to EGFR tyrosine kinase inhibitors in the H1975 lung cancer cell line harboring T790M mutation.* Int J Oncol, 2013. **42**(6): p. 2094-102.
18. Montero, J. and A. Letai, *Dynamic BH3 profiling-poking cancer cells with a stick.* Mol Cell Oncol, 2016. **3**(3): p. e1040144.
19. Oxnard, G.R., et al., *New strategies in overcoming acquired resistance to epidermal growth factor receptor tyrosine kinase inhibitors in lung cancer.* Clin Cancer Res, 2011. **17**(17): p. 5530-7.
20. Katayama, R., et al., *Therapeutic strategies to overcome crizotinib resistance in non-small cell lung cancers harboring the fusion oncogene EML4-ALK.* Proc Natl Acad Sci U S A, 2011. **108**(18): p. 7535-40.
21. Zhang, C.H. and Y.P. Zhang, *Maximizing the commercial value of personalized therapeutics and companion diagnostics.* Nat Biotechnol, 2013. **31**(9): p. 803-5.
22. Amidon, G.L., et al., *A theoretical basis for a biopharmaceutic drug classification: the correlation of in vitro drug product dissolution and in vivo bioavailability.* Pharm Res, 1995. **12**(3): p. 413-20.
23. Gallo, J.M., *Pharmacokinetic/ pharmacodynamic-driven drug development.* Mt Sinai J Med, 2010. **77**(4): p. 381-8.
24. Chun, S.G., et al., *Isolated central nervous system progression on Crizotinib: an Achilles heel of non-small cell lung cancer with EML4-ALK translocation?* Cancer Biol Ther, 2012. **13**(14): p. 1376-83.
25. Trepel, J., et al., *Targeting the dynamic HSP90 complex in cancer.* Nat Rev Cancer, 2010. **10**(8): p. 537-49.
26. Xu, W., et al., *Chaperone-dependent E3 ubiquitin ligase CHIP mediates a degradative pathway for c-ErbB2/Neu.* Proc Natl Acad Sci U S A, 2002. **99**(20): p. 12847-52.
27. Chatterjee, S., et al., *HSP90 inhibitors in lung cancer: promise still unfulfilled.* Clin Adv Hematol Oncol, 2016. **14**(5): p. 346-56.
28. Banerji, U., et al., *Phase I pharmacokinetic and pharmacodynamic study of 17-allylamino, 17-demethoxygeldanamycin in patients with advanced malignancies.* J Clin Oncol, 2005. **23**(18): p. 4152-61.
29. Supko, J.G., et al., *Preclinical pharmacologic evaluation of geldanamycin as an antitumor agent.* Cancer Chemother Pharmacol, 1995. **36**(4): p. 305-15.
30. Samuni, Y., et al., *Reactive oxygen species mediate hepatotoxicity induced by the Hsp90 inhibitor geldanamycin and its analogs.* Free Radic Biol Med, 2010. **48**(11): p. 1559-63.
31. Ying, W., et al., *Ganetespib, a unique triazolone-containing Hsp90 inhibitor, exhibits potent antitumor activity and a superior safety profile for cancer therapy.* Mol Cancer Ther, 2012. **11**(2): p. 475-84.
32. Smith, V., et al., *Comparison of 17-dimethylaminoethylamino-17-demethoxy-geldanamycin (17DMAG) and 17-allylamino-17-demethoxygeldanamycin (17AAG) in vitro: effects on Hsp90 and client proteins in melanoma models.* Cancer Chemother Pharmacol, 2005. **56**(2): p. 126-37.
33. Kim, Y.S., et al., *Update on Hsp90 inhibitors in clinical trial.* Curr Top Med Chem, 2009. **9**(15): p. 1479-92.
34. Biamonte, M.A., et al., *Heat shock protein 90: inhibitors in clinical trials.* J Med Chem, 2010. **53**(1): p. 3-17.

35. Brough, P.A., et al., *4,5-diarylisoxazole Hsp90 chaperone inhibitors: potential therapeutic agents for the treatment of cancer.* J Med Chem, 2008. **51**(2): p. 196-218.
36. Sequist, L.V., et al., *Activity of IPI-504, a novel heat-shock protein 90 inhibitor, in patients with molecularly defined non-small-cell lung cancer.* J Clin Oncol, 2010. **28**(33): p. 4953-60.
37. Socinski, M.A., et al., *A multicenter Phase II study of ganetespib monotherapy in patients with genotypically-defined advanced non-small cell lung cancer.* Clin Cancer Res, 2013.
38. Sang, J., et al., *Targeted Inhibition of the Molecular Chaperone Hsp90 Overcomes ALK Inhibitor Resistance in Non-Small Cell Lung Cancer.* Cancer Discov, 2013. **3**(4): p. 430-43.
39. Ramalingam, S., et al., *A randomized phase II study of ganetespib, a heat shock protein 90 inhibitor, in combination with docetaxel in second-line therapy of advanced non-small cell lung cancer (GALAXY-1).* Ann Oncol, 2015. **26**(8): p. 1741-8.
40. Johnson, M.L., et al., *Phase I/II Study of HSP90 Inhibitor AUY922 and Erlotinib for EGFR-Mutant Lung Cancer With Acquired Resistance to Epidermal Growth Factor Receptor Tyrosine Kinase Inhibitors.* J Clin Oncol, 2015. **33**(15): p. 1666-73.
41. Ritossa, F., *A new puffing pattern induced by temperature shock and DNP in Drosophila.* Experienta, 1962. **18**: p. 571-573.
42. Ritossa, F., *New puffs induced by temperature shock, DNP and salicilate in salivary chromosomes of D. melanogaster. Drosophila* Information Service, 1963. ***37***: p. 122-123.
43. Ritossa, F., *Experimental activation of specific loci in polytene chromosome of Drosophila.* Exp Cell Res, 1963. **35**: p. 601-607.
44. Ritossa, F., *Discovery of the heat shock response.* Cell Stress Chaperones, 1996. **1**(2): p. 97-8.
45. Brugge, J.S., E. Erikson, and R.L. Erikson, *The specific interaction of the Rous sarcoma virus transforming protein, pp60src, with two cellular proteins.* Cell, 1981. **25**(2): p. 363-72.
46. Oppermann, H., et al., *Two cellular proteins that immunoprecipitate with the transforming protein of Rous sarcoma virus.* Virology, 1981. **113**(2): p. 736-51.
47. Wang, X., et al., *HSP27, 70 and 90, anti-apoptotic proteins, in clinical cancer therapy (Review).* Int J Oncol, 2014. **45**(1): p. 18-30.
48. Kampinga, H.H., et al., *Guidelines for the nomenclature of the human heat shock proteins.* Cell Stress Chaperones, 2009. **14**(1): p. 105-11.
49. Bagatell, R., et al., *Hsp90 inhibitors deplete key anti-apoptotic proteins in pediatric solid tumor cells and demonstrate synergistic anticancer activity with cisplatin.* Int J Cancer, 2005. **113**(2): p. 179-88.
50. Ahmed, F., R.A. Williams, and K.E. Smith, *Microbial transformation of steroids--IX. Purification of progesterone hydroxylase cytochrome P-450 from Phycomyces blakesleeanus.* J Steroid Biochem Mol Biol, 1995. **52**(2): p. 203-8.
51. Vasko, R.C., et al., *Mechanistic studies of Sansalvamide A-amide: an allosteric modulator of Hsp90.* ACS Med Chem Lett, 2010. **1**(1): p. 4-8.

52. Shiau, A.K., et al., *Structural Analysis of E. coli hsp90 reveals dramatic nucleotide-dependent conformational rearrangements.* Cell, 2006. **127**(2): p. 329-40.
53. Mickler, M., et al., *The large conformational changes of Hsp90 are only weakly coupled to ATP hydrolysis.* Nat Struct Mol Biol, 2009. **16**(3): p. 281-6.
54. Hessling, M., K. Richter, and J. Buchner, *Dissection of the ATP-induced conformational cycle of the molecular chaperone Hsp90.* Nat Struct Mol Biol, 2009. **16**(3): p. 287-93.
55. Ali, M.M., et al., *Crystal structure of an Hsp90-nucleotide-p23/Sba1 closed chaperone complex.* Nature, 2006. **440**(7087): p. 1013-7.
56. Li, J. and J. Buchner, *Structure, function and regulation of the hsp90 machinery.* Biomed J, 2013. **36**(3): p. 106-17.
57. Kim, H.R., H.S. Kang, and H.D. Kim, *Geldanamycin induces heat shock protein expression through activation of HSF1 in K562 erythroleukemic cells.* IUBMB Life, 1999. **48**(4): p. 429-33.
58. Hu, Y. and N.F. Mivechi, *HSF-1 interacts with Ral-binding protein 1 in a stress-responsive, multiprotein complex with HSP90 in vivo.* J Biol Chem, 2003. **278**(19): p. 17299-306.
59. Gupta, R.S., *Phylogenetic analysis of the 90 kD heat shock family of protein sequences and an examination of the relationship among animals, plants, and fungi species.* Mol Biol Evol, 1995. **12**(6): p. 1063-73.
60. Sreedhar, A.S., et al., *Hsp90 isoforms: functions, expression and clinical importance.* FEBS Lett, 2004. **562**(1-3): p. 11-5.
61. Eustace, B.K., et al., *Functional proteomic screens reveal an essential extracellular role for hsp90 alpha in cancer cell invasiveness.* Nat Cell Biol, 2004. **6**(6): p. 507-14.
62. Lele, Z., et al., *Disruption of zebrafish somite development by pharmacologic inhibition of Hsp90.* Dev Biol, 1999. **210**(1): p. 56-70.
63. Gruppi, C.M., Z.F. Zakeri, and D.J. Wolgemuth, *Stage and lineage-regulated expression of two hsp90 transcripts during mouse germ cell differentiation and embryogenesis.* Mol Reprod Dev, 1991. **28**(3): p. 209-17.
64. Millson, S.H., et al., *Expressed as the sole Hsp90 of yeast, the alpha and beta isoforms of human Hsp90 differ with regard to their capacities for activation of certain client proteins, whereas only Hsp90beta generates sensitivity to the Hsp90 inhibitor radicicol.* FEBS J, 2007. **274**(17): p. 4453-63.
65. Chan, C.T., et al., *Molecular imaging of the efficacy of heat shock protein 90 inhibitors in living subjects.* Cancer Res, 2008. **68**(1): p. 216-26.
66. Grammatikakis, N., et al., *The role of Hsp90N, a new member of the Hsp90 family, in signal transduction and neoplastic transformation.* J Biol Chem, 2002. **277**(10): p. 8312-20.
67. Zurawska, A., J. Urbanski, and P. Bieganowski, *Hsp90n - An accidental product of a fortuitous chromosomal translocation rather than a regular Hsp90 family member of human proteome.* Biochim Biophys Acta, 2008. **1784**(11): p. 1844-6.
68. Song, H.Y., et al., *Identification of a protein with homology to hsp90 that binds the type 1 tumor necrosis factor receptor.* J Biol Chem, 1995. **270**(8): p. 3574-81.

69. Felts, S.J., et al., *The hsp90-related protein TRAP1 is a mitochondrial protein with distinct functional properties.* J Biol Chem, 2000. **275**(5): p. 3305-12.
70. Montesano Gesualdi, N., et al., *Tumor necrosis factor-associated protein 1 (TRAP-1) protects cells from oxidative stress and apoptosis.* Stress, 2007. **10**(4): p. 342-50.
71. Kang, B.H., *TRAP1 regulation of mitochondrial life or death decision in cancer cells and mitochondria-targeted TRAP1 inhibitors.* BMB Rep, 2012. **45**(1): p. 1-6.
72. Agorreta, J., et al., *TRAP1 regulates proliferation, mitochondrial function, and has prognostic significance in NSCLC.* Mol Cancer Res, 2014. **12**(5): p. 660-9.
73. Marzec, M., D. Eletto, and Y. Argon, *GRP94: An HSP90-like protein specialized for protein folding and quality control in the endoplasmic reticulum.* Biochim Biophys Acta, 2012. **1823**(3): p. 774-87.
74. Van, P.N., F. Peter, and H.D. Soling, *Four intracisternal calcium-binding glycoproteins from rat liver microsomes with high affinity for calcium. No indication for calsequestrin-like proteins in inositol 1,4,5-trisphosphate-sensitive calcium sequestering rat liver vesicles.* J Biol Chem, 1989. **264**(29): p. 17494-501.
75. Holmes, J.L., et al., *Silencing of HSP90 cochaperone AHA1 expression decreases client protein activation and increases cellular sensitivity to the HSP90 inhibitor 17-allylamino-17-demethoxygeldanamycin.* Cancer Res, 2008. **68**(4): p. 1188-97.
76. Panaretou, B., et al., *Activation of the ATPase activity of hsp90 by the stress-regulated cochaperone aha1.* Mol Cell, 2002. **10**(6): p. 1307-18.
77. Taipale, M., et al., *Quantitative analysis of HSP90-client interactions reveals principles of substrate recognition.* Cell, 2012. **150**(5): p. 987-1001.
78. Connell, P., et al., *The co-chaperone CHIP regulates protein triage decisions mediated by heat-shock proteins.* Nat Cell Biol, 2001. **3**(1): p. 93-6.
79. Vaughan, C.K., et al., *Hsp90-dependent activation of protein kinases is regulated by chaperone-targeted dephosphorylation of Cdc37.* Mol Cell, 2008. **31**(6): p. 886-95.
80. Johnson, T.R., et al., *The proteasome inhibitor PS-341 overcomes TRAIL resistance in Bax and caspase 9-negative or Bcl-xL overexpressing cells.* Oncogene, 2003. **22**(32): p. 4953-63.
81. Yang, X., et al., *Hsp70 promotes chemoresistance by blocking Bax mitochondrial translocation in ovarian cancer cells.* Cancer Lett, 2012. **321**(2): p. 137-43.
82. Beere, H.M., et al., *Heat-shock protein 70 inhibits apoptosis by preventing recruitment of procaspase-9 to the Apaf-1 apoptosome.* Nat Cell Biol, 2000. **2**(8): p. 469-75.
83. Powers, M.V., P.A. Clarke, and P. Workman, *Dual targeting of HSC70 and HSP72 inhibits HSP90 function and induces tumor-specific apoptosis.* Cancer Cell, 2008. **14**(3): p. 250-62.
84. Hanahan, D. and R.A. Weinberg, *The hallmarks of cancer.* Cell, 2000. **100**(1): p. 57-70.
85. Nanbu, K., et al., *Expression of heat shock proteins HSP70 and HSP90 in endometrial carcinomas. Correlation with clinicopathology, sex steroid receptor status, and p53 protein expression.* Cancer, 1996. **77**(2): p. 330-8.

86. Yano, M., et al., *Expression and roles of heat shock proteins in human breast cancer.* Jpn J Cancer Res, 1996. **87**(9): p. 908-15.
87. Strik, H.M., et al., *Heat shock protein expression in human gliomas.* Anticancer Res, 2000. **20**(6B): p. 4457-62.
88. Hauser, P., et al., *Expression and prognostic examination of heat shock proteins (HSP 27, HSP 70, and HSP 90) in medulloblastoma.* J Pediatr Hematol Oncol, 2006. **28**(7): p. 461-6.
89. Ferrarini, M., et al., *Unusual expression and localization of heat-shock proteins in human tumor cells.* Int J Cancer, 1992. **51**(4): p. 613-9.
90. Kamal, A., et al., *A high-affinity conformation of Hsp90 confers tumour selectivity on Hsp90 inhibitors.* Nature, 2003. **425**(6956): p. 407-10.
91. Hardcastle, A., et al., *A duplexed phenotypic screen for the simultaneous detection of inhibitors of the molecular chaperone heat shock protein 90 and modulators of cellular acetylation.* Mol Cancer Ther, 2007. **6**(3): p. 1112-22.
92. da Silva, V.C. and C.H. Ramos, *The network interaction of the human cytosolic 90 kDa heat shock protein Hsp90: A target for cancer therapeutics.* J Proteomics, 2012. **75**(10): p. 2790-802.
93. Amar, V., et al., *Large cystic renal cell carcinoma leading to diagnostic dilemma: a case report.* Indian J Surg, 2013. **75**(Suppl 1): p. 103-5.
94. Chen, Y.X., et al., *Dexamethasone enhances cell resistance to chemotherapy by increasing adhesion to extracellular matrix in human ovarian cancer cells.* Endocr Relat Cancer, 2010. **17**(1): p. 39-50.
95. Dias, N. and C.A. Stein, *Potential roles of antisense oligonucleotides in cancer therapy. The example of Bcl-2 antisense oligonucleotides.* Eur J Pharm Biopharm, 2002. **54**(3): p. 263-9.
96. Fortugno, P., et al., *Regulation of survivin function by Hsp90.* Proc Natl Acad Sci U S A, 2003. **100**(24): p. 13791-6.
97. Pandey, P., et al., *Negative regulation of cytochrome c-mediated oligomerization of Apaf-1 and activation of procaspase-9 by heat shock protein 90.* EMBO J, 2000. **19**(16): p. 4310-22.
98. Chakraborty, A., et al., *HSP90 regulates cell survival via inositol hexakisphosphate kinase-2.* Proc Natl Acad Sci U S A, 2008. **105**(4): p. 1134-9.
99. Forsythe, H.L., et al., *Stable association of hsp90 and p23, but Not hsp70, with active human telomerase.* J Biol Chem, 2001. **276**(19): p. 15571-4.
100. Keppler, B.R., A.T. Grady, and M.B. Jarstfer, *The biochemical role of the heat shock protein 90 chaperone complex in establishing human telomerase activity.* J Biol Chem, 2006. **281**(29): p. 19840-8.
101. Kim, R.H., et al., *Association of hsp90 to the hTERT promoter is necessary for hTERT expression in human oral cancer cells.* Carcinogenesis, 2008. **29**(12): p. 2425-31.
102. Neckers, L. and P. Workman, *Hsp90 molecular chaperone inhibitors: are we there yet?* Clin Cancer Res, 2012. **18**(1): p. 64-76.
103. Chen, G., et al., *Hsp90 stress potentiates rapid cellular adaptation through induction of aneuploidy.* Nature, 2012. **482**(7384): p. 246-50.
104. Arlander, S.J., et al., *Hsp90 inhibition depletes Chk1 and sensitizes tumor cells to replication stress.* J Biol Chem, 2003. **278**(52): p. 52572-7.

105. Senju, M., et al., *Hsp90 inhibitors cause G2/M arrest associated with the reduction of Cdc25C and Cdc2 in lung cancer cell lines.* J Cancer Res Clin Oncol, 2006. **132**(3): p. 150-8.
106. O'Connell, B.C., et al., *HSP90 inhibition enhances antimitotic drug-induced mitotic arrest and cell death in preclinical models of non-small cell lung cancer.* PLoS One, 2014. **9**(12): p. e115228.
107. Gallegos Ruiz, M.I., et al., *Integration of gene dosage and gene expression in non-small cell lung cancer, identification of HSP90 as potential target.* PLoS One, 2008. **3**(3): p. e0001722.
108. Acquaviva, J., et al., *Targeting KRAS Mutant Non-Small Cell Lung Cancer with the Hsp90 Inhibitor Ganetespib.* Mol Cancer Ther, 2012.
109. Bao, R., et al., *Targeting heat shock protein 90 with CUDC-305 overcomes erlotinib resistance in non-small cell lung cancer.* Mol Cancer Ther, 2009. **8**(12): p. 3296-306.
110. Chen, Z., et al., *Inhibition of ALK, PI3K/MEK, and HSP90 in murine lung adenocarcinoma induced by EML4-ALK fusion oncogene.* Cancer Res, 2010. **70**(23): p. 9827-36.
111. Normant, E., et al., *The Hsp90 inhibitor IPI-504 rapidly lowers EML4-ALK levels and induces tumor regression in ALK-driven NSCLC models.* Oncogene, 2011. **30**(22): p. 2581-6.
112. Morris, S.W., et al., *Fusion of a kinase gene, ALK, to a nucleolar protein gene, NPM, in non-Hodgkin's lymphoma.* Science, 1994. **263**(5151): p. 1281-4.
113. Bischof, D., et al., *Role of the nucleophosmin (NPM) portion of the non-Hodgkin's lymphoma-associated NPM-anaplastic lymphoma kinase fusion protein in oncogenesis.* Mol Cell Biol, 1997. **17**(4): p. 2312-25.
114. Morris, S.W., et al., *ALK, the chromosome 2 gene locus altered by the t(2;5) in non-Hodgkin's lymphoma, encodes a novel neural receptor tyrosine kinase that is highly related to leukocyte tyrosine kinase (LTK).* Oncogene, 1997. **14**(18): p. 2175-88.
115. Wellstein, A., *ALK receptor activation, ligands and therapeutic targeting in glioblastoma and in other cancers.* Front Oncol, 2012. **2**: p. 192.
116. Soda, M., et al., *Identification of the transforming EML4-ALK fusion gene in non-small-cell lung cancer.* Nature, 2007. **448**(7153): p. 561-6.
117. Choi, Y.L., et al., *Identification of novel isoforms of the EML4-ALK transforming gene in non-small cell lung cancer.* Cancer Res, 2008. **68**(13): p. 4971-6.
118. Inamura, K., et al., *EML4-ALK fusion is linked to histological characteristics in a subset of lung cancers.* J Thorac Oncol, 2008. **3**(1): p. 13-7.
119. Koivunen, J.P., et al., *EML4-ALK fusion gene and efficacy of an ALK kinase inhibitor in lung cancer.* Clin Cancer Res, 2008. **14**(13): p. 4275-83.
120. Shinmura, K., et al., *EML4-ALK fusion transcripts, but no NPM-, TPM3-, CLTC-, ATIC-, or TFG-ALK fusion transcripts, in non-small cell lung carcinomas.* Lung Cancer, 2008. **61**(2): p. 163-9.
121. Martelli, M.P., et al., *EML4-ALK rearrangement in non-small cell lung cancer and non-tumor lung tissues.* Am J Pathol, 2009. **174**(2): p. 661-70.
122. Shaw, A.T., et al., *Clinical features and outcome of patients with non-small-cell lung cancer who harbor EML4-ALK.* J Clin Oncol, 2009. **27**(26): p. 4247-53.

123. Wong, D.W., et al., *The EML4-ALK fusion gene is involved in various histologic types of lung cancers from nonsmokers with wild-type EGFR and KRAS.* Cancer, 2009. **115**(8): p. 1723-33.
124. Takeuchi, K., et al., *Multiplex reverse transcription-PCR screening for EML4-ALK fusion transcripts.* Clin Cancer Res, 2008. **14**(20): p. 6618-24.
125. Fukuyoshi, Y., et al., *EML4-ALK fusion transcript is not found in gastrointestinal and breast cancers.* Br J Cancer, 2008. **98**(9): p. 1536-9.
126. Perner, S., et al., *EML4-ALK fusion lung cancer: a rare acquired event.* Neoplasia, 2008. **10**(3): p. 298-302.
127. Takahashi, T., et al., *Clinicopathologic features of non-small-cell lung cancer with EML4-ALK fusion gene.* Ann Surg Oncol, 2010. **17**(3): p. 889-97.
128. Sasaki, T., et al., *The biology and treatment of EML4-ALK non-small cell lung cancer.* Eur J Cancer, 2010. **46**(10): p. 1773-80.
129. Takeuchi, K., et al., *KIF5B-ALK, a novel fusion oncokinase identified by an immunohistochemistry-based diagnostic system for ALK-positive lung cancer.* Clin Cancer Res, 2009. **15**(9): p. 3143-9.
130. Rikova, K., et al., *Global survey of phosphotyrosine signaling identifies oncogenic kinases in lung cancer.* Cell, 2007. **131**(6): p. 1190-203.
131. Shaw, A.T. and J.A. Engelman, *ALK in lung cancer: past, present, and future.* J Clin Oncol, 2013. **31**(8): p. 1105-11.
132. Jemal, A., et al., *Annual report to the nation on the status of cancer, 1975-2001, with a special feature regarding survival.* Cancer, 2004. **101**(1): p. 3-27.
133. Chia, P.L., et al., *Prevalence and natural history of ALK positive non-small-cell lung cancer and the clinical impact of targeted therapy with ALK inhibitors.* Clin Epidemiol, 2014. **6**: p. 423-32.
134. Marzec, M., et al., *Inhibition of ALK enzymatic activity in T-cell lymphoma cells induces apoptosis and suppresses proliferation and STAT3 phosphorylation independently of Jak3.* Lab Invest, 2005. **85**(12): p. 1544-54.
135. Takezawa, K., et al., *Role of ERK-BIM and STAT3-survivin signaling pathways in ALK inhibitor-induced apoptosis in EML4-ALK-positive lung cancer.* Clin Cancer Res, 2011. **17**(8): p. 2140-8.
136. Kwak, E.L., et al., *Anaplastic lymphoma kinase inhibition in non-small-cell lung cancer.* N Engl J Med, 2010. **363**(18): p. 1693-703.
137. Gridelli, C., et al., *Second-line treatment of advanced non-small cell lung cancer.* J Thorac Oncol, 2008. **3**(4): p. 430-40.
138. Choi, Y.L., et al., *EML4-ALK mutations in lung cancer that confer resistance to ALK inhibitors.* N Engl J Med, 2010. **363**(18): p. 1734-9.
139. Zhang, S., et al., *Crizotinib-resistant mutants of EML4-ALK identified through an accelerated mutagenesis screen.* Chem Biol Drug Des, 2011. **78**(6): p. 999-1005.
140. Heuckmann, J.M., et al., *ALK mutations conferring differential resistance to structurally diverse ALK inhibitors.* Clin Cancer Res, 2011. **17**(23): p. 7394-401.
141. Doebele, R.C., et al., *Mechanisms of resistance to crizotinib in patients with ALK gene rearranged non-small cell lung cancer.* Clin Cancer Res, 2012. **18**(5): p. 1472-82.
142. Costa, D.B., et al., *CSF concentration of the anaplastic lymphoma kinase inhibitor crizotinib.* J Clin Oncol, 2011. **29**(15): p. e443-5.

143. Chun, S.G., et al., *Isolated central nervous system progression on Crizotinib: An Achilles heel of non-small cell lung cancer with EML4-ALK translocation?* Cancer Biol Ther, 2012. **13**(14).
144. Shaw, A.T. and J.A. Engelman, *Ceritinib in ALK-rearranged non-small-cell lung cancer.* N Engl J Med, 2014. **370**(26): p. 2537-9.
145. Seto, T., et al., *CH5424802 (RO5424802) for patients with ALK-rearranged advanced non-small-cell lung cancer (AF-001JP study): a single-arm, open-label, phase 1-2 study.* Lancet Oncol, 2013. **14**(7): p. 590-8.
146. Kodama, T., et al., *Antitumor activity of the selective ALK inhibitor alectinib in models of intracranial metastases.* Cancer Chemother Pharmacol, 2014. **74**(5): p. 1023-8.
147. Shaw, A.T., et al., *Resensitization to Crizotinib by the Lorlatinib ALK Resistance Mutation L1198F.* N Engl J Med, 2016. **374**(1): p. 54-61.
148. Egorin, M.J., et al., *Plasma pharmacokinetics and tissue distribution of 17-(allylamino)-17-demethoxygeldanamycin (NSC 330507) in CD2F1 mice1.* Cancer Chemother Pharmacol, 2001. **47**(4): p. 291-302.
149. Nagaraju, G.P., et al., *Antiangiogenic effects of ganetespib in colorectal cancer mediated through inhibition of HIF-1alpha and STAT-3.* Angiogenesis, 2013. **16**(4): p. 903-17.
150. Nagaraju, G.P., et al., *HSP90 inhibition downregulates thymidylate synthase and sensitizes colorectal cancer cell lines to the effect of 5FU-based chemotherapy.* Oncotarget, 2014. **5**(20): p. 9980-91.
151. Miyajima, N., et al., *The HSP90 inhibitor ganetespib synergizes with the MET kinase inhibitor crizotinib in both crizotinib-sensitive and -resistant MET-driven tumor models.* Cancer Res, 2013. **73**(23): p. 7022-33.
152. Webber, P.J., et al., *Combination of heat shock protein 90 and focal adhesion kinase inhibitors synergistically inhibits the growth of non-small cell lung cancer cells.* Oncoscience, 2015. **2**(9): p. 765-76.
153. Lai, C.H., et al., *HSP-90 inhibitor ganetespib is synergistic with doxorubicin in small cell lung cancer.* Oncogene, 2014. **33**(40): p. 4867-76.
154. Gomez-Casal, R., et al., *The HSP90 Inhibitor Ganetespib Radiosensitizes Human Lung Adenocarcinoma Cells.* Cancers (Basel), 2015. **7**(2): p. 876-907.
155. Proia, D.A., et al., *Synergistic activity of the Hsp90 inhibitor ganetespib with taxanes in non-small cell lung cancer models.* Invest New Drugs, 2012. **30**(6): p. 2201-9.
156. Vaughan, C.K., et al., *A common conformationally coupled ATPase mechanism for yeast and human cytoplasmic HSP90s.* FEBS J, 2009. **276**(1): p. 199-209.
157. Prodromou, C., et al., *Structural basis of the radicicol resistance displayed by a fungal hsp90.* ACS Chem Biol, 2009. **4**(4): p. 289-97.
158. Millson, S.H., et al., *Features of the Streptomyces hygroscopicus HtpG reveal how partial geldanamycin resistance can arise with mutation to the ATP binding pocket of a eukaryotic Hsp90.* FASEB J, 2011. **25**(11): p. 3828-37.
159. Robbins, N., M.D. Leach, and L.E. Cowen, *Lysine deacetylases Hda1 and Rpd3 regulate Hsp90 function thereby governing fungal drug resistance.* Cell Rep, 2012. **2**(4): p. 878-88.

160. Rao, R., et al., *HDAC6 inhibition enhances 17-AAG--mediated abrogation of hsp90 chaperone function in human leukemia cells.* Blood, 2008. **112**(5): p. 1886-93.
161. Institute, B. *Tumorscape - Copy Number Alterations Across Multiple Cancer Types*. [cited 2015; Available from: http://www.broadinstitute.org/tumorscape/.
162. Cheng, Q., et al., *Amplification and high-level expression of heat shock protein 90 marks aggressive phenotypes of human epidermal growth factor receptor 2 negative breast cancer.* Breast Cancer Res, 2012. **14**(2): p. R62.
163. Gaspar, N., et al., *Acquired resistance to 17-allylamino-17-demethoxygeldanamycin (17-AAG, tanespimycin) in glioblastoma cells.* Cancer Res, 2009. **69**(5): p. 1966-75.
164. McCollum, A.K., et al., *P-Glycoprotein-mediated resistance to Hsp90-directed therapy is eclipsed by the heat shock response.* Cancer Res, 2008. **68**(18): p. 7419-27.
165. Kim, H.J., et al., *P-glycoprotein confers acquired resistance to 17-DMAG in lung cancers with an ALK rearrangement.* BMC Cancer, 2015. **15**(1): p. 553.
166. Bertram, J., et al., *Increase of P-glycoprotein-mediated drug resistance by hsp 90 beta.* Anticancer Drugs, 1996. **7**(8): p. 838-45.
167. Guo, W., et al., *Formation of 17-allylamino-demethoxygeldanamycin (17-AAG) hydroquinone by NAD(P)H:quinone oxidoreductase 1: role of 17-AAG hydroquinone in heat shock protein 90 inhibition.* Cancer Res, 2005. **65**(21): p. 10006-15.
168. Guo, W., et al., *The bioreduction of a series of benzoquinone ansamycins by NAD(P)H:quinone oxidoreductase 1 to more potent heat shock protein 90 inhibitors, the hydroquinone ansamycins.* Mol Pharmacol, 2006. **70**(4): p. 1194-203.
169. Strassburg, C.P., S. Kalthoff, and U. Ehmer, *Variability and function of family 1 uridine-5'-diphosphate glucuronosyltransferases (UGT1A).* Crit Rev Clin Lab Sci, 2008. **45**(6): p. 485-530.
170. Landmann, H., et al., *UDP glucuronosyltransferase 1A expression levels determine the response of colorectal cancer cells to the heat shock protein 90 inhibitor ganetespib.* Cell Death Dis, 2014. **5**: p. e1411.
171. Acquaviva, J., et al., *FGFR3 translocations in bladder cancer: differential sensitivity to HSP90 inhibition based on drug metabolism.* Mol Cancer Res, 2014. **12**(7): p. 1042-54.
172. Whitesell, L. and S.L. Lindquist, *HSP90 and the chaperoning of cancer.* Nat Rev Cancer, 2005. **5**(10): p. 761-72.
173. Samant, R.S., P.A. Clarke, and P. Workman, *E3 ubiquitin ligase Cullin-5 modulates multiple molecular and cellular responses to heat shock protein 90 inhibition in human cancer cells.* Proc Natl Acad Sci U S A, 2014. **111**(18): p. 6834-9.
174. Ehrlich, E.S., et al., *Regulation of Hsp90 client proteins by a Cullin5-RING E3 ubiquitin ligase.* Proc Natl Acad Sci U S A, 2009. **106**(48): p. 20330-5.
175. Ambati, S.R., et al., *Pre-clinical efficacy of PU-H71, a novel HSP90 inhibitor, alone and in combination with bortezomib in Ewing sarcoma.* Mol Oncol, 2014. **8**(2): p. 323-36.

176. Richardson, P.G., et al., *Tanespimycin and bortezomib combination treatment in patients with relapsed or relapsed and refractory multiple myeloma: results of a phase 1/2 study.* Br J Haematol, 2011. **153**(6): p. 729-40.
177. Gerlinger, M., et al., *Intratumor heterogeneity and branched evolution revealed by multiregion sequencing.* N Engl J Med, 2012. **366**(10): p. 883-92.
178. Schrodl, K., et al., *Response to chemotherapy, reexposure to crizotinib and treatment with a novel ALK inhibitor in a patient with acquired crizotinib resistance.* Respiration, 2014. **88**(3): p. 262-4.
179. Chen, W.V., et al., *Identification and validation of PDGF transcriptional targets by microarray-coupled gene-trap mutagenesis.* Nat Genet, 2004. **36**(3): p. 304-12.
180. Kong, J., et al., *Slingshot: a PiggyBac based transposon system for tamoxifen-inducible 'self-inactivating' insertional mutagenesis.* Nucleic Acids Res, 2010. **38**(18): p. e173.
181. *Drug: 17-AAG - CancerRxGene - Genomics of Drug Sensitivity in Cancer*. http://www.cancerrxgene.org/translation/Drug/1026#scatter_1026_1010.
182. Ceulemans, S., K. van der Ven, and J. Del-Favero, *Targeted Screening and Validation of Copy Number Variations*, in *Genomic Structural Variants: Methods and Protocols*, L. Feuk, Editor. 2012, Humana Press: New York. p. 311-328.
183. Harewood, L., E. Chaignat, and R. Alexandre, *Structural Variation and Its Effect on Expression*, in *Genomic Structural Variants: Methods and Protocols*, L. Feuk, Editor. 2012, Humana Press: New York. p. 173-186.
184. Conrad, D.F., et al., *Origins and functional impact of copy number variation in the human genome.* Nature, 2010. **464**(7289): p. 704-12.
185. Stranger, B.E., et al., *Relative impact of nucleotide and copy number variation on gene expression phenotypes.* Science, 2007. **315**(5813): p. 848-53.
186. Auer, H., *Expression divergence and copy number variation in the human genome.* Cytogenet Genome Res, 2008. **123**(1-4): p. 278-82.
187. Ait Yahya-Graison, E., et al., *Classification of human chromosome 21 gene-expression variations in Down syndrome: impact on disease phenotypes.* Am J Hum Genet, 2007. **81**(3): p. 475-91.
188. Weckselblatt, B. and M.K. Rudd, *Human Structural Variation: Mechanisms of Chromosome Rearrangements.* Trends Genet, 2015. **31**(10): p. 587-99.
189. Stephens, P.J., et al., *Massive genomic rearrangement acquired in a single catastrophic event during cancer development.* Cell, 2011. **144**(1): p. 27-40.
190. Kodama, T., et al., *A novel mechanism of EML4-ALK rearrangement mediated by chromothripsis in a patient-derived cell line.* J Thorac Oncol, 2014. **9**(11): p. 1638-46.
191. Vissers, L.E.L.M. and P. Stankiewicz, *Microdeletion and Microduplication Syndromes*, in *Genomic Structural Variants: Methods and Protocols*, L. Feuk, Editor. 2012, Humana Press: New York. p. 29-75.
192. Lee, J.A., et al., *Spastic paraplegia type 2 associated with axonal neuropathy and apparent PLP1 position effect.* Ann Neurol, 2006. **59**(2): p. 398-403.
193. Shen, Z., *Genomic instability and cancer: an introduction.* Journal of Molecular Cell Biology, 2011. **3**(1): p. 1-3.

194. Ferguson, L.R., et al., *Genomic instability in human cancer: Molecular insights and opportunities for therapeutic attack and prevention through diet and nutrition.* Semin Cancer Biol, 2015.
195. Gillies, R.J., D. Verduzco, and R.A. Gatenby, *Evolutionary dynamics of carcinogenesis and why targeted therapy does not work.* Nat Rev Cancer, 2012. **12**(7): p. 487-93.
196. Beroukhim, R., et al., *The landscape of somatic copy-number alteration across human cancers.* Nature, 2010. **463**(7283): p. 899-905.
197. Valabrega, G., F. Montemurro, and M. Aglietta, *Trastuzumab: mechanism of action, resistance and future perspectives in HER2-overexpressing breast cancer.* Ann Oncol, 2007. **18**(6): p. 977-84.
198. Montemurro, F., G. Valabrega, and M. Aglietta, *Trastuzumab-based combination therapy for breast cancer.* Expert Opin Pharmacother, 2004. **5**(1): p. 81-96.
199. Fiala, O., et al., *Epidermal Growth Factor Receptor Gene Amplification in Patients with Advanced-stage NSCLC.* Anticancer Res, 2016. **36**(1): p. 455-60.
200. Katayama, R., et al., *Mechanisms of acquired crizotinib resistance in ALK-rearranged lung Cancers.* Sci Transl Med, 2012. **4**(120): p. 120ra17.
201. Kummar, S., et al., *Utilizing targeted cancer therapeutic agents in combination: novel approaches and urgent requirements.* Nat Rev Drug Discov, 2010. **9**(11): p. 843-56.
202. Mendez, P. and J.L. Ramirez, *Copy number gains of FGFR1 and 3q chromosome in squamous cell carcinoma of the lung.* Transl Lung Cancer Res, 2013. **2**(2): p. 101-11.
203. Martin, V., et al., *Increase of MET gene copy number confers resistance to a monovalent MET antibody and establishes drug dependence.* Mol Oncol, 2014. **8**(8): p. 1561-74.
204. Bean, J., et al., *MET amplification occurs with or without T790M mutations in EGFR mutant lung tumors with acquired resistance to gefitinib or erlotinib.* Proc Natl Acad Sci U S A, 2007. **104**(52): p. 20932-7.
205. Schmidt, M.L., et al., *Favorable prognosis for patients 12 to 18 months of age with stage 4 nonamplified MYCN neuroblastoma: a Children's Cancer Group Study.* J Clin Oncol, 2005. **23**(27): p. 6474-80.
206. Ladanyi, M., *Implications of P16/CDKN2A deletion in pleural mesotheliomas.* Lung Cancer, 2005. **49 Suppl 1**: p. S95-8.
207. Zhu, C.Q., et al., *Immunohistochemical markers of prognosis in non-small cell lung cancer: a review and proposal for a multiphase approach to marker evaluation.* J Clin Pathol, 2006. **59**(8): p. 790-800.
208. Dimou, A., et al., *MET gene copy number predicts worse overall survival in patients with non-small cell lung cancer (NSCLC); a systematic review and meta-analysis.* PLoS One, 2014. **9**(9): p. e107677.
209. Fidler, M.J., et al., *PTEN and PIK3CA gene copy numbers and poor outcomes in non-small cell lung cancer patients with gefitinib therapy.* Br J Cancer, 2011. **105**(12): p. 1920-6.
210. Gorre, M.E., et al., *Clinical resistance to STI-571 cancer therapy caused by BCR-ABL gene mutation or amplification.* Science, 2001. **293**(5531): p. 876-80.

211. Wang, T.L., et al., *Digital karyotyping identifies thymidylate synthase amplification as a mechanism of resistance to 5-fluorouracil in metastatic colorectal cancer patients.* Proc Natl Acad Sci U S A, 2004. **101**(9): p. 3089-94.
212. Albertson, D.G., *Gene amplification in cancer.* Trends Genet, 2006. **22**(8): p. 447-55.
213. Gorlick, R., et al., *Intrinsic and acquired resistance to methotrexate in acute leukemia.* N Engl J Med, 1996. **335**(14): p. 1041-8.
214. de Bruin, E.C., et al., *Spatial and temporal diversity in genomic instability processes defines lung cancer evolution.* Science, 2014. **346**(6206): p. 251-6.
215. Butts, C., et al., *Tecemotide (L-BLP25) versus placebo after chemoradiotherapy for stage III non-small-cell lung cancer (START): a randomised, double-blind, phase 3 trial.* Lancet Oncol, 2014. **15**(1): p. 59-68.
216. Reck, M., et al., *Ipilimumab in combination with paclitaxel and carboplatin as first-line therapy in extensive-disease-small-cell lung cancer: results from a randomized, double-blind, multicenter phase 2 trial.* Ann Oncol, 2013. **24**(1): p. 75-83.
217. Brahmer, J., et al., *Nivolumab versus Docetaxel in Advanced Squamous-Cell Non-Small-Cell Lung Cancer.* N Engl J Med, 2015. **373**(2): p. 123-35.
218. NH, S., A. SJ, and B. JR, *Preliminary data from a multi-arm expansion study of MEDI4736, an antiPD-L1 antibody.*, in *J. Clin Oncol*. 2014.
219. Olshen, A.B., et al., *Circular binary segmentation for the analysis of array-based DNA copy number data.* Biostatistics, 2004. **5**(4): p. 557-72.
220. Venkatraman, E.S. and A.B. Olshen, *A faster circular binary segmentation algorithm for the analysis of array CGH data.* Bioinformatics, 2007. **23**(6): p. 657-63.
221. Mermel, C.H., et al., *GISTIC2.0 facilitates sensitive and confident localization of the targets of focal somatic copy-number alteration in human cancers.* Genome Biol, 2011. **12**(4): p. R41.
222. Pollmann, M., et al., *Human EML4, a novel member of the EMAP family, is essential for microtubule formation.* Exp Cell Res, 2006. **312**(17): p. 3241-51.
223. Roskoski, R., Jr., *Anaplastic lymphoma kinase (ALK): structure, oncogenic activation, and pharmacological inhibition.* Pharmacol Res, 2013. **68**(1): p. 68-94.
224. Richards, M.W., et al., *Crystal structure of EML1 reveals the basis for Hsp90 dependence of oncogenic EML4-ALK by disruption of an atypical beta-propeller domain.* Proc Natl Acad Sci U S A, 2014. **111**(14): p. 5195-200.
225. Corp, S.P., *Ganetespib. Background Information for the pediatric subcommittee meeting of the oncologic drugs advisory committee.* 2014, Food and Drug Administration: www.fda.gov.
226. Heuckmann, J.M., et al., *Differential protein stability and ALK inhibitor sensitivity of EML4-ALK fusion variants.* Clin Cancer Res, 2012. **18**(17): p. 4682-90.
227. Togashi, Y., et al., *KLC1-ALK: a novel fusion in lung cancer identified using a formalin-fixed paraffin-embedded tissue only.* PLoS One, 2012. **7**(2): p. e31323.
228. Grizzle, W.E., W.C. Bell, and K.C. Sexton, *Issues in collecting, processing and storing human tissues and associated information to support biomedical research.* Cancer Biomark, 2010. **9**(1-6): p. 531-49.

229. Bao, X.H., et al., *Antiproliferative effect of the HSP90 inhibitor NVP-AUY922 is determined by the expression of PTEN in esophageal cancer.* Oncol Rep, 2013. **29**(1): p. 45-50.
230. Busacca, S., et al., *Resistance to HSP90 inhibition involving loss of MCL1 addiction.* Oncogene, 2015.
231. Abe, Y., et al., *Interpretation of the effects of protein kinase C inhibitors on human UDP-glucuronosyltransferase 1A (UGT1A) proteins in cellulo.* Drug Metab Pharmacokinet, 2011. **26**(3): p. 256-65.
232. Touzeau, C., et al., *BH3 profiling identifies heterogeneous dependency on Bcl-2 family members in multiple myeloma and predicts sensitivity to BH3 mimetics.* Leukemia, 2015.
233. Del Gaizo Moore, V. and A. Letai, *BH3 profiling--measuring integrated function of the mitochondrial apoptotic pathway to predict cell fate decisions.* Cancer Lett, 2013. **332**(2): p. 202-5.
234. Clarke, P.A., et al., *Gene expression profiling of human colon cancer cells following inhibition of signal transduction by 17-allylamino-17-demethoxygeldanamycin, an inhibitor of the hsp90 molecular chaperone.* Oncogene, 2000. **19**(36): p. 4125-33.
235. Cui, N., et al., *Effects of heat stress on the level of heat shock protein 70 on the surface of hepatocellular carcinoma Hep G2 cells: implications for the treatment of tumors.* Tumour Biol, 2013. **34**(2): p. 743-8.
236. McCollum, A.K., et al., *Up-regulation of heat shock protein 27 induces resistance to 17-allylamino-demethoxygeldanamycin through a glutathione-mediated mechanism.* Cancer Res, 2006. **66**(22): p. 10967-75.
237. Liu, B., et al., *Computational methods for detecting copy number variations in cancer genome using next generation sequencing: principles and challenges.* Oncotarget, 2013. **4**(11): p. 1868-81.
238. Wang, Y., M. Cottman, and J.D. Schiffman, *Molecular inversion probes: a novel microarray technology and its application in cancer research.* Cancer Genet, 2012. **205**(7-8): p. 341-55.
239. Hunter, S.M., et al., *Copy number aberrations in benign serous ovarian tumors: a case for reclassification?* Clin Cancer Res, 2011. **17**(23): p. 7273-82.
240. Brewster, A.M., et al., *Copy number imbalances between screen- and symptom-detected breast cancers and impact on disease-free survival.* Cancer Prev Res (Phila), 2011. **4**(10): p. 1609-16.
241. Lee, H.W., et al., *Genomic copy number alterations associated with the early brain metastasis of non-small cell lung cancer.* Int J Oncol, 2012. **41**(6): p. 2013-20.
242. Dellinger, A.E., et al., *Comparative analyses of seven algorithms for copy number variant identification from single nucleotide polymorphism arrays.* Nucleic Acids Res, 2010. **38**(9): p. e105.
243. Rueda, O.M. and R. Diaz-Uriarte, *Finding Recurrent Copy Number Alteration Regions: A Review of Methods.* Current Bioinformatics, 2010. **5**(1): p. 1-17.
244. Kaye, J.A., et al., *DNA breaks promote genomic instability by impeding proper chromosome segregation.* Curr Biol, 2004. **14**(23): p. 2096-106.

245. Shibata, T., et al., *Genetic classification of lung adenocarcinoma based on array-based comparative genomic hybridization analysis: its association with clinicopathologic features.* Clin Cancer Res, 2005. **11**(17): p. 6177-85.
246. Zhang, Y.J., et al., *Amplification and overexpression of cyclin D1 in human hepatocellular carcinoma.* Biochem Biophys Res Commun, 1993. **196**(2): p. 1010-6.
247. Higuchi, E., et al., *Prognostic significance of cyclin D1 and p16 in patients with intermediate-risk head and neck squamous cell carcinoma treated with docetaxel and concurrent radiotherapy.* Head Neck, 2007. **29**(10): p. 940-7.
248. Zhang, L.Q., et al., *The role of cyclin D1 expression and patient's survival in non-small-cell lung cancer: a systematic review with meta-analysis.* Clin Lung Cancer, 2012. **13**(3): p. 188-95.
249. Dienstmann, R., et al., *Genomic aberrations in the FGFR pathway: opportunities for targeted therapies in solid tumors.* Ann Oncol, 2014. **25**(3): p. 552-63.
250. Goetz, R. and M. Mohammadi, *Exploring mechanisms of FGF signalling through the lens of structural biology.* Nat Rev Mol Cell Biol, 2013. **14**(3): p. 166-80.
251. Newton, A.C. and L.C. Trotman, *Turning off AKT: PHLPP as a drug target.* Annu Rev Pharmacol Toxicol, 2014. **54**: p. 537-58.
252. Steed, E., et al., *MarvelD3 couples tight junctions to the MEKK1-JNK pathway to regulate cell behavior and survival.* J Cell Biol, 2014. **204**(5): p. 821-38.
253. Gao, J., et al., *Integrative analysis of complex cancer genomics and clinical profiles using the cBioPortal.* Sci Signal, 2013. **6**(269): p. pl1.
254. Cerami, E., et al., *The cBio cancer genomics portal: an open platform for exploring multidimensional cancer genomics data.* Cancer Discov, 2012. **2**(5): p. 401-4.
255. Bashyam, M.D., et al., *Array-based comparative genomic hybridization identifies localized DNA amplifications and homozygous deletions in pancreatic cancer.* Neoplasia, 2005. **7**(6): p. 556-62.
256. Antonarakis, E.S. and A.J. Armstrong, *Evolving standards in the treatment of docetaxel-refractory castration-resistant prostate cancer.* Prostate Cancer Prostatic Dis, 2011. **14**(3): p. 192-205.
257. Jamal-Hanjani, M., et al., *Tracking genomic cancer evolution for precision medicine: the lung TRACERx study.* PLoS Biol, 2014. **12**(7): p. e1001906.
258. *Genome-wide mutagenesis screens for drug resistance in cancer*. Available from: http://www.sanger.ac.uk/science/projects/genome-wide-mutagenesis-screens-drug-resistance-cancer.
259. Chen, S., et al., *Genome-wide CRISPR screen in a mouse model of tumor growth and metastasis.* Cell, 2015. **160**(6): p. 1246-60.

8 Appendix

EML4-ALK Patient sample phenotyping primers

Forward Primers:	**Sequence:**
V1-FW	ACTGTAGAGCCCACACCTGG
V2-FW	TGGTCCCCAGACAACAAGTA
V3a/b-FW	GCAGACAAGCATAAAGATGTCATCATC
V4-FW	ACTGGAGGAGGGAAAGACAGA
V5a-FW	TGAGGCGTCTTGCAATCTCT
V5b-FW	AGTCTCAAGTAAAGGTTCAGAGC
V6-FW	ACTACTGTAGAGCCCACACCTG
Reverse Primers:	
V1/2/3ab/5a-REV	TGCATGGCTTGCAGCTCC
V4-REV	GTCGGTCATGATGGTCGAGG
V5b/6-REV	GGTGGTCAGCTGCAACATG
RT-Primers:	
V1/2/3ab/5a-RT	AGCTCCATCTGCATGGCTTG
V4-RT	GTTGGGGTTGTAGTCGGTCA
V5b/6-RT	CTGCAGGTGGGTGGTCAG
Probes:	
V1/2/3ab/5a-PB	TGCTTCCGGCGGT
V4-PB	CAGCTTGTACTCAGGG
V5b/6-PB	TCAAGGGCCAGGCTGC

Antibody	Company	Address	ID	Dilution	Molecular Weight (kda)
AKT	CST	Danvers, MA, USA	9272	1:1000	60
ALK (31F12)	CST	Danvers, MA, USA	3791	1:1000	220, various EML4-ALK sizes
Alpha tubulin	Abcam	Cambridge, MA, USA	ab4074	1:5000	50
BAK	CST	Danvers, MA, USA	3814	1:1000	25
BAX	CST	Danvers, MA, USA	2772	1:1000	20
BCL-2	CST	Danvers, MA, USA	2872	1:1000	28
BCL-xL	CST	Danvers, MA, USA	2764	1:1000	30
Cleaved caspase 9	CST	Danvers, MA, USA	9501	1:1000	37
ERK(1/2)	CST	Danvers, MA, USA	9102	1:2000	44/42
GAPDH	Abcam	Cambridge, MA, USA	ab8245	1:10000	37
GFP (4B10)	CST	Danvers, MA, USA	2955	1:1000	25
Goat Anti-Mouse HRP	CST	Danvers, MA, USA	7076	1:5000	N/A
Goat Anti-Rabbit HRP	CST	Danvers, MA, USA	7074	1:5000	N/A
HSP72	CST	Danvers, MA, USA	4872	1:1000	72
HSP90	CST	Danvers, MA, USA	4874	1:1000	90
MCL-1 (C2)	SC	Dallas, TX, USA	sc-377487	1:1000	40
p-AKT (Ser473)	CST	Danvers, MA, USA	9271	1:1000	60
p-ALK (Tyr1604)	CST	Danvers, MA, USA	3341	1:1000	220, various EML4-ALK sizes
PARP	CST	Danvers, MA, USA	9542	1:1000	89, 116
p-ERK(1/2) (Thr 202/Tyr204)	CST	Danvers, MA, USA	9101	1:1000	44/42
Phospho-Stat3 (Tyr705) (3E2)	CST	Danvers, MA, USA	9138	1:1000	79,86
STAT3 (124H6)	CST	Danvers, MA, USA	9139	1:1000	79,86
UGT1A (H-300)	SC	Dallas, TX, USA	sc-15847	1:1000	55

Table 6.1-1 *List of antibodies used. SC = Santa-Cruz Biotech, CST = Cell Signaling Technology*